ISSN : 0019-5693

INDIAN JOURNAL
OF
THEORETICAL PHYSICS

VOLUME 65 NOS. 3, 4

JULY, 2017 — DECEMBER, 2017

Published by the
CALCUTTA INSTITUTE OF THEORETICAL PHYSICS
(Formerly, INSTITUTE OF THEORETICAL PHYSICS)
"BIGNAN KUTIR"
4/1, MOHAN BAGAN LANE, KOLKATA-700 004

(UGC approved and refereed Journal)

ISSN : 0019-5693

INDIAN JOURNAL
OF
THEORETICAL PHYSICS

VOLUME 65 **NOS. 3, 4**

JULY, 2017 — DECEMBER, 2017

Published by the

CALCUTTA INSTITUTE OF THEORETICAL PHYSICS

(Formerly, INSTITUTE OF THEORETICAL PHYSICS)

"BIGNAN KUTIR"

4/1, MOHAN BAGAN LANE, KOLKATA-700 004

(UGC approved and refereed Journal)

ISSN : 0019-5693

INDIAN JOURNAL
OF
THEORETICAL PHYSICS

[Founder President : Late Prof. K. C. Kar, D.Sc.]

VOLUME 65 **NOS. 3, 4**

JULY, 2017 — DECEMBER, 2017

Director **: D. K. Basu**

Secretary **: S. K. Sarkar**

Co-Published by the

WILCOX BOOKS & PERIODICALS CO.

8/2/A, Neogipara Road, Kolkata - 700 036

INDIAN JOURNAL
OF
THEORETICAL PHYSICS
"BIGNAN KUTIR"
4/1, MOHAN BAGAN LANE, KOLKATA-700 004, INDIA

SUBSCRIPTION RATE

INDIA : (For Library & Institute)
₹ 1500.00 for Vol. 64, 2016 and onwards
FOREIGN : $ 350 for Vol. 64, 2016 and onwards
Drafts, Orders, Enquiries & Claim for Non-Receipt of Journal should be sent to :

WILCOX BOOKS & PERIODICALS CO.
8/2/A, NEOGIPARA ROAD
KOLKATA - 700 036 (INDIA)
Website : www.wilcoxjournals.com
E-mail : wilcoxbooks@yahoo.com
: wilcoxbooks@gmail.com
Phone : 91-3325771147
Mobile : 91-9231675520

C O N T E N T S

INDIAN JOURNAL OF THEORETICAL PHYSICS, VOL. 65, NOS. 3 & 4, 2017

Evidence of multifractality of the pion production process at 60 GeV/n

Md. Abdul Kayum Jafry,
Department of Physics, Shibpur Dinobundhoo Institution (College),
412/1 G.T. Road (South), Howrah-711102, India
e-mail: akjafry@yahoo.com

Dipak Ghosh and Argha Deb
Nuclear and Particle Physics Research Centre, Department of Physics,
Jadavpur University, Kolkata-700 032, India

[**Abstract** : To study the dynamical fluctuation of pions produced in 60 *GeV/n* ^{16}*O–AgBr* interaction in η and ϕ space, we have used G_q moment, which can suppress the statistical noise. In both η and ϕ spaces fractal nature has been observed which is of dynamical origin.]

Keywords: Heavy ion interactions, produced particles, mutifractality.
PACS: 25.70 Pq, 24.60 Ky

1. Introduction

Non-statistical fluctuations in high energy collisions have been observed with much attention to understand the multi-particle production mechanism[1-4]. Bialas and Peschanski[5, 6] observed a power law dependence of the normalized factorial moments of the multiplicity distribution on the rapidity bin-width. Such a power law dependence of the normalized factorial moments is a signature of self-similarity in the fluctuation pattern of multi-particle production. It has been suggested that the probability distribution of the particle density has fractal properties[7]. Different methods have been proposed for studying the fractal structures in multi-particle data[8-12]. Hwa proposed[10, 11] an approach in terms of G_q moments, which can reveal the multi-fractal structure of the particle spectra. But for low multiplicity events, the fractal moments G_q are dominated by statistical noise. In order to suppress statistical noise, Hwa Pan[12] modified the

definetion of G_q moments, by introducing a step function which can act as a filter for the low multiplicity events.

The motivation of this paper is to investigate the fractal behavior of multiplicity fluctuations in $^{16}O–AgBr$ interactions in both pseudo-rapidity and azimuthal dimensions using the modified definition of the G_q moments[12]. We have studied the fractal indices as well as their dependence on the order of the moments. In this paper we report for the investigation of the fractal behavior in pseudo-rapidity as well as azimuth space. The relation between the fractal and intermittency indices has also been studied. In order to study this relation, we perform a multi-fractal analysis of the data using the noise suppressed G_q moments. It would be further interesting to investigate the intermittency in terms of multi-fractals, for this will provide another window to understand the dynamics of particle production process.

2. Experimental Method

The study was performed on pions produced in $^{16}O–AgBr$ interactions at 60 *GeV/n*. The data sets used in this present analysis were obtained from Ilford *G*5 emulsion tracks exposed to ^{16}O beam of energy 60 *GeV/n* at *CERN SPS*. A Leitz Metaloplan microscope with a 10*x* objective and 10*x* ocular lens provided with a semi-automatic scanning stage was used to scan the plates. Each plate was scanned by two independent observers to increase the scanning efficiency. The interactions have been selected after 1*cm* from the leading edge of the plate. The final measurements were done using an oil-immersion 100*x* objective. The measuring system fitted with it has 1 μm resolution along the *x* and *y* axes and 0.5 μm resolutions along the *z* axis. Here the nuclear emulsion serves the purpose of target as well as detector.

Our detector can resolve particles differing by 0.1 unit in pseudorapidity scale and about 5^0 in azimuthal angle space. It is worthwhile to mention that the emulsion technique possesses a very high spatial resolution which makes it a very effective detector for studying fluctuation phenomena.

After scanning, the events were chosen according to the following criteria :

(*i*) The incident beam track should not exceed 3^0 from the main beam direction in the pellicle. It is done to ensure that we have taken the real projectile beam.

(*ii*) Events showing interactions within 20 μm from the top or bottom surface of the pellicle were rejected. It is done to reduce the loss of tracks as well as to reduce the error in angle measurement.

(*iii*) The selection of the primary interactions is made by following the incident beam track in the backward direction until it reaches the leading edge.

According to the usual emulsion terminology[13], relativistic charged particles with ionisation $I \leq 1.4\, I_0$, (I_0 being the minimum ionisation) and velocity $\geq 0.7c$, are termed as shower tracks. They are mostly pions. With the above selection criterion, we have chosen 250 events of ^{16}O–*AgBr* interactions at 60 *GeV/n* for this analysis.

The shower tracks are identified from each event and their emission angles θ with respect to the beam direction and azimuthal angle ϕ determined by measuring the space co-ordinates (*x,y,z*) of a point on each shower track, the point of interaction and a point on the incident track. Pseudo-rapidity η of all shower particles were determined from measured space angle θ with reference to the beam by the relation $\eta = -\ln \tan(\theta/2)$. The average multiplicity of produced particles of the sample is 63.74 ± 2.3.

3. Method of Analysis

Let us consider a pseudorapidity interval $\Delta\eta$ which is divided into *M* bins of size $\delta\eta = \Delta\eta/M$. Let *N* be the total multiplicity in the considered η interval, *M* be the number of bins into which the total interval has been divided and n_m be the *m*-th bin multiplicity. The modified form of multifractal multiplicity moments of order *q* suggested by Hwa and Pan[12] is defined by

$$\langle G_q \rangle = \sum_{m=1}^{M} (n_m / N)^q \; \theta(n_m - q) \qquad \ldots \quad (1)$$

where $\theta(n_m - q)$ is the usual step function which is equal to 1 for $n_m \geq q$ and 0 for $n_m < q$. For very large multiplicity $N/M >> q$, the step function, as in the case of statistical system, is not essential and the two definitions coincide. But in the particle production phenomenon N is much less than M and the θ function exerts a crucial influence on the G_q moments.

A self similar particle production process is characterized by a power-law behavior[10,11]

$$\langle G_q \rangle \propto M^{-\tau q} \quad \ldots \quad (2)$$

where τ_q are the fractal indices which can be obtained from the slope

$$\tau_q = \left(\frac{\delta \langle \ln G_q(M) \rangle}{\delta \ln(M)} \right) \quad \ldots \quad (3)$$

on a double logarithmic plot, after averaging over all events in the sample.

For an ensemble of events, the averaging is done as,

$$\langle G_q \rangle = (1/Nev) \ \Sigma \ G_q \quad \ldots \quad (4)$$

where *Nev* is the total no. of events in the ensemble.

One of the most important aspects of multi-fractal analysis is the extraction of the generalized dimensions D_q. The generalized (Renyi) dimensions are given by

$$D_q = [1/(q-1)] \ \tau_q \quad \ldots \quad (5)$$

If $D_{q'} = D_q = 1$, it would indicate that the multi-particle spectrum does not have any fractal structure. For geometrically monofractal structure of multi-particle spectra $D_{q'} = D_q \neq 1$. On the other hand multi-fractality in the particle production process manifests itself as $D_{q'} > D_q$ for $q' < q$.

We calculated the $\langle G_q \rangle$ moments using Eq. (1) and Eq. (4) for $q = 2,3,\ldots 6$ in the η and ϕ interval. For the analysis we have considered the pseudo-rapidity interval $\Delta\eta = 4$ around the peak of the distribution. For the ϕ space we have used the total 2π interval. Fig.1(*a*) depicts the variation of $\ln \langle G_q \rangle$ with $\ln(M)$ for the η interval and Fig.1(*b*) depicts the variation of $\ln \langle G_q \rangle$ with $\ln(M)$ for the ϕ interval. A linear dependence of $\ln \langle G_q \rangle$ on $\ln (M)$ is observed in both cases, which indicates self-similarity in the

particle production process. The exponent τ_q of the power law behaviour is obtained by curve fitting (least square fitting). τ_q values for η and ϕ are presented in Table I and Table II respectively.

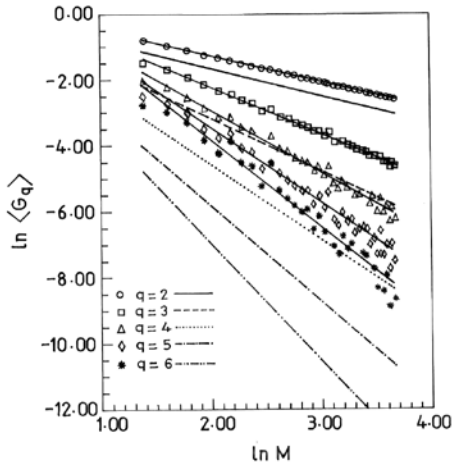

Fig.1(*a*)

Plot of ln< G_q > vs. ln(M) for q=2 to 6 in η interval.

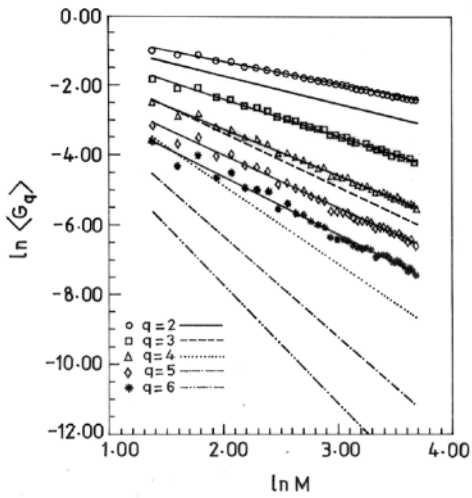

Fig.1(*b*)

Plot of ln< G_q > vs. ln(M) for q = 2 to 6 in φ interval.

(Symbols represent data, lines represent statistical noise;
Error bars are not shown to avoid clumsiness.)

Table I

Parameters of G_q moment analysis for q = 2 to 6 in the pseudo rapidity interval.

Q	τ_q	τ_q^{stat}	τ_q^{dyn}	D_q^{dyn}
2	0.788±0.004	0.836±0.006	0.952±0.007	0.952±0.007
3	1.403±0.016	1.598±0.010	1.805±0.019	0.903±0.010
4	1.862±0.039	2.279±0.024	2.582±0.046	0.861±0.015
5	2.246±0.067	2.915±0.066	3.331±0.094	0.833±0.024
6	2.618±0.094	3.559±0.117	4.059±0.150	0.812±0.030

Table II

Parameters of G_q moment analysis for q = 2 to 6 in the azimuthal interval.

Q	τ_q	τ_q^{stat}	τ_q^{dyn}	D_q^{dyn}
2	0.660±0.006	0.812±0.004	0.848±0.007	0.848±0.007
3	1.091±0.012	1.563±0.009	1.527±0.015	0.764±0.008
4	1.349±0.017	2.254±0.018	2.095±0.025	0.699±0.008
5	1.522±0.025	2.885±0.046	2.637±0.052	0.659±0.013
6	1.667±0.033	3.413±0.140	3.254±0.144	0.651±0.029

To obtain the statistical noise contribution to $\langle G_q \rangle$, N particles of each event are distributed randomly throughout the considered η and ϕ interval. The G^{st}_q value of each event is calculated with the redistributed particles and the average of G^{st}_q is obtained by using (4). The best fit curves are plotted in Fig.1(*a*) and Fig.1(*b*). The fitted slopes τ^{st}_q are listed in Table I and Table II. For $q \geq 3$, the $\langle G^{st}_q \rangle$ is much smaller than $\langle G_q \rangle$ in the best fit region, which reveals the dynamical effect prominently and thus demonstrates the superiority of the modified definition over the old definition. For q=2 and 3, there is no significant suppression of statistical fluctuations. So for both pseudo-rapidity and azimuthal intervals, the suppression of statistical noise is apparent from the figures for greater than three.

The dynamical contribution to the G_q moments can be expressed by[14]

$$<G_q>^{dyn} = [<G_q>/<G_q>^{st}] M^{(1-q)} \quad \ldots \quad (6)$$

where $<G_q>^{st}$ can be determined by distributing the N particles of an event randomly in $\Delta\eta$.

The dynamical contributions to the slope τ_q can be expressed by

$$\tau_q^{dyn} = \tau_q - \tau^{st}_q + q - 1 \quad \ldots \quad (7)$$

where the τ^{st}_q is the statistical part of the slope.

When $< G^{st}_q>$ is equal to $<G_q>$, a trivial dynamical effect gives the result,

$$<G_q>^{dyn} = M^{(1-q)} \quad \ldots \quad (8)$$

Under such condition,

$$\tau_q^{dyn} = q - 1 \quad \ldots \quad (9)$$

So any deviation of τ_q^{dyn} from $(q - 1)$ indicates the presence of dynamical information.

We have extracted the dynamical part of τ_q according to the formula (7) for q = 2 to 6 for both the cases of η and ϕ . Table I and II contain the τ_q^{dyn} values in each case. In each case τ_q^{dyn} differs significantly from $(q–1)$, indicating the dynamical origin of the observed fluctuation.

We have calculated D_q^{dyn} [$= \tau_q^{dyn} / (q–1)$] from the values of τ_q^{dyn} for different orders and the values are shown in Table I (for η space). We have also calculated D_q^{dyn} for FRITIOF data and are given in Table III. D_q^{dyn} for the FRITIOF events are almost equal to the topological dimension ($D_q \approx 1$). But for the experimental events the deviation of D_q^{dyn} from the topological dimension is non-vanishing and non-trivial indicating the presence of fractality in the particle production process. Moreover, the dimension values decrease with order which is a hint of multi-fractal geometry. Similar results are obtained for ϕ space also (Table II).

Table III

Parameters of G_q moment analysis for q = 2 to 6 in the pseudo-rapidity interval for FRITIOF data.

q	τ_q	τ_q^{stat}	τ_q^{dyn}	D_q^{dyn}
2	0.845±0.005	0.850±0.006	0.995±0.006	0.995±0.007
3	1.689±0.014	1.704±0.015	1.985±0.018	0.993±0.010
4	2.547±0.035	2.563±0.025	2.984±0.042	0.995±0.016
5	3.395±0.070	3.363±0.068	4.032±0.095	1.008±0.025
6	4.108±0.096	4.469±0.114	4.638±0.155	0.928±0.032

Simple intermittency analysis were performed by KLM[15], HELIOS[16], EMU01[17], WA80[18] on emulsion data at *SPS* energies. From intermittency exponents (α_q) one can calculate the generalized dimension D_q [= 1– α_q / (q–1)][12]. Though calculated values of generalized dimensions are different from that of ours, all the data reveal hint of multi-fractality. The difference in values may be attributed to the different method of analysis. Mulifractality analysis was also performed recently by several scientists on emulsion data at *SPS* energies[22-24].

The self-similar property of multi-particle production at high energy can be investigated by factorial moments (F_q) and by fractal moments (G_q). It is natural to search for some correlation between the G_q moment and the F_q moment, thus providing a fractal interpretation for intermittency. The fractal index τ_q measures the strength of fractality, while the intermittency index α_q is a measure of the strength of the intermittency. Thus, a correspondence between intermittency and multi-fractality can be obtained by relating the indices α_q and τ_q . Since the deviation of α_q from zero is a measure of dynamical fluctuation, it can be compared to the deviation of τ_q^{dyn} from (q–1).

Subtracting the statistical contribution from τ_q, Eq. (7) gives,

$$\tau_q - \tau^{st}_q = \tau_q^{dyn} - q + 1 \approx -\alpha_q$$

$$i.e. \quad \alpha_q \approx q - 1 - \tau_q^{dyn} \qquad \ldots \quad (10)$$

which can be directly compared to the slopes α_q obtained from the factorial moments[12].

The intermittency exponents α_q for order q = 2 to 6 in the pseudo-rapidity interval and azimuthal interval are shown in Table IV and Table V respectively[19].

Table IV

Intermittency exponents α_q for order q = 2 to 6 in the pseudo-rapidity interval.

	q=2	q=3	q=4	q=5	q=6
α_q	0.174±0.004	0.570±0.013	1.130±0.032	1.729±0.052	2.312±0.072

Table V

Intermittency exponents α_q for order q = 2 to 6 in the azimuthal interval.

	q=2	q=3	q=4	q=5	q=6
α_q	0.251±0.007	0.698±0.018	1.282±0.034	1.923±0.057	2.569±0.082

The relationship is not exact because F_q and G_q are different moments and approach each other only in the limiting case of infinite N. It is clear from (10) that the derivation of α_q from zero is equivalent to the deviation of τ_q^{dyn} from (q–1). Thus for the comparison of the fractal behavior of $<F_q>$ and $<G_q>$, we should compare α_q and (q–1 – τ_q^{dyn})[12,20]. We have plotted the value for α_q (solid circles) and the value for (q–1 – τ_q^{dyn}) (open circles) with the order q in Fig. 2(*a*) for the η interval and Fig. 2(*b*) for the ϕ interval. It is observed from these Figs. that in each case the two values α_q and (q–1 – τ_q^{dyn}) are not equal but both of them increase with the order q.

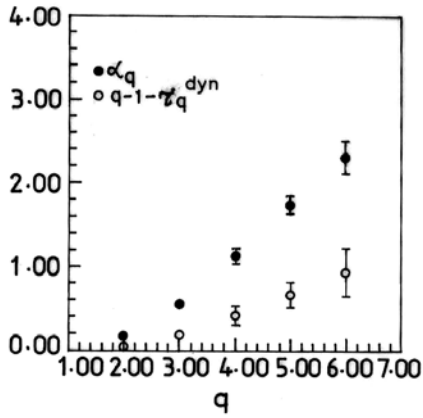

Fig. 2(*a*)

Compaison of the exponents of α_q of F_q and $(q-1-\tau_q^{dyn})$ of G_q in η interval.

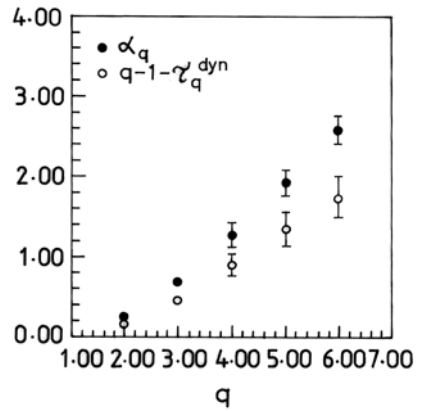

Fig. 2(*b*)

Compaison of the exponents of α_q of F_q and $(q-1-\tau_q^{dyn})$ of G_q in φ interval.

The information dimension D_1 of a self-similar set may be given by

$$D_q = Lim_{\delta\eta\to 0} \frac{\sum (n_m/N) \ln(n_m/N)\Theta (n_m - q)}{\ln \delta\eta} \quad \text{for } q = 1$$

which describes how the information entropy[21]

$$S = -\Sigma\ (n_m/N)\ \ln(n_m/N)\ \theta(n_m - 1) \qquad \ldots\ (11)$$

varies with decreasing widths of the pseudo-rapidity bins.

Since the intermittency index increases with the increase of q, we observe for a deviation of D_q from 1.0 at large q. One might also search for a deviation of D_q from unity where the statistics are best *i.e.* $q = 1$. Hence we look in more detail at the particular case $q = 1$, where D_1 is the derivative of the entropy S with respect to ln $\delta\eta$. Hence calculation of entropy should be needed. We have calculated the value for horizontally averaged entropy $< S >$ using Eq. (11) and we have plotted this with respect to ln (M) in Fig. 3(a). It is observed from the Fig. that the points approach a straight line with a characteristic slope D_1. It should be investigated whether this tendency to approach a straight line is a real dynamical effect or just a result of saturation (bend over) at large M due to finite multiplicity. We, therefore, calculate $<S^{stat}>$ in a manner similar to the calculation of $<G^{stat}>$ using (11). $<S^{stat}>$ of the randomized event is then interpreted as the average maximum entropy $<S_{max}>$ attainable for every event.The values of the normalized entropy $<S>/<S_{max}>$ are plotted in Fig. 3(b). we have compared the normalized entropy $<S>/<S_{max}>$ of the experimental events with that of the FRITIOF data.

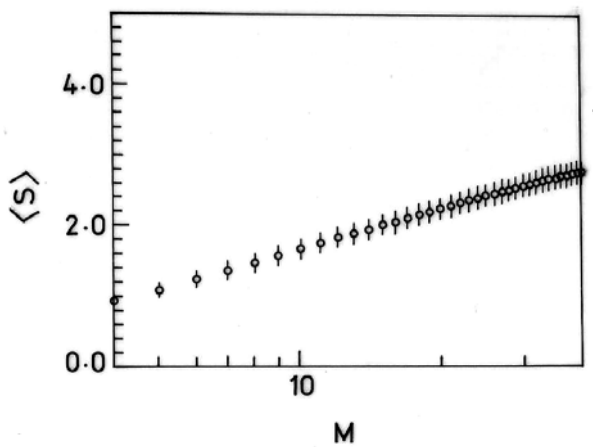

Fig. 3(a)

$< S >$ as a function of ln (M) in η interval.

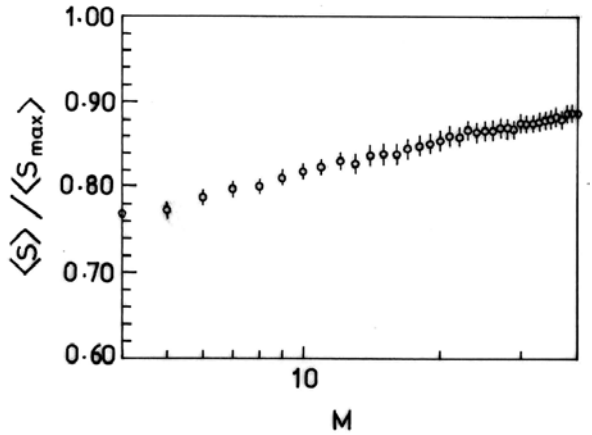

Fig. 3(*b*)

Plot of $<S>/<S_{max}>$ vs. ln (M) in η interval.

For the sake of comparison we have calculated $<S>/<S_{max}>$ for the FRITIOF events. It is observed that the normalized entropy is almost unity in each phase space whereas the experimental data show the monotonic increase of normalized entropy suggesting non-random behavior in ^{16}O–*AgBr* interaction at 60 *GeV/n*.

This analysis reveals multi - fractality in the pionisation process in ^{16}O – *AgBr* interaction at 60 *GeV/n*. Further this fractal analysis indicates clearly that the modified G_q moment indeed suppresses statistical noise. Suppression is very prominent for order greater than three. $<G_q>$ exhibits asymptotic power law behavior. The extracted dynamical signal (q–1 – τ_q^{dyn}) has a rough link with the intermittency exponents α_q .

Acknowledgement

We would like to express our gratitude to Prof. P .L. Jain , Buffalo State University, U.S.A, for providing us with the exposed and developed emulsion plates used for this work. Md. Abdul Kayum Jafry would like to acknowledge the financial help sanctioned by the University Grant Commission (Govt. of India) under his Minor Research Project.

References

1. Intermittency in High Energy Collisions, Proceedings of the Santa Fe Workshop, Santa Fe, New Mexico, (1990), edited by F. Cooper, R. C. Hwa and I. Sarcevic– World Scientific, Singapore, (1991).
2. Kittel, W. − In proceedings of the Twentieth International Symposium on Multi Particle Dynamics, Gut Holmeeke, Germany, (1990), edited by R. Baier and D. Wegener − World Scientific, Singapore, p. 401(1991).
3. Bialas, A. − In Quark Matter '90, Proceedings of the Eighth International Conference on Ultra relativistic Nucleus-Nucleus Collisions, Menton, France, edited by J.P.Blaizot et. al. – Nucl. Phys., **A 525**, 345c (1991).
4. Fluctuations and Fractal Structures, Proceedings of the Ringberg Workshop on Multi Particle Production, Rringberg Caslte, Germany, (1991), edited by R.C.Hwa, W.Ochs and N. Schmitz – World Scientific, Singapore, (1992).
5. Bialas, A. and Peschanski, R. − Nucl. Phys., **B 273**, 703 (1986).
6. Bialas, A. and Peschanski, R. − Nucl. Phys., **B 308**, 857 (1988).
7. Mandelbrot, B.B. −The Fractal Geometry of Nature, Freeman, New York, (1982); Paladin, G. and Vulpiany, A. − Phys. Rep., **156** ,147 (1987).
8. Dremin, I. M. − Modern Physics Lett., **A3**, 1333 (1998); Caruthers, P. – Int. J. Mod. Phys., **A4**, 5587 (1989); Brax, Ph. and Peschansky, R. – Nucl. Phys., **B 346,** 65 (1990).
9. Lipa, P. and Bushbeck, B. − Phys. Lett., **B 223**, 465 (1988).
10. Hwa, R.C. − Phys. Rev., **D 41**, 1456 (1990).
11. Chiu, C.B. and Hwa, R.C. − Phys. Rev., **D 43**, 100 (1991).
12. Hwa, R.C. and Pan, J.C. – Phys. Rev., **D 45**, 1476 (1992).
13. Powell, C.F., Fowler, P.H. and Perkins, D.H. − The Study of Elementary Particles by Photographic Methods, Pergamon, Newyork, (1959).
14. Chiu, C.B., Fialkowski, K. and Hwa, R.C. − Mod. Phys. Lett., **A 5**, 2651 (1990).
15. KLM Collab. − Phys. Rev. Lett., **62**, 733 (1989).
16. HELLIOS Collab. − Phys. Lett., **B 252,** 303 (1990).

17. EMU01 Collab. − Z. Phys., **C 49** , 395 (1991).
18. WA80 Collab. − Phys. Lett., **B 221** ,427 (1989).
19. Ghosh, D. et.al. − Phys. Rev., **D 51,** 3298 (1995).
20. Ghosh, D. et.al. − Z. Phys., **C 71,** 243 (1996).
21. K.L.M. Collab. − Phys. Rev., **D 48 ,** 3174 (1993).
22. Ahmad, N. and Kamal, A. et al. − Journal of Modern Physics, **5**, 1288 (2014).
23. Rasool, M. H. et al. − Chaos Soliton's & Fractals, **84**, 58 (2016).
24. Bhattacharyya, S. and Ghosh, D. et al. − Nucl. Phys., **A 390** , 4144 (2011).

INDIAN JOURNAL OF THEORETICAL PHYSICS, VOL. 65, NOS. 3 & 4, 2017

Global stability analysis to control growth of tumor in an immune-tumor-normal cell model with drug administration in the form of chemotherapy

Ranu Paul, Ms. Anusmita Das and Hemanta Kr. Sarmah
Department of Mathematics, Gauhati University,
Guwahati-781014, Assam, India

[**Abstract:** The main objective of this paper is to present a control policy for an immune-tumor-normal cell model with drug administration in the form of chemotherapy following certain model through both local and global stability analysis of tumor free equilibrium points. By constructing a simple quadratic Lyapunov function we determined a range for the drug administration rate so that the tumor free state can be made globally stable.]

Keywords: Equilibrium points, Local stability, Global stability, Lyapunov function.

1. Introduction

Cancer is still a leading cause of death in the world. Yet, much is still not known about the mechanism by which the disease gets incorporated in the cell system and how it can be cured. Growth of tumor cells for cancer is very complex in nature as it involves many biological factors. Cancer is caused due to unnatural growth of malignant cells which form tumor. A tumor is a non-linear dynamical system in which bad cells spread very quickly and eventually overwhelm good cells in the body. Majority of the tumor growth models are formulated in the form of differential equations. More recently, interest of the researchers has been shifted towards discrete models also.

Till date many authors have proposed many tumor cell growth models[8,9,10,11,13,15,17,21] and have suggested various control policies that include treatment such as immunotherapy[4,7,19], drug therapy (chemotherapy)[1,3,6,9,16,18], use of tumor cell targetting viruses etc.[2].

In 2003, de Pillis, et. al.[12] constructed a mathematical model of tumor growth and immune system interaction. In 2006, Novozhilov, et. al.[2] presented a model of tumor therapy using oncolytic viruses that specifically

target tumor cells. In 2009, Kirschner, et. al.[4] investigated the global dynamics to show under what conditions tumor clearance can be achieved. In 2012, Wilson & Levy[18] proposed a model related to immunotherapy using transforming growth factor β (*TGF-*β).

In the model proposed by Pillis, et. al.[12], the authors assumed that the immune and tumor cells compete in a predator prey fashion whereas the normal cells and tumor cells compete for available resources. Drug therapy was assumed to kill all types of cells *viz*. normal cells, immune cells and tumor cells but with different killing rates. Using optimal control theory with constraints and numerical simulations, the authors obtained new therapy protocols which they compared with traditional pulsed periodic treatment. The authors showed that though the optimal control generated therapies proposed by them produce larger oscillations in the tumor population over time, however, by the end of the treatment period, total tumor size become smaller than that achieved through traditional pulsed therapy, and the normal cell population suffers nearly no oscillations.

In the present paper we have followed the tumor growth model suggested by de Pillis[12]. But in contrast to Pillis' model[12], we have assumed that the drug administration in the form of chemotherapy follows the logistic growth law with a per capita decay rate of the drug once being injected. Moreover, in the immune system equation (first equation), we have replaced Michaelis-Menten form of the function by the Lotka-Voltera from. Further, in contrast to[12], in the last term of the first three equations of the model, we have assumed that the drug kills all types of cells with the linear response curve $(V) = aV$, in all cases instead of an exponential one. Here (V) is the fraction cell kill for a given amount of drug, V, at the tumor site.

With the above mentioned changes in the model[12] we have done our investigation which proceeds as follows: The model formulation is given in section 2. In section 3, we determined conditions for the existence of the equilibrium points. Local stability analysis of the equilibrium points is done in section 4. In section 5, we have shown the existence of a Lyapunov function having simple form and then applied the Lyapunov second method to globally stabilize the locally stable tumor free equilibrium point E_2 which is the only realistic one (out of the four) and determined a range for the rate of drug administration to reduce the tumor size to zero and stabilize it

irrespective of the initial size of the tumor. Numerical simulation to validate our results is done in section 6 and section 7 contains concluding remarks.

2. The model

The tumor growth model we considered in this paper is :

$$\frac{dI}{dt} = s + c_1 IT - d_1 I - a_1 VI$$

$$\frac{dT}{dt} = r_1 T(1 - b_1 T) - c_2 IT - c_3 TN - a_2 VT$$

$$\frac{dN}{dt} = r_2 N(1 - N) - c_4 TN - a_3 VN$$

$$\frac{dV}{dt} = \alpha_3 V(1 - \beta_3 V) - d_2 V$$

where, $I(t)$, $T(t)$, $N(t)$ and $V(t)$ denotes the number of immune cells, number of tumor cells, number of normal cells and the amount of drug administered at time t respectively. The unit of cells are normalised by taking the carrying capacity of normal cells equal to one.

Further, s is the constant number of immune cells already present in the body, d_1 is the natural death rate of immune cells, r_1 is the intrinsic tumor growth rate, $1/b_1$ is the tumor population carrying capacity, α_3 is the intrinsic rate of drug application, $1/\beta_3$ is the maximum drug carrying capacity, d_2 is the per capita decay rate of the drug after being injected and a_1, a_2 and a_3 are the kill rates of the immune cells, the tumor cells and the normal cells respectively due to drug administration.

3. Existence of the equilibrium point

Equilibrium points of the system are given by

$$\frac{\mathrm{dI}}{\mathrm{dt}} = 0 \Rightarrow \mathrm{I} = \frac{s}{d_1 + a_1 \mathrm{V} - c_1 \mathrm{T}}; \qquad \frac{dT}{dt} = 0 \Rightarrow T = 0,\ T = \frac{r_1 - c_2 I - c_3 N - a_2 V}{r_1 b_1}$$

$$\frac{dN}{dt} = 0 \Rightarrow N = 0,\ N = \frac{r_2 - c_4 T - a_3 V}{r_2}; \qquad \frac{dV}{dt} = 0 \Rightarrow V = 0,\ V = \frac{\alpha_3 - d_2}{\alpha_3 \beta_3} = \mathrm{V}^*$$

Since $N = 0$ signifies that the patient will die due to nullity of normal cells, we discard the equilibrium points with $N = 0$ and check the stability of the other equilibrium points with $N \neq 0$.

Thus, the possible equilibrium points are :

E_1 (N_1, 0, I_1, 0), E_2 (N_2, 0, I_2, V_2), E_3 (N_3, T_3, I_3, 0) and E_4 (N_4, T_4, I_4, V_4).

(*i*) The equilibrium point E_1 (N_1, 0, I_1, 0) lies in the *N-I* plane with $N_1 > 0$, $I_1 > 0$ and $T_1 = V_1 = 0$ where $N_1 = 1$, $I_1 = s/d_1$.

(*ii*) The equilibrium point E_2 (N_2, 0, I_2, V_2) lies in the *N-I-V* space with N_2, I_2, $V_2 > 0$ and $T_2 = 0$. Here $V_2 = V*$, $N_2 = \frac{r_2 - a_3 V^*}{r_2}$, $I_2 = \frac{s}{d_1 + a_1 V^*}$

(*iii*) The equilibrium point E_3 (N_3, T_3, I_3, 0) lies in the *N-T-I* space with N_3, T_3, $I_3 > 0$ and $V_3 = 0$.

Here $N_3 = \frac{r_2 - c_4 T_3}{r_2}$, $T_3 = \frac{r_1 - c_2 I_3 - c_3 N_3}{r_1 b_1}$, $I_3 = \frac{s}{d_1 - c_1 T_3}$

Thus, we get,

$$T_3 = \frac{r_1 - c_2 I_3 - c_3 N_3}{r_1 b_1} = \frac{1}{b_1} - \frac{c_2}{r_1 b_1}\left(\frac{s}{d_1 - c_1 T_3}\right) - \frac{c_3}{r_1 b_1}\left(\frac{r_2 - c_4 T_3}{r_2}\right)$$

which gives the equation, $A_1 T^2_3 + B_1 T_3 + C_1 = 0$
where,

$A_1 = (c_1 c_3 c_4 - r_1 r_2 c_1 b_1)$

$B_1 = (r_1 r_2 b_1 d_1 + c_1 r_1 r_2 - c_1 c_3 r_2 - c_3 c_4 d_1)$

$C_1 = (c_2 s r_2 - r_1 r_2 d_1 + c_3 r_2 d_1)$

Solving we get, $T_3 = \frac{-B_1 \pm \sqrt{B_1^2 - 4A_1 C_1}}{2A_1}$. For the existence of T_3, the discriminant must be positive *i.e.* $B_1^2 - 4A_1 C_1 \geq 0$

(*iv*) The co-existing equilibrium point E_4 (N_4, T_4, I_4, V_4) lies in the *N-T-I-V* space with N_4, T_4, I_4 and $V_4 > 0$ where

$$I_4 = \frac{s}{d_1 + a_1 V^* - c_1 T_4}, \quad T_4 = \frac{r_1 - c_2 I_4 - c_3 N_4 - a_2 V^*}{r_1 b_1}, \quad N_4 = \frac{r_2 - c_4 T_4 - a_3 V^*}{r_2},$$

$V_4 = \frac{\alpha_3 - d_2}{\alpha_3 \beta_3} = V^*$ (say).

Therefore,

$$T_4 = \frac{1}{b_1} - \frac{c_2}{r_1 b_1}\left(\frac{s}{d_1 + a_1 V^* - c_1 T_4}\right) - \frac{c_3}{r_1 b_1}\left(\frac{r_2 - c_4 T_4 - a_3 V^*}{r_2}\right) - \frac{a_2 V^*}{r_1 b_1}$$

$$\Rightarrow A_2 T_4^2 + B_2 T_4 + C_2 = 0$$

where,

$$A_2 = c_1 c_3 c_4 - r_1 r_2 b_1 c_1$$

$$B_2 = r_1 r_2 b_1 d_1 + r_1 r_2 b_1 a_1 V^* + c_1 r_1 r_2 - c_1 c_3 r_2 - c_3 c_4 d_1 - c_3 c_4 a_1 V^* + c_1 c_3 a_3 V^* - c_1 a_2 r_2 V^*$$

$$C_2 = c_2 s r_2 - r_1 r_2 d_1 - r_1 r_2 a_1 V^* + c_3 r_2 d_1 + r_2 c_3 a_1 V^* - d_1 c_3 a_3 V^* - a_1 c_3 a_3 V^{*2} + a_2 r_2 d_1 V^* + a_1 a_2 r_2 V^{*2}.$$

Solving, we get,

$$T_4 = \frac{-B_2 \pm \sqrt{B_2^2 - 4A_2 C_2}}{2A_2}.$$

Thus, for the existence of T_4, we must have $B_2^2 - 4A_2 C_2 \geq 0$.

4. Local stability analysis of the equilibrium points

For the stability of the equilibrium points E_1, E_2, E_3, E_4, the real part of all the eigen values of Jacobian matrix of the linearized system at the corresponding equilibrium points must be less than zero. Below, we have checked for each of the equilibrium points.

For the equilibrium point E_1:

This critical point lies in the *N-I* plane with $T=V=0$, $N=1=N_1$, $I = \frac{s}{d_1} = I_1$.

The Jacobian matrix of the system at E_1 is,

$$J_{E_1} = \begin{pmatrix} -r_2.1 & -c_4.1 & 0 & -a_3.1 \\ 0 & r_1 - c_2.{}^{s}/_{d_1} - c_3.1 & 0 & 0 \\ 0 & c_1.{}^{s}/_{d_1} & -d_1 & -a_1.{}^{s}/_{d_1} \\ 0 & 0 & 0 & \alpha_3 - d_2 \end{pmatrix}$$

The eigen values are found to be,

$\lambda_1 = -r_1$, $\lambda_1 = r_1 - c_1 s/d_1 - c_3$, $\lambda_3 = -d_1 < 0$ and $\lambda_4 = \alpha_3 - d_2 > 0$ (since, $\alpha_3 \geq d_2$ as amount of drug administered cannot be negative).

So, the equilibrium point E_1 is unstable which suggests the fact that without any drug administration or treatment policy, the tumor size cannot be diminished to zero.

For the equilibrium point E_2:

The equilibrium point $E_2(N_2 = \frac{r_2 - a_3V^*}{r_2}, 0, I_2 = \frac{s}{d_1 + a_1V^*}, V_2 = V^*)$ lies in the *NIV*-plane.

The Jacobian matrix of the system at E_2 is

$$J_{E_2} = \begin{pmatrix} r_2 - 2r_2N_2 - a_3V^* & -c_4N_2 & 0 & -a_3N_2 \\ 0 & r_1 - c_2I_2 - c_3N_2 - a_2V^* & 0 & 0 \\ 0 & c_1I_2 & -d_1 - a_1V^* & -a_1I_2 \\ 0 & 0 & 0 & \alpha_3 - 2\alpha_3\beta_3V^* - d_2 \end{pmatrix}$$

with the following eigen values,

$$\lambda_1 = r_2 - 2r_2N_2 - a_3V^* = \frac{a_3\alpha_3 - a_3d_2 - r_2\alpha_3\beta_3}{\alpha_3\beta_3}$$

$$\lambda_2 = r_1 - c_2I_2 - c_3N_2 - a_2V^* = r_1 - c_2.\frac{s}{d_1 + a_1V^*} - c_3.\frac{r_2 - a_3V^*}{r_2} - a_2V^*$$

$$\lambda_3 = -d_1 - a_1V^* < 0$$

$$\lambda_4 = \alpha_3 - 2\alpha_3\beta_3\,\frac{\alpha_3 - d_2}{\alpha_3\beta_3}.-d_2 = -\alpha_3 + d_2 < 0.$$

For the equilibrium point E_2 to be stable we must have $\lambda_1 < 0$ which gives $\alpha_3 < \frac{a_3d_2}{a_3 - r_2\beta_3}$

Thus, we have, $1 \leq \frac{\alpha_3}{d_2} < \frac{a_3}{a_3 - r_2\beta_3}$ … (1)

For $\lambda_2 < 0$, we get, $PV^{*2} + QV^* + R < 0$

where,

$$P = a_1\left(\frac{c_3a_3}{r_2} - a_2\right),\ Q = d_1\left(\frac{c_3a_3}{r_2} - a_2\right) + (r_1 - c_3)a_1,\ R = (r_1 - c_3)d_1 - c_2s$$

$$\Rightarrow P\left(\frac{\alpha_3 - d_2}{\alpha_3\beta_3}\right)^2 + Q\left(\frac{\alpha_3 - d_2}{\alpha_3\beta_3}\right) + R < 0$$

$$\Rightarrow (P + Q\beta_3 + R\beta_3^2)\alpha_3^2 - (2Pd_2 + Qd_2\beta_3)\alpha_3 + Pd_2^2 < 0$$

$$\Rightarrow F\alpha_3^2 + G\alpha_3 + H < 0 \quad \ldots \quad (2)$$

where,

$$\mathrm{F} = P + Q\beta_3 + R\beta_3^2, \quad G = -(2Pd_2 + Qd_2\beta_3) \text{ and } \quad H = Pd_2^2.$$

So for $\lambda_2 < 0$, α_3 should satisfy the inequality (2).

The other two eigenvalues λ_3 and λ_3 are always negative for all admissible values of α_3.

Thus, for the equilibrium point E_2 to be stable, the drug administration rate α_3 must satisfy the inequalities (1) and (2) together.

For the equilibrium point E_3:

This equilibrium point lies in the *NTI*-plane since, $V_3 = 0$ and

$$N_3 = \frac{r_2 - c_4 T_3}{r_2}, \quad T_3 = \frac{r_1 - c_2 I_3 - c_3 N_3}{r_1 b_1}, \quad I_3 = \frac{s}{d_1 - c_1 T_3}$$

The Jacobian matrix of the system at E_2 is

$$J_{E_3} = \begin{pmatrix} r_2 - 2r_2 N_3 - c_4 \mathrm{T}_3 & -c_4 N_3 & 0 & -a_3 N_3 \\ -\mathrm{c}_3 \mathrm{T}_3 & r_1 - 2\mathrm{r}_1 \mathrm{b}_1 \mathrm{T}_3 - c_2 I_3 - c_3 N_3 & -\mathrm{c}_2 \mathrm{T}_3 & -\mathrm{a}_2 \mathrm{T}_3 \\ 0 & c_1 I_3 & -d_1 + c_1 \mathrm{T}_3 & -\mathrm{a}_1 \mathrm{I}_3 \\ 0 & 0 & 0 & \alpha_3 - d_2 \end{pmatrix}$$

One of the eigen values of the Jacobian matrix at this equilibrium points is found to be

$$\lambda_4 = \alpha_4 - d_2 > 0 \,,$$

which confirms that this equilibrium point is unstable always. Physically, it means that without any drug administration tumor growth cannot be stopped and so cannot be stabilized to a certain size and so it will go on increasing in size.

For the equilibrium point E_4 :

This equilibrium point lies in the *NTIV*-space.

Here,

$$I_4 = \frac{s}{d_1 + a_1 V^* - c_1 T_4}, \quad T_4 = \frac{r_1 - c_2 I_4 - c_3 N_4 - a_2 V^*}{r_1 b_1}, \quad N_4 = \frac{r_2 - c_4 T_4 - a_3 V^*}{r_2},$$

$$V_4 = \frac{\alpha_3 - d_2}{\alpha_3 \beta_3} = V^* .$$

The Jacobian matrix of the system at E_4 becomes,

$$J_{E_4} = \begin{pmatrix} A & -c_4N_4 & 0 & -a_3N_4 \\ -c_3T_4 & B & -c_2T_4 & -a_2T_4 \\ 0 & c_1I_4 & C & -a_1I_4 \\ 0 & 0 & 0 & D \end{pmatrix}$$

Let, $A = r_2 - 2r_2N_4 - c_4T_4 - a_3V^*$, $B = r_1 - 2r_1b_1T_4 - c_2I_4 - c_3N_4 - a_2V^*$

$C = -d_1 + c_1T_4 - a_1V^*$, $D = \alpha_3 - 2\alpha_3\beta_3V^* - d_2$

The characteristic equation of J_{E4} is

$$(D-\lambda)[(A-\lambda)(B-\lambda)(C-\lambda) + c_1c_2(A-\lambda)T_4I_4 + c_3c_4(C-\lambda)N_4T_4] = 0.$$

One of the eigen value is,

$$\lambda = D \text{ i.e. } \lambda = \alpha_3 - 2\alpha_3\beta_3\left(\frac{\alpha_3 - d_2}{\alpha_3\beta_3}\right) - d_2 = -\alpha_1 + d_1 < 0.$$

The other eigen values are derived from the equation,

$$(A-\lambda)(B-\lambda)(C-\lambda) + c_1c_2(A-\lambda)T_4I_4 + c_3c_4(C-\lambda)N_4T_4 = 0$$

$$\Rightarrow \lambda^3 + \{-(A+B+C)\}\lambda^2 + \{(AB+BC+CA) + c_3c_4N_4T_4 + c_1c_2T_4I_4\}\lambda + (c_3c_4CN_4T_4 - c_1c_2T_4I_4A - ABC) = 0$$

$$\Rightarrow \lambda^3 + X\lambda^2 + Y\lambda + Z = 0.$$

By Routh-Hurwitz stability criteria[14], E_4 is stable when

$$X > 0,\ Z > 0 \text{ and } XZ > Y$$

Now,

$$X > 0 \Rightarrow -(A+B+C) > 0$$

$$\Rightarrow 2r_2N_4 + c_4T_4 + a_3V^* + 2r_1b_1T_4 + c_2I_4 + c_3N_4 + a_2V^* + d_1 + a_1V^* > r_1 + r_2 + c_1T_4 \quad Z > 0 \quad \ldots \quad (3)$$

$$\Rightarrow c_3c_4CN_4T_4 - c_1c_2T_4I_4A - ABC > 0 \text{ and } XZ > Y \quad \ldots \quad (4)$$

$$\Rightarrow \{-(A+B+C)\}(c_3c_4CN_4T_4 - c_1c_2T_4I_4A - ABC) > \{(AB+BC+CA) + c_3c_4N_4T_4 + c_1c_2T_4I_4\} \quad \ldots \quad (5)$$

Thus, E_4 will be locally stable if conditions (3), (4) and (5) are satisfied simultaneously.

5. Global stability analysis of the tumor free equilibrium point E_2

In 2001, A. Rantzer in his paper "A dual to Lyapunov's stability theorm" introduced the concept of global stability and its analysis through Lyapunov Method that has opened a new research direction in nonlinear differential equations analysis. To study the condition of global stability for steady states of non-linear differential equations two well known methods are used. One technique is Bendixson-Dulac's criterion and the other technique is Lyapunov method[20]. But Bendixson-Dulac's criteria has the limitation that it can only be used in the two dimensional systems. But the Lyapunov second method is a powerful technique for multidimensional system.

The principle advantage of Lyapunov's method is the fact that it does not require the knowledge of solutions of the nonlinear differential equation. However, the method requires an auxiliary function called Lyapunov function that is difficult to construct. The second Lyapunov method is a powerful technique for multidimensional systems. There is no systematic method for constructing Lyapunov function for mathematical models. On the other hand the Lyapunov functions for a given system are not unique. It turns out that Lyapunov functions can always be found for any stable system and hence if a system is stable, a Lyapunov function exists and vice versa.

***Lyapunov stability theorem*:** Let E be an open subset of R^4 containing an isolated equilibrium point x_0. Suppose that f is continuously differentiable and then E a continuous differentiable function, say (x), which satisfy the following conditions :

(i) $W(x_0) = 0$

(ii) $W(x) > 0,$ if $x \neq x_o$ where $x \in E$

Then

(i) If $\dot{W}(x) \leq 0$ $\forall\, x \in E, x_0$ is stable.

(ii) If $\dot{W}(x) < 0$ $\forall\, x \in E, x_0$ is asymptotically stable.

(iii) If $\dot{W}(x) > 0$ $\forall\, x \in E, x_0$ is unstable.

In our model the main objective is to make the tumor free equilibrium point globally stable which means the total eradication of the tumor cells. We tried to achieve this goal by the Lyapunov second method. The only tumor free equilibrium point for our model which is locally stable is $E_2\ (N_2, 0, I_2, V_2)$.

We consider the function defined by

$$W = \left(\frac{N - N_2}{N_2}\right)^2 + \left(\frac{I - I_2}{I_2}\right)^2 + \left(\frac{V - V_2}{V_2}\right)^2 + (T - T_2)^2$$

Evidently, $(E_2) = 0$ and $W(E) > 0 \; \forall \; E \neq E_2$ in the *NIVT*-plane containing the equilibrium point E_2. So, it is a Lyapunov function.

Now,

$$\dot{W} = \frac{2}{N_2^2}(N - N_2)\dot{N} + \frac{2}{I_2^2}(I - I_2)\dot{I} + \frac{2}{V_2^2}(V - V_2)\dot{V} + 2(T - T_2)\dot{T}$$

$$= \frac{2}{N_2^2}(N - N_2)\{r_2 N(1 - N) - c_4 TN - a_3 VN\} + \frac{2}{I_2^2}(I - I_2)(s + c_1 IT - d_1 I - a_1 VI)$$

$$+ \frac{2}{V_2^2}(V - V_2)(\alpha_3 V(1 - \beta_3 V) - d_2 V) + 2(T - T_2)\{r_1 T(1 - b_1 T) - c_2 IT - c_3 TN - a_2 VT\} \quad \ldots \quad (6)$$

Since, at the equilibrium point E_2, $\frac{dN}{dt} = \frac{dI}{dt} = \frac{dV}{dt} = 0$ and $T = 0$

So,

$$r_2 N_2(1 - N_2) - c_4 T_2 N_2 - a_3 N_2 V_2 = 0;$$

$$s + c_1 I_2 T_2 - d_1 I_2 - a_1 I_2 V_2 = 0; \; \alpha_3 V_2(1 - \beta_3 V_2) - d_2 V_2 = 0;$$

$$r_1 T_2(1 - b_1 T_2) - c_2 I_2 T_2 - c_3 N_2 T_2 - a_2 V_2 T_2 = 0$$

Incorporating the above terms in (6), we get

$$\dot{W} = \frac{2}{N_2^2}(N - N_2)^2\{r_2 - r_2(N + N_2) - c_4 T - a_3 V\} + (N - N_2)(I - I_2).$$

$$0 - \frac{2a_3}{N_2}(N - N_2)(V - V_2) - \frac{2c_4}{N_2}(N - N_2)(T - T_2)$$

$$+ \frac{2}{I_2^2}(I - I_2)^2\{-(d_1 - c_1 T + a_1 V)\} + (N - N_2)(I - I_2).$$

$$0 + \frac{2c_1}{I_2}(I - I_2)(T - T_2) + \frac{2}{I_2}(-a_1)(I - I_2)(V - V_2) + \frac{2}{V_2^2}(V - V_2)^2$$

$$\times\{\alpha_3 - \alpha_3\beta_3(V + V_2) - d_2\} + 2(T - T_2)^2\{r_1 - r_1 b_1(T + T_2)$$

$$- c_2 I - c_3 N - a_2 V\} = -X^T,$$

where $X^T = (N–N_2, I–I_2, V–V_2, T–T_2)$ and A is a symmetric matrix given by

$$\begin{pmatrix} \frac{2}{N_2^2}\{-r_2 + r_2(N+N_2) + c_4T + a_3V\} & 0 & \frac{a_3}{N_2} & \frac{c_4}{N_2} \\ 0 & \frac{2}{I_2^2}(d_1 - c_1T + a_1V) & \frac{a_1}{I_2} & -\frac{c_1}{I_2} \\ \frac{a_3}{N_2} & \frac{a_1}{I_2} & \frac{2}{V_2^2}\{-\alpha_3 + \alpha_3\beta_3(V+V_2) + d_2\} & 0 \\ \frac{c_4}{N_2} & -\frac{c_1}{I_2} & 0 & 2\{-r_1 + r_1b_1(T+T_2) + c_2I + c_3N + a_2V\} \end{pmatrix}$$

$$= \begin{pmatrix} a_{11} & 0 & a_{13} & a_{14} \\ 0 & a_{22} & a_{23} & a_{24} \\ a_{31} & a_{32} & a_{33} & 0 \\ a_{41} & a_{42} & 0 & a_{44} \end{pmatrix}$$

$$\Rightarrow \dot{W} < 0,$$

if the matrix A is positive definite *i.e*. if all the principal minors of A are positive.

Now, the first principal minor

$$M_1 = |a_{11}| = \frac{2}{N_2^2}\{-r_2 + r_2(N+N_2) + c_4T + a_3V\} > 0$$

only if $-r_2 + r_2(N+N_2) + c_4T + a_3V > 0$

$$\Rightarrow -r_2 + r_2\left(1 + \frac{r_2 - a_3V^*}{r_2}\right) + c_4.\frac{1}{b_1} + a_3.\frac{1}{\beta_3} > 0$$

[Since, $0 \le N \le 1, 0 \le T \le \frac{1}{b_1}$ and $0 \le V \le \frac{1}{\beta_3}$ and $^s/_{d_1} \le I \le 1$]

$$\Rightarrow \alpha_3 > \frac{-a_3d_2}{(r_2 + \frac{c_4}{b_1})\beta_3}, \text{ which always holds.} \qquad \ldots \quad (7)$$

Therefore, $M_1 > 0$

Again, for the second principal minor, $M_2 = \begin{vmatrix} a_{11} & 0 \\ 0 & a_{22} \end{vmatrix} > 0$ holds if

$a_{11}a_{22} > 0 \Rightarrow a_{11} > 0$ [if, $a_{22} = \frac{2}{I_2^2}(d_1 - c_1T + a_1V) > 0$]

$\Rightarrow \alpha_3 > \frac{-a_3d_2}{(r_2 + \frac{c_4}{b_1})\beta_3}$, which is the same condition as mentioned in (7)

and $a_{22} > 0 \; if \;\; d_1 + a_1.\frac{1}{\beta_3} > c_1.\frac{1}{b_1}$ … (8)

Therefore, $M_2 > 0$ if $\frac{1}{\beta_3} > \frac{a_1 b_1}{c_1 - b_1 \, d_1}$ holds in the system else the equilibrium point E_2 can not be globally stabilized whatever range we take for the rate of drug administration.

The third principal minor $M_3 = \begin{vmatrix} a_{11} & 0 & a_{13} \\ 0 & a_{22} & a_{23} \\ a_{31} & a_{32} & a_{33} \end{vmatrix} = a_{11}(a_{22}a_{33} - a_{23}^2) - a_{13}^2 a_{22} > 0$

If $a_{11}a_{22}a_{33} - (a_{11}a_{23}^2 + a_{22}a_{13}^2) > 0$

$$=> a_{11}[\frac{a_{22}a_{33}}{2} - a_{23}^2] + a_{22}[\frac{a_{11}a_{33}}{2} - a_{13}^2] > 0.$$

This can happen when $\frac{a_{22}a_{33}}{2} - a_{23}^2 > 0$ and $\frac{a_{11}a_{33}}{2} - a_{13}^2 > 0$

Now,

$$\frac{a_{22}a_{33}}{2} - a_{23}^2 > 0$$

$$=>\frac{2}{I_2^2}(d_1 - c_1 T + a_1 V)\frac{2}{V_2^2}\alpha_3\beta_3 V - 2\left(\frac{a_1}{I_2}\right)^2 > 0$$

$$=> \Delta_1\alpha_3^3 - \Delta_2\alpha_3^2 + \Delta_3\alpha_3 - \Delta_4 > 0 \quad \text{… (9)}$$

where, $\Delta_1 = 2(d_1\beta_3 + a_1)\beta_3$, $\Delta_2 = a_1^2$, $\Delta_3 = 2a_1^2 d_2$ and $\Delta_4 = a_1^2 d_2^2$

Again,

$$\frac{a_{11}a_{33}}{2} - a_{13}^2 > 0$$

$$=>\frac{2}{N_2^2}\{-r_2 + r_2(N + N_2) + c_4 T + a_3 V\}\frac{2}{V_2^2}\alpha_3\beta_3 V - 2\left(\frac{a_3}{N_2}\right)^2 > 0$$

$$=> \Delta_1'\alpha_3^3 + \Delta_2'\alpha_3^2 + \Delta_3'\alpha_3 - \Delta_4' > 0 \quad \text{… (10)}$$

where, $\Delta_1' = 2(r_2 + \frac{c_4}{b_1})\beta_3^2$, $\Delta_2' = 2a_3 d_2\beta_3 - a_3^2$, $\Delta_3' = 2a_3^2 d_2$, $\Delta_4' = a_3^2 d_2^2$.

Therefore, $M_3 > 0$ if condition (9) and (10) together are satisfied by the rate of drug administration α_3.

Lastly, the fourth principal minor $M_4 = \begin{vmatrix} a_{11} & 0 & a_{13} & a_{14} \\ 0 & a_{22} & a_{23} & a_{24} \\ a_{31} & a_{32} & a_{33} & 0 \\ a_{41} & a_{42} & 0 & a_{44} \end{vmatrix} > 0$ if

$$=> \frac{16}{V_2^2}\left(r_2 + \frac{a_3 d_2}{\alpha_3 \beta_3} + c_4 \frac{1}{b_1}\right)\left(d_1 + a_1 \frac{1}{\beta_3}\right)\alpha_3 \left(c_2 + c_3 + a_2 \frac{1}{\beta_3}\right)$$

$$- 4a_1^2 \left(r_2 + \frac{a_3 d_2}{\alpha_3 \beta_3} + c_4 \frac{1}{b_1}\right)\left(-r_1 + c_2 \times \frac{s}{d_1}\right) + 4a_3^2 \left(d_1 - c_1 \frac{1}{b_1}\right)\left(c_2 + c_3 + a_2 \frac{1}{\beta_3}\right)$$

$$- \frac{4c_4^2}{V_2^2}\alpha_3 \left(d_1 - c_1 \frac{1}{b_1}\right) + 2a_1 a_3 c_1 c_4 + a_3^2 c_1^2 + a_1^2 c_4^2 > 0. \quad \ldots \quad (11)$$

Therefore, $M_4 > 0$ if condition (11) is satisfied by the rate of drug administration α_3.

So the matrix A is positive definite if α_3 satisfy the inequalities (8), (9), (10) and (11) simultaneously.

Thus, the equilibrium point E_2 satisfies all the conditions of Lyapunov stability theorem with the restriction for α_3 given by (8), (9), (10) and (11) *i.e.* for the tumor free equilibrium point E_2 to be globally asymptotically stable, we must restrict the intrinsic rate of drug administration α_3 by the condition (1), (8) and (9) simultaneously.

6. Numerical simulation

In this section, we present a long term dynamical behaviour of the tumor cells, immune cells and normal cells. Following 1(a) and 1(b) are the plots of number of normal cells and tumor cells Vs. time respectively for the parameter values within the range for the global stability of the tumor free equilibrium point E_2.

The plots clearly shows the stability of the equilibrium point E_2. The parameter value we chose to plot the graph are :

s = 0.05, c_1 = 0.2,$_1$ = 0.2,$_1$ = 0.2, r_1 = 0.4, r_2 = 0.35, b_1 = 1.5,

c_2 = 0.3, c_3 = 0.2, c_4 = 0.25, a_2 = 0.5, a_3 = 0.25, d_2 = 0.05

and the initial points are taken as $N(0)$ = 0.9, $T(0)$ = 10^{-5}, $I(0)$ = 0.25, $V(0)$ = 10^{-5}

Further, we considered β_3 = 0.7 and α_3 = 0.075

(For the above considered parameter values the range for α_3 is $0.05 \leq \alpha_3 \leq 2.5$)

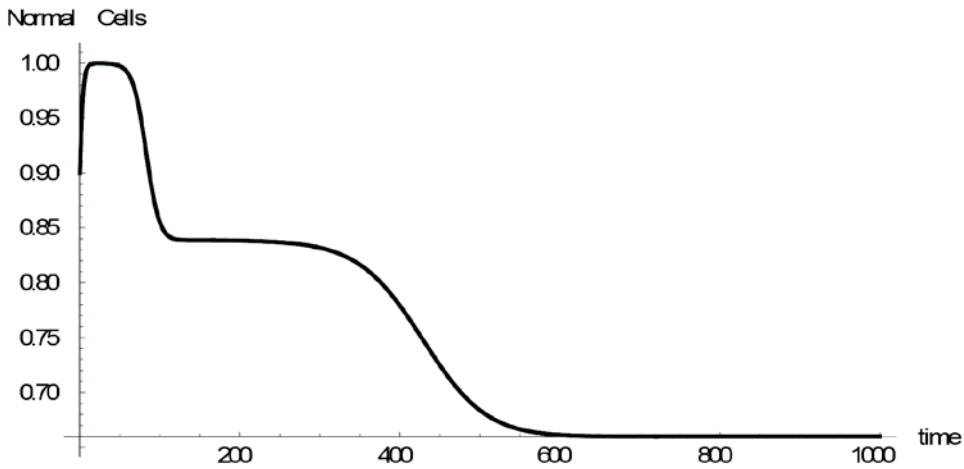

Fig 1(*a*)
Number of Normal Cells Vs. Time.

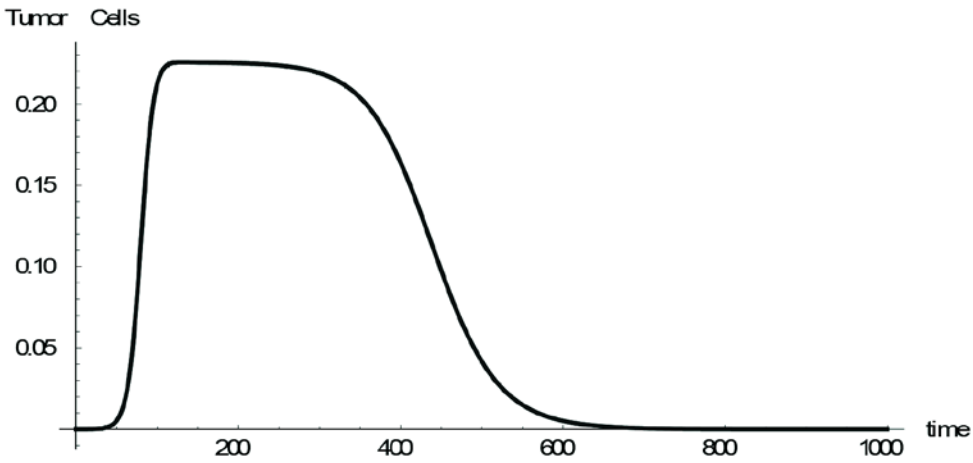

Fig. 1(*b*)
Number of Tumor Cells Vs. Time.

From the figure1(*b*) it is seen that there is a decay in the tumor size and after some time the tumor size stabilizes to zero volume whereas the no. of normal cells stabilizes to the 65 percent (approximately) of the body cell population.

The vector field plot along with four trajectories and the equilibrium point E_2 (with the same set of parameter values taken in fig 1) is shown below :

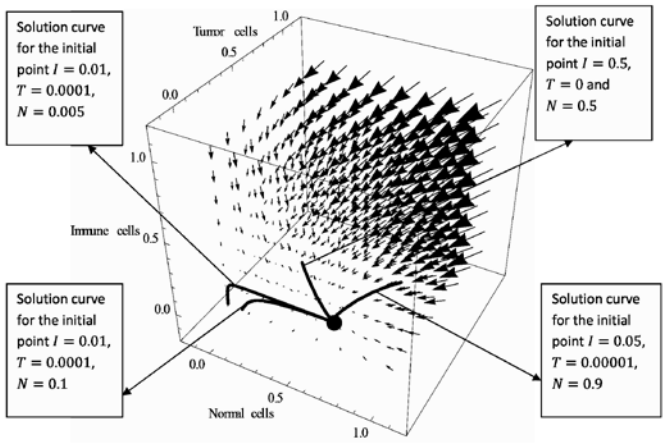

Fig. 2

From the vector field plot (Fig. 2) we see that any trajectory starting from any initial point within the basin of attraction converges to the equilibrium point E_2 (represented by the large black dot). This represents the fact that the body will recover from the tumor whatever be the initial conditions.

7. Conclusion

In this paper we analyzed the local stability of the equilibrium points. Global stability analysis of the locally stable tumor free equilibrium point was carried out by constructing a Lyapunov function and a range was determined for drug administration rate to see that the tumor size can be reduced to zero if we adopt a proper control policy. Numerical verification of our results has also been carried out through some diagrams.

References

1 Devi, Anuradha and Ghosh, Aditya − Some Control Policies for Control of Cancer, Nonlinear analysis and differential equations, **Vol. 4**, No.1, 27-41(2016).

2. Novozhilov, A. S., Benezovskaya, F.S. and Koonin, E.V. et.al. − Mathematical modeling of tumour therapy with oncolytic viruses: Regimes with complete tumour elimination within the framework of deterministic models. Biology Direct, (2006).

3. Dibrov, B. F., Zhabotinsky, A. M., Neyfakh, Y. A., Orlova, M.P. and Churikova, L.I. − Mathematical model of cancer chemotherapy. Periodic schedules of phase-specific

cytotoxic-agent administration increasing the selectivity of therapy. Mathematical Bioscience, An International Journal, **73,** No. 1, 1-31 (1985).

4. Kirschner, D. − On the global dynamics of a model for tumor immunotherapy, Mathematical bioscience and Engineering, **6** (2009).
5. Kirschner, D. and Panetta, J. − Modeling immune therapy of the tumor-immune interaction, Journal of Mathematical Biology, **37(3) ,** 235–252 (1998).
6. Shochat, E., Hart, D. and Agur, Z. − Using computer simulations for evaluating the efficacy of breast cancer chemotherapy protocols, Mathematical models and Methods in Applied Science, **9**, No. 4, 599-615 (1999).
7. Frascoli, Federico, Peter S. Kim, Hughes, Barry D. and Landman, Kerry A. − A dynamical model of tumor immunotherapy, Mathematical Bioscience, **253**, 50-62 (2014).
8. Narula, Gurpreet Kaur − A study of population dynamics of tumor cells in the presence of Normal and Immune cells, International Journal of Scientific Engineering research, **Vol. 4**, Issue 4, April, ISSN 2229-5518 (2013).
9. Adam , J.A. − The dynamics growth- factor - modified immune response to cancer growth: One dimensional models, Mathematical and Computer Modelling, **17(3)**, 83-106 (1993).
10. Adam , J. A. and Panetta, J. − A simple mathematical model and alternative paradigm for certain chemotherapeutic regimens, Mathematical and computer Modelling, **22(8)**, 49-60 (1995).
11. de Pillis , L. G. and Radunskaya, A. − A mathematical tumor model with immune resistance and drug therapy: an optimal control approach, Journal of Theoretical Medicine, **3**, 79-100 (2001).
12. de Pillis, L.G. and Radunskaya, A.E. − The Dynamics of Optimally Controlled Tumor Model, A Case Study,Mathematical and Computer Modelling **37**, 1221-1244 (2003).
13. Eisen, M. − Mathematical models in cell Biology and cancer chemotherapy, Spinger-Verlag, Berlin (1979).
14. Gopal, M. − Control systems: Principles and Design, Tata McGraw-Hill Education, 2nd Ed. (2002).
15. Owen, M. and Sherratt, J. − Modeling the macrophage invasion of tumours: Effects on growth and composition, IMA Journal of Mathematics Applied in Medicine and Biology, **15**, 165-185 (1998).
16. Martin, R. B. − optimal control drug scheduling of cancer chemotherapy. Automatica, The journal of IFAC, the International Federation of Automatic Control, **28(6)**, 1113-1123 (1992).

17. Martin, R. B., Fisher, M. E., Minchin, R. F. and Teo, K. L. − A mathematical model of cancer chemotherapy with an optimal selection of parameters, Mathematical Biosciences, An International Journal, **99(2)**, 205-230 (1990).
18. Paul, Ranu − Stability analysis of critical points to control growth of tumor in an Immune-Tumor-Normal cell-Drug model, International Journal of Applied Mathematics & Statistical Sciences, **Vol 5**, 43-52 (2016).
19. Wilson, S. and Levy, D. − A mathematical model of the enhancement of tumor vaccine efficacy by immune therapy, Bulletin of mathematical biology, **74**, 1485-1500 (2012).
20. Lynch Stephen − Dynamical Systems with Applications using Mathematica, Birkhäuser, (2007).
21. Kuznetsov, V., Makalkin, I., Taylor, M. and Perelson, A. − Nonlinear dynamics of immunogenic tumurs: parameter estimation and global bifurcation analysis, Bull, of Math. Bio., **56(2)**, 295-321 (1994).

INDIAN JOURNAL OF THEORETICAL PHYSICS, VOL. 65, NOS. 3 & 4, 2017

Oscillatory Bingham plastic flow between two confocal elliptic cylinders

Anup Kumar Karak

Asst. Professor of Mathematics, Berhampore Girls' College,
Berhampore -742101, India
e-mail: karak_anup@yahoo.in

[Abstract : The present investigation deals with the oscillatory flow of Bingham plastic fluid between two confocal elliptic cylinders. The inner cylinder is assumed to be at rest and the flow is caused by the rotation of the outer one. By transforming the confocal ellipses in the z-plane ($z = x + iy$) conformally to concentric circles in the non-dimensional ζ - plane ($\zeta = \xi + i\eta$), the problem has been solved by the use of perturbation technique. The approximate velocity distribution has been calculated and the results are presented in graphical form.]

1. Introduction

During the past several decades, rheology and continuum mechanics have bean emphasised for one–phase materials, specially to polimer solutions and polymer melts[1]. Surprisingly, less attention has been made to materials such as slurries, pastes, suspension etc. which are encountered in industrial problems. Many of these materials have a yield stress and a critical value below which they do not deform and above which deformation and flow arise according to different constitutive relations; these are called viscoplastic materials. Viscoplastic models include the Bingham plastic, Herschel-Bulkley, Casson etc. However, all these models are discontinuous and analytical solutions are difficult to obtain except for some simple cases. It may be mentioned that Bingham[2] was the first to describe such types of flows in this way.

The flow of yield stress is encountered in many situations of engineering, industrial and geophysical aspects. For instance, mud and slurries are dealt with not only in off-shore construction, but also in mining and agro –and food–industries (*e.g.* fertilisers, margarine, mayonnaise, ketchup etc). In such cases, a minimum stress is to be applied to the material to start

flowing. As for example, we have the yield stress material like fresh concrete whose rheological properties are important[3,4,5]. Also, lahars resulting from rainfalls in volcanic areas show similar behavior[6,7]. Such properties are also manifested in the slow failure of muddy soils.

Despite the apparent diversity, these materials, to a first approximation, can be described as Bingham plastics in a good number of situations. At low stress, they behave like solids and at high stress they flow like viscous fluids. In its simplified form, a yield stress and a viscosity define them nearly completely.

Extensive theoretical works on the slumping of viscoplastic material were achieved mostly in the framework of longwave approximation[8, 9, 10]. Using limit analysis, predictions have been made for yield stress material in the problems of cylinders and rectangles for incipient failure conditions[11]. However the complex interplay of geometry and rheology in the gravity flow of Bingham materials still needs clarification. As high values of the yield stress imply small lateral deformation, so, in general, it is often assumed that plastic viscosity plays no role in the slumping system[12, 13]. Yet, for low field stress, shear deformation and viscous stresses are likely to be important to the overall deformation. Also the specific role of the plastic viscosity may depend on the initial geometry of the system.

In the present investigation, it is our aim to consider the oscillatory flow of Bingham plastic fluid between two confocal elliptic cylinders, the inner surface of which is at rest while the flow is caused by the rotation of the outer one. Using conformal transformation, the confocal ellipses are reduced to concentric circles and then the problem is solved by perturbation technique. The approximate velocity distribution is shown in graphical form.

2. Fundamental equations

The rheological equations of state are[2]:

$$\begin{aligned} p'_{ii} &= 3ke \ (\text{in elastic regions}, \tfrac{1}{2}\, p'_{ij} p'_{ij} \le \nu^2) \\ p'_{ij} &= 2\mu e'_{ij} \ (\text{in elastic regions}, \tfrac{1}{2}\, p'_{ij} p'_{ij} \le \nu^2) \\ p'_{ij} &= 2\eta e'_{ij} \ (\text{in flow regions}, \tfrac{1}{2}\, p'_{ij} p'_{ij} \ge \nu^2) \end{aligned} \qquad \dots \quad (1)$$

with $\eta = \eta_1 + \nu(2e'_{il}e'_{il})^{-\frac{1}{2}}$.

In the above, η_1 is the reciprocal of mobility, v is the constant yield value, μ is the constant rigidity modulus in the elastic, k (non necessarily constant) is the bulk modulus, e'_{ij} is the rate of strain tensor, p'_{ij} is the stress tensor, $e = e_{ii}$ is the dilatation and e_{ij} is the strain tensor. The prime denotes deviatoric components of tensor.

Since we are non concerned with elastic deformation, so the elastic region is treated as rigid. The transition conditions to be satisfied on the yield surface are : (*i*) the velocity must be continuous and (*ii*) the rate of strain tensor e'_{ij} must vanish.

The equations of motion are

$$\frac{\partial p'_{ij}}{\partial x_j} + \frac{\partial p'_{ij}}{\partial x_j} + X_i = \rho \frac{\partial w_i}{\partial t}, \qquad \ldots \quad (2)$$

X_i being the body force, w_i the velocity components and ρ the density.

3. The problem

Let us consider the unsteady flow of Bingham plastic between two confocal elliptic cylinders. The inner cylinder is assumed to be at rest while the flow is caused by the rotation of the outer one. The distance between the foci of the elliptic section is taken as *d*. The plastic flows axially parallel to the generator of the cylinders and the pressure gradient is assumed to be zero. The velocity components are taken as $\{0, 0, W(x, y, z, t)\}$ referred to Cartesian set of axes and time *t*.

The boundary conditions are:

$W = 0$ at the inner cylinder,

$W = W_0 f(t)$ at the outer cylinder, $\qquad \ldots \quad (3)$

where W_0 is constant and *f*(*t*) is a function of *t*.

4. Solutions

We have only two non-zero components of e'_{ij} given by

$$e'_{xz} = \frac{1}{2}\frac{\partial W}{\partial x} \text{ and } e'_{yz} = \frac{1}{2}\frac{\partial W}{\partial y} \qquad \ldots \quad (4)$$

Hence the equation (2) gives

$$\frac{\partial}{\partial x}\left(\eta \frac{\partial W}{\partial x}\right) + \frac{\partial W}{\partial y}\left(\eta \frac{\partial W}{\partial y}\right) = \frac{\partial W}{\partial t}, \qquad \ldots \quad (5)$$

where

$$\eta = \eta_1 + \nu\left\{\left(\frac{\partial W}{\partial x}\right)^2 + \left(\frac{\partial W}{\partial y}\right)^2\right\}^{-\frac{1}{2}}. \quad \ldots \quad (6)$$

Transforming equations (5) and (6) into conjugate complex variables $z = x + iy$ and $\bar{z} = x - iy$,

we get

$$\frac{\partial}{\partial z}\left(\eta\frac{\partial W}{\partial z}\right) + \frac{\partial W}{\partial \bar{z}}\left(\eta\frac{\partial W}{\partial \bar{z}}\right) = \frac{1}{2}\rho\frac{\partial W}{\partial t}, \quad \ldots \quad (7)$$

with

$$\eta = \eta_1 + 2\nu\left\{\frac{\partial W}{\partial z}\frac{\partial W}{\partial \bar{z}}\right\}^{-\frac{1}{2}}. \quad \ldots \quad (8)$$

Substituting (8) into (7) and rearranging we get

$$4\eta_1\frac{\partial^2 W}{\partial z\partial\bar{z}} + \nu\left[\frac{\partial}{\partial z}\left\{\frac{\partial W}{\partial \bar{z}}\left(\frac{\partial W}{\partial z}\frac{\partial W}{\partial \bar{z}}\right)^{-\frac{1}{2}}\right\} + \frac{\partial}{\partial \bar{z}}\left\{\frac{\partial W}{\partial \bar{z}}\left(\frac{\partial W}{\partial z}\frac{\partial W}{\partial \bar{z}}\right)^{-\frac{1}{2}}\right\}\right] = \frac{\partial W}{\partial t}. \ldots \quad (9)$$

Now the confocal ellipses in the z-plane may be transformed conformally to the concentric circles of dimensionless radii a and b ($1<a<b$) in the non-dimensional ζ - plane by the transformation

$$z = \frac{d}{4}\left(\zeta + \frac{1}{\zeta}\right), \quad \bar{z} = \frac{d}{4}\left(\bar{\zeta} + \frac{1}{\bar{\zeta}}\right) \quad \ldots \quad (10)$$

where $\zeta = re^{i\theta}$ and $\bar{\zeta} = re^{-i\theta}$.

The distance d between the foci of the elliptic sections may be taken as the typical distance in the z-plane to define the dimensionless number $\sigma = \frac{\nu d}{\eta_1 W_o}$.

Using (10), the equation (9) is transformed to

$$\frac{1}{W_o}\frac{\partial^2 W}{\partial\zeta\partial\bar{\zeta}} - \frac{\kappa}{W_o}\left(1 - \frac{1}{\zeta^2}\right)\left(1 - \frac{1}{\bar{\zeta}^2}\right)\frac{\partial W}{\partial\zeta} = -\frac{\sigma}{16}\frac{\partial}{\partial\zeta}\left[\frac{\partial W}{\partial\bar{\zeta}}\left\{\frac{\left(1-\frac{1}{\zeta^2}\right)\left(1-\frac{1}{\bar{\zeta}^2}\right)}{\frac{\partial W}{\partial\zeta}\frac{\partial W}{\partial\bar{\zeta}}}\right\}^{\frac{1}{2}}\right]$$

$$+ \text{Complex conjugate expression} \quad \ldots \quad (11)$$

where $\kappa = \frac{\rho d^2}{16\eta_1}$, a constant quantity.

The equation (10) is to be solved subject to the boundary conditions

$$\left.\begin{aligned} & W = 0 && \text{when } |\zeta| = a \\ \text{and} \quad & W = \bar{W}_0 e^{\frac{i\lambda t}{\kappa}} && \text{when } |\zeta| = b \end{aligned}\right\} \quad \ldots \quad (12)$$

We now assume σ to be sufficiently small for convergence so that a solution of (11) can be developed with successive approximations for W equal to partial sum of the series

$$W = \bar{W}_0 (W_o + \sigma W_1 + \sigma^2 W_2 + \ldots\ldots) \quad \ldots \quad (13)$$

Substituting this into (11) and equating different powers of σ from both sides, we get the following differential equations for W_o, W_1, ...

$$\frac{\partial^2 W_o}{\partial\zeta\partial\bar{\zeta}} - \kappa\left(1-\frac{1}{\zeta^2}\right)\left(1-\frac{1}{\bar{\zeta}^2}\right)\frac{\partial W_o}{\partial\zeta} = 0, , \quad \ldots \quad (14)$$

$$\frac{\partial^2 W_1}{\partial\zeta\partial\bar{\zeta}} - \kappa\left(1-\frac{1}{\zeta^2}\right)\left(1-\frac{1}{\bar{\zeta}^2}\right)\frac{\partial W_1}{\partial\zeta} = -\frac{1}{16}\frac{\partial}{\partial\zeta}\left[\frac{\partial W_o}{\partial\bar{\zeta}}\left\{\frac{\left(1-\frac{1}{\zeta^2}\right)\left(1-\frac{1}{\bar{\zeta}^2}\right)}{\frac{\partial W_o}{\partial\zeta}\,\frac{\partial W_o}{\partial\bar{\zeta}}}\right\}^{\frac{1}{2}}\right]$$

$$+ \text{ Complex conjugate expression} \quad \ldots. \quad (15)$$

For each approximation to W, the boundary conditions are as follows:

$$\left.\begin{aligned} & W_o = 0, && W_n = 0\ (n \geq 1) \text{ on } |\zeta| = a; \\ \text{and} \quad & W_o = e^{\frac{i\lambda t}{\kappa}}, && W_n = 0\ (n \geq 1) \text{ on } |\zeta| = b. \end{aligned}\right\} \quad \ldots \quad (16)$$

Again to solve the equations (14) and (15) we assume that the parameter λ is small and $0 < \lambda < 1$. Then we may take

$$W_o(\zeta, \bar{\zeta}, t) = [W_{00}(\zeta, \bar{\zeta}) + \lambda W_{01}(\zeta, \bar{\zeta}) + \ldots.] e^{\frac{i\lambda t}{\kappa}} \quad \ldots \quad (17)$$

so that Eq. (14) gives by equating powers of λ

$$\left.\begin{aligned} & \frac{\partial^2 W_{oo}}{\partial\zeta\partial\bar{\zeta}} = 0, \\ & \frac{\partial^2 W_{o1}}{\partial\zeta\partial\bar{\zeta}} - \left(1-\frac{1}{\zeta^2}\right)\left(1-\frac{1}{\bar{\zeta}^2}\right) W_{oo} = 0 \end{aligned}\right\} \quad \ldots \quad (18)$$

and the boundary conditions give

$$\left.\begin{aligned} W_{oo} = 0, \quad W_{on} = 0\ (n \geq 1) \text{ on } |\zeta| = \mathrm{a}\,; \\ \text{and} \quad W_{oo} = 1 \quad W_{on} = 0\ (n \geq 1) \text{ on } |\zeta| = \mathrm{b}. \end{aligned}\right\} \quad \ldots \quad (19)$$

Solutions of the equations (18) subject to (19) are

$$W_{oo} = \frac{1}{2L} \log\left(\frac{\zeta\bar{\zeta}}{a^2}\right), \quad \ldots \quad (20)$$

$$W_{o1} = \frac{1}{2L}\left[\log\left(\frac{\zeta\bar{\zeta}}{a^2}\right).\left(\zeta\bar{\zeta} + \frac{1}{\zeta\bar{\zeta}} + \frac{\bar{\zeta}}{\zeta} + \frac{\zeta}{\bar{\zeta}}\right) - 2\left(\zeta\bar{\zeta} - \frac{1}{\zeta\bar{\zeta}}\right)\right] + \text{harmonic function}$$

$$= \frac{1}{L}\left[\left(r^2 + \frac{1}{r^2}\right) log\left(\frac{r}{a}\right) - \left(r^2 - \frac{1}{r^2}\right) + 2log\left(\frac{r}{a}\right).cos2\theta\right]$$

$$+ \mathrm{A} + \mathrm{B}\ log\ r + \left(\alpha_0 r^2 + \frac{2\beta_0}{r^2}\right)\cos 2\theta \quad \ldots \quad (21)$$

where $\mathrm{L} = log\left(\frac{b}{a}\right)$ and

$$\left.\begin{aligned} A &= \frac{1}{L^2}\left\{\left(a^2 - \frac{1}{a^2}\right)\log b - \left(b^2 - \frac{1}{b^2}\right)\log a + L\left(b^2 + \frac{1}{b^2}\right)\log a\right\}, \\ B &= \frac{1}{L^2}\left\{\left(b^2 - \frac{1}{b^2}\right)\log b - \left(a^2 - \frac{1}{a^2}\right) + L\left(b^2 + \frac{1}{b^2}\right)\right\}, \\ \alpha_0 &= \frac{2b^2}{b^4 - a^4}, \quad \beta_0 = \frac{b^2 a^4}{b^4 - a^4}. \end{aligned}\right\}$$

$$\ldots \quad (22)$$

Thus the expression for W_0 is obtained from Eqs. (17), (19) and (20) as

$$W_0 = e^{\frac{i\lambda t}{\kappa}}\left[\frac{1}{L} log\left(\frac{r}{a}\right) - \frac{i\lambda}{L^2}\left\langle\left\{L\left(b^2 + \frac{1}{b^2}\right) log\left(\frac{r}{a}\right) - L\left(r^2 + \frac{1}{r^2}\right) log\left(\frac{r}{a}\right) + L\left(r^2 - \frac{1}{r^2}\right)\right\}\right.\right.$$

$$\left.\left. + \frac{2L}{b^4 - a^4}\left\{\mathrm{b}^2\left(r^2 - \frac{a^4}{r^2}\right)\mathrm{L} - (b^4 - a^4) log\left(\frac{r}{a}\right)\right\}\cos 2\theta\right\rangle\right] \quad (23)$$

Now to solve the equation (13) by the use of (23), we first note that the right hand side of Eq. (15) becomes independent of time. Hence we assume

$$W_1(\zeta, \bar{\zeta}, t) = W_s(\zeta, \bar{\zeta}) + W_u(\zeta, \bar{\zeta}, t), \quad \ldots \quad (24)$$

where $W_s\ (\zeta\ ,\bar{\zeta})$ and $W_u\ (\zeta\ ,\bar{\zeta},t)$ represent the steady and unsteady parts of W_1 respectively.

Substituting Eq. (24) into Eq. (15) and then equating the steady and unsteady parts, we get

$$\frac{\partial^2 W_s}{\partial\zeta\partial\bar{\zeta}} = -\frac{1}{16}\frac{\partial}{\partial\zeta}\left[\frac{\partial W_0}{\partial\bar{\zeta}}\left\{\frac{\left(1-\frac{1}{\zeta^2}\right)\left(1-\frac{1}{\bar{\zeta}^2}\right)}{\frac{\partial W_0}{\partial\zeta}\frac{\partial W_0}{\partial\bar{\zeta}}}\right\}^{\frac{1}{2}}\right] + \text{Complex conjugate expression} \quad \ldots (25)$$

$$\frac{\partial^2 W_u}{\partial\zeta\partial\bar{\zeta}} = \kappa\left(1-\frac{1}{\zeta^2}\right)\left(1-\frac{1}{\bar{\zeta}^2}\right)\frac{\partial W_u}{\partial t}. \quad \ldots (26)$$

The boundary conditions for W_s and W_u are

$$W_s = W_u = 0 \text{ on } |\zeta| = a, b. \quad \ldots (27)$$

Using (23), we have from (25)

$$\begin{aligned}\frac{\partial^2 W_s}{\partial\zeta\partial\bar{\zeta}} = & -\frac{1}{16}\left[\left\{\frac{\zeta}{\bar{\zeta}}\left(1-\frac{1}{\zeta^2}\right)\left(1-\frac{1}{\bar{\zeta}^2}\right)\right\}^{\frac{1}{2}} - \frac{i\lambda}{L}\left\{2L\left(\frac{\zeta}{\bar{\zeta}}-\frac{\bar{\zeta}}{\zeta}\right)\right.\right.\\ & \times\left(\frac{b^2\zeta\bar{\zeta}}{b^4-a^4}-\frac{b^2a^4}{(b^4-a^4)\zeta\bar{\zeta}}-\frac{1}{2L}\,log\left(\frac{\zeta\bar{\zeta}}{a^2}\right)\right)-\left(b^2+\frac{1}{b^2}\right)-\frac{1}{L}\left(a^2-\frac{1}{a^2}\right)\\ & +\frac{1}{L}\left(b^2-\frac{1}{b^2}\right)+\left(\zeta\bar{\zeta}-\frac{1}{\zeta\bar{\zeta}}\right)\log\left(\frac{\zeta\bar{\zeta}}{a^2}\right)-\left(\zeta\bar{\zeta}+\frac{1}{\zeta\bar{\zeta}}\right)-2\mathrm{L}\left(\frac{\zeta}{\bar{\zeta}}+\frac{\bar{\zeta}}{\zeta}\right)\\ & \left.\left.\times\left(\frac{b^2\zeta\bar{\zeta}}{b^4-a^4}+\frac{b^2a^4}{(b^4-a^4)\zeta\bar{\zeta}}-\frac{1}{2L}\right)\right\}\right] + \text{Complex conjugate expression.}\end{aligned}$$

Integrating we get

$$\begin{aligned}W_s = & -\frac{1}{16}\int^{\bar{\zeta}}\left\{\frac{\zeta}{\bar{\zeta}}\left(1-\frac{1}{\zeta^2}\right)\left(1-\frac{1}{\bar{\zeta}^2}\right)\right\}^{\frac{1}{2}}d\bar{\zeta}+\frac{i\lambda}{16L}\int^{\bar{\zeta}}\left[\left\{2L\left(\frac{\zeta}{\bar{\zeta}}-\frac{\bar{\zeta}}{\zeta}\right)\right.\right.\\ & \times\left(\frac{b^2\zeta\bar{\zeta}}{b^4-a^4}-\frac{b^2a^4}{(b^4-a^4)\zeta\bar{\zeta}}-\frac{1}{2L}\,log\left(\frac{\zeta\bar{\zeta}}{a^2}\right)\right)-\left(b^2+\frac{1}{b^2}\right)-\frac{1}{L}\left(a^2-\frac{1}{a^2}\right)\\ & +\frac{1}{L}\left(b^2-\frac{1}{b^2}\right)+\left(\zeta\bar{\zeta}-\frac{1}{\zeta\bar{\zeta}}\right)\log\left(\frac{\zeta\bar{\zeta}}{a^2}\right)-\left(\zeta\bar{\zeta}+\frac{1}{\zeta\bar{\zeta}}\right)-2\mathrm{L}\left(\frac{\zeta}{\bar{\zeta}}+\frac{\bar{\zeta}}{\zeta}\right)\\ & \left.\left.\times\left(\frac{b^2\zeta\bar{\zeta}}{b^4-a^4}+\frac{b^2a^4}{(b^4-a^4)\zeta\bar{\zeta}}-\frac{1}{2L}\right)\right\}+\left(\frac{\zeta}{\bar{\zeta}}\right)^{\frac{1}{2}}\left\{1-\frac{1}{2}\left(\frac{1}{\zeta^2}+\frac{1}{\bar{\zeta}^2}\right)+\ldots\ldots\right\}\right]d\bar{\zeta}\end{aligned}$$

+ Complex conjugate expression + Harmonic function.

This implies

$$W_s = -\frac{1}{4}r + \frac{1}{48r^2} + \frac{1}{12r}\cos 2\theta + \frac{i\lambda}{16L}\left[-\frac{4r}{L}\left\{\left(b^2 + \frac{1}{b^2}\right)L + \left(a^2 - \frac{1}{a^2} - b^2 + \frac{1}{b^2}\right)\right\} + \frac{8}{3}r^2 \log\frac{r}{a} - \frac{8}{3}\log\frac{r}{a} - \frac{20}{9}r^2 + \frac{r}{4} + 8\left(\frac{5}{9}r - \frac{2L}{3}\frac{b^2a^4}{(b^4-a^4)r} + \frac{4}{3}r\log\frac{r}{a} - \frac{2L}{5}\frac{b^2r^2}{(b^4-a^4)}\right)\cos 2\theta\right] + A_1 + B_1 \log r + \left(\alpha_1 r^2 + \frac{2\beta_1}{r^2}\right)\cos 2\theta \,. \quad \ldots (28)$$

Using boundary conditions (27), we have

$$A_1 = \frac{1}{4L}(a\log b - b\log a) + \frac{1}{48L}\left(\frac{\log a}{b^2} - \frac{\log b}{a^2}\right) + \frac{i\lambda}{4L^2}\left[(a\log b - b\log a) \times \left\{\left(b^2 + \frac{1}{b^2}\right)L + \left(a^2 - \frac{1}{a^2} - b^2 + \frac{1}{b^2}\right)\right\} + \frac{2}{3}b^2L^2\log a + \frac{2}{3}L^2\log a + \frac{5L}{3}(a^3\log b - b^3\log a) - \frac{L}{ab}(b\log b - a\log a)\right.$$

$$B_1 = \frac{1}{4L}(\mathrm{b} - \mathrm{a}) + \frac{1}{48L}\left(\frac{1}{a^3} - \frac{1}{b^3}\right) + \frac{i\lambda}{4L^3}\left[L(b-a)\left(b^2 + \frac{1}{b^2}\right) + \left(a^2 - \frac{1}{a^2} - b^2 + \frac{1}{b^2}\right) - \frac{2}{3}b^3L^2 - \frac{2}{3}L^2 + \frac{5L}{3}(b^2 - a^2) - \frac{(b-a)L}{ab}\right]$$

$$\alpha_1 = -\frac{(b-a)}{12\,(b^4-a^4)} + \frac{i\lambda}{2L}\left\{-\frac{5}{9}\frac{b^3-a^3}{b^4-a^4} + \frac{2}{3}La^4b^2\frac{(b-a)}{(b^4-a^4)^2} + \frac{2}{5}Lb^2\frac{b^5-a^5}{b^4-a^4} - \frac{4}{3}\frac{b^3L}{b^4-a^4}\right\}$$

$$\beta_1 = -\frac{ab}{24}\frac{b^3-a^3}{b^4-a^4} - \frac{i\lambda a^3b^3}{4L}\left\{\frac{5}{9}\frac{b-a}{b^4-a^4} - \frac{2}{3}La^2\frac{b^2-a^2}{(b^4-a^4)^2} + \frac{5}{2}ab^3\frac{(b-a)}{(b^4-a^4)^2} - \frac{4}{3}\frac{aL}{b^4-a^4}\right\}$$

Hence, we have to the first order of λ

$$W_s = \frac{1}{4L}\left(b\log\frac{r}{a} + a\log\frac{b}{r} - r\log\frac{b}{a}\right) - \frac{1}{48a^3b^2L}\left(\mathrm{b}^3\log\frac{b}{a} + \mathrm{a}^3\log\frac{r}{a}\right.$$

$$\left. - \frac{\mathrm{a}^3\mathrm{b}^3}{\mathrm{r}^3}\log\frac{b}{a}\right) - \frac{1}{12(b^4-a^4)}\left\{(b-a)r^2 - \frac{b^4-a^4}{r} + \frac{(b^3-a^3)ab}{r^2}\right\}\cos 2\theta$$

$$+\frac{i\lambda}{4L^3}\left[\left\langle\left\{\left(b^2 + \frac{1}{b^2}\right)\mathrm{L} + \left(a^2 - \frac{1}{a^2} - b^2 + \frac{1}{b^2}\right)\right\}\left(b\log\frac{r}{a} + a\log\frac{b}{r} - r\log\frac{b}{a}\right)\right.\right.$$

$$\left. + \frac{2}{3}L^3(r^3 - b^3)\log\frac{r}{a} + \mathrm{L}\left(\frac{1}{r}\log\frac{b}{a} - \frac{1}{a}\log\frac{b}{r} - \frac{1}{b}\log\frac{r}{a}\right)\right\rangle$$

$$+\left\langle\frac{5}{9}\left\{r - \frac{b^3-a^3}{b^4-a^4}\,r^2 - \frac{\mathrm{a}^3\mathrm{b}^3(\mathrm{b}-\mathrm{a})}{(b^4-a^4)\mathrm{r}^2}\right\} + \frac{4}{3}\left\{r\log\frac{r}{a} - \frac{b^2r^2}{b^4-a^4}\,L + \frac{a^4b^3}{(b^4-a^4)r^2}\,L\right\}\right.$$

$$\left. + \frac{2}{3}\mathrm{a}^4\mathrm{b}^2\mathrm{L}\left\{\frac{r^2(b-a)}{(b^4-a^4)^2} + \frac{ab(b^3-a^3)}{(b^4-a^4)^2r^2} - \frac{1}{(b^4-a^4)r}\right\}\right.$$

$$\left. - \frac{2}{5}b^2L\left\{\frac{r^3}{b^4-a^4} - \frac{(b^5-a^5)r^2}{(b^4-a^4)^2} + \frac{\mathrm{a}^4\mathrm{b}^4(\mathrm{b}-\mathrm{a})}{(b^4-a^4)r^2}\right\}\right\rangle\cos 2\theta\Big] \quad \ldots \quad (29)$$

Again, to solve the equation (26) we assume

$$W_u(\zeta, \bar{\zeta}, t) = [W_{10}(\zeta, \bar{\zeta}) + \lambda W_{11}(\zeta, \bar{\zeta}) + \ldots.]\, e^{\frac{i\lambda t}{\kappa}} \quad \ldots \quad (30)$$

Putting this value in Eq. (26) and then equating different powers of λ, we get

$$\frac{\partial^2 W_{10}}{\partial\zeta\partial\bar{\zeta}} = 0, \quad \ldots \quad (31)$$

$$\frac{\partial^2 W_{11}}{\partial\zeta\partial\bar{\zeta}} - i\left(1 - \frac{1}{\zeta^2}\right)\left(1 - \frac{1}{\bar{\zeta}^2}\right)W_{10} = 0, \quad \ldots \quad (32)$$

while the boundary conditions (27) give

$$W_{1n} = 0 \text{ on } |\zeta| = a, b \ (n = 0, 1, \ldots.) \quad \ldots \quad (33)$$

Solving Eqs. (31) and (32) subject to (33) we get

$$W_{1n}(\zeta, \bar{\zeta}, t) = 0 \ (n \geq 0)$$

so that

$$W_u(\zeta, \bar{\zeta}, t) = 0$$

and hence $W_1(\zeta, \bar{\zeta}, t) = W_s(\zeta, \bar{\zeta})$.

This shows that W_1 is independent of time *t*.

Thus, we have finally to the first order of σ and λ

$$W(\zeta, \bar{\zeta}, t) = \bar{W}_0[W_0(\zeta, \bar{\zeta}, t) + \sigma W_1(\zeta, \bar{\zeta}) + \ldots] \quad \ldots \quad (34)$$

where $W_0(\zeta, \bar{\zeta}, t)$ and $W_1(\zeta, \bar{\zeta})$ are given by Eqs. (28) and (29) respectively.

5. Numerical results

To get a physical insight into the problem, we consider the case when $a = 2$, $b = 3$ corresponding respectively to inner boundary with semi-major and semi-minor axes $\frac{5d}{4}$ and $\frac{3d}{4}$ and outer boundary with semi-major and semi-minor axes $\frac{5d}{3}$ and $\frac{4d}{3}$. These values satisfy the conditions of the ellipse being confocal. The variations of W_0 for different values of *r* and λ at $\theta = 0$ are shown in Figure 1 while those of W_1 are depicted through Figure 2. Figure 3 gives the representation of the velocity for different values of λ for $\sigma = 0.5$.

Figures 1 and 2 show that W_0 and W_1 both increase with increase of λ. W_0 increases from the inner to the outer boundary of the cylinders while W_1 attains its maximum at the middle part of it. It is also noted from Figure 3 that the velocity increases with increasing values of σ.

For numerical calculations, we have chosen $\frac{\lambda t}{\kappa} = \frac{\pi}{2}$ and taken only real parts of the functions from physical point of view.

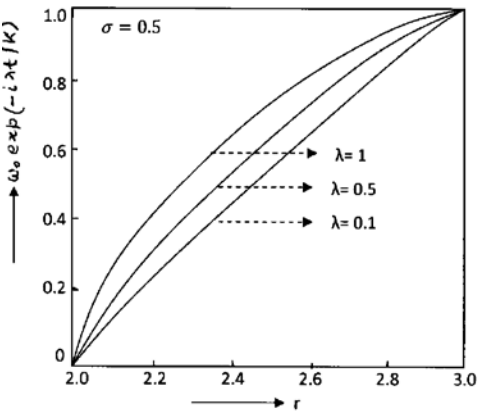

Fig. 1

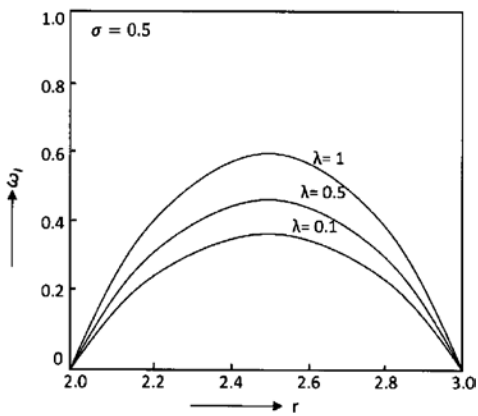

Fig. 2

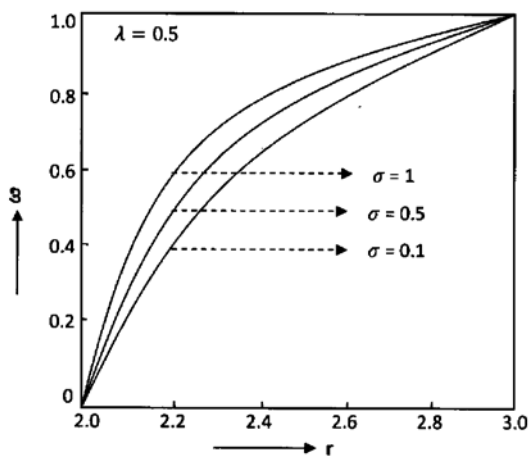

Fig. 3

References

1. Bird, R.B, Dai, G.C. and Yaruso, B. J. − The Rheology and flow of viscoplastic materials, Rev. Chem. Eng., **1**, 1-70 (1983).
2. Bingham, E. C. − Fluidity and plasticity, McGraw-Hill, New York (1922).
3. Ferraris, C.F. and de Larrard F. − Modified slump test to measure rheological parameters of fresh concrete, Cem. Concr Aggregates, **20** , 241-247 (1998).
4. Schowalter, W.R. and Christensen, G. − Toward a rationalization of the slump test for fresh concrete; Comparison of calculations and experiments, J. Rheol, **42**, 865-870 (1998).

5. Roussel, N., Stefani, C. and Leroy, R. − From mini-cone test to Abrams cone test: Measurement of cement-based materials yield stress using slump test, Cem. Concr.Res., **35** , 817-822 (2005).
6. Whipple, K.X. − Open-channel flow of Bingham fluids: Applications in debris-flow research, J. Geol., **105 ,** 243-262 (1997).
7. Tallarico, A. and Dragoni, M. − A three-dimensional Bingham model channelled Lava flows, J. Geophys. Res., **105** , 2569-2580 (2000).
8. Balmforth, N.J., Craster, R.V., Peronac, P., Rustd, A.C. and Sassie, R. − Viscoplastic dam breaks and the Bostarick consistometer, J.Non-Newtonian Fluid Mech., **142 ,** 63-78 (2007).
9. Dubash, N., Balmforth, N.J., Slima, A.C. and Cochard, S. − What is the final shape of a Viscoplastic slump?, J. Non-Newtonian Fluid Mech., **158 ,** 91-100 (2009).
10. Hogg, A.J. and Matson, G.P. − Slumps of viscoplastic fluids on slopes, J. Non-Newtonian Fluid Mech., **158** , 101-112 (2009).
11. Chamberlain, J.A., Horrobin, D.J., Landman, K.A. and Sader, J.E. − Upper and lower bounds for incipient failure in a body under gravitational loading, J. Appl. Mech., **71,** 586-589 (2004).
12. Sader, J.E. and Davidson, M.R. − Scaling behaviour for gravity induced flow of a yield stress materials, J. Rheol, **49** , 105-112 (2005).
13. Roussel, N. and Coussot, P. − Fifty-cent rheometer' for yield stress measurements: From slump to spreading flow, J. Rheol., **49**, 705-718 (2005).

INDIAN JOURNAL OF THEORETICAL PHYSICS, VOL. 65, NOS. 3 & 4, 2017

On the threshold value of IMF B_Z in relation with geomagnetic storm and Dst index

Adrija Banerjee, Amaresh Bej*

Department of Physics,
Indian Institute of Engineering Science and Technology,
Shibpur, P.O. - Botanic Garden, Howrah-711103, West Bengal, India
*E-mail : amaresh_bej@yahoo.com

T. N. Chatterjee

Department of Electronics, Dinabandhu Andrews College,
54, Raja S.C. Mullick Road, Garia, Kolkata-700084, India

and

Abhijit Majumdar

Department of Physics,
Indian Institute of Engineering Science and Technology,
Shibpur, P.O. - Botanic Garden, Howrah-711103, West Bengal, India

[**Abstract :** *Dst* index, an widely known global measurement of the magnitude, duration and occurrence of geomagnetic storm, is a time-series, primarily controlled by the B_Z component of the interplanetary magnetic field (*IMF*) and the solar wind emitted from the Sun. The direction and intensity of *IMF* B_Z plays a significant role in determining the strength of the solar wind-magnetosphere coupling and also the amount of energy transferred into the magnetosphere. In the present paper, the effect of *IMF* B_Z on this coupling is studied for the entire 23^{rd} solar cycle and different threshold values of B_Z had been observed for each year.]

Key-words : Solar wind-magnetosphere interactions, Interplanetary magnetic fields, *Dst* index, Time series analysis.

1. Introduction

Geomagnetic storm is a physical phenomenon having complex dynamical structure and stochastic nature. The Sun emits a stream of plasma particles, known as solar wind which is coming towards the Earth with an average speed of 400 *Km./sec*. The solar wind interacts with the terrestrial

magnetosphere, a cusp is formed and a number of energized particles are injected into the magnetosphere through the cusp. These injected particles then generate a ring current around the Earth which in turn lowers down the magnitude of the horizontal magnetic field from its average value. This decrement is measured in nano Tesla and termed as Disturbance storm time (*Dst*) index. Four magnetometer stations, namely Hermanus (33.3° south, 80.3° in magnetic dipole latitude and longitude), Kakioka (26.0° north, 206.0°), Honolulu (21.0° north, 266.4°), and San Juan (29.9° north, 3.2°) had been chosen to record the data as their specific position is beyond the influence of auroral activities or equatorial electrojet currents[1,2]. The negative value of *Dst* index is a direct measurement of geomagnetic storm obeying the scale : upto -100 *nT* means moderate storm, between -100 *nT* and -250 *nT* intense storm and less than -250 *nT* indicates super storm.

Geomagnetic storm has severe damaging effect on the Earth's electrical and technical hardware. Intense or super storm can completely collapse the power grids to cause massive black out in a large area, disturbs the navigation and satellite communications, destroys computer networks and in general can cause several human hazards and enormous monetary losses. The upper latitude regions of the Earth, specifically the regions belonging to Scandinavia, Russia, Canada or U.S. are the most affected ones[3,4,5,6].

To understand the actual dynamics of the geomagnetic storm, *Dst* index had been studied and analysed extensively using various approaches in the last decades. In the year of 1975, Burton et al.[7] first proposed an empirical relationship of *Dst* index based on the solar wind and *IMF* B_Z. Since then, a number of works had been published investigating the nature[8-12] of *Dst* index in relationship with the other parameters.

As numerous previous works had suggested, *IMF* B_Z plays a key role in the solar wind-magnetosphere coupling and the occurrence of geomagnetic storm. According to Lu et al.[13], when the direction of the *IMF* B_Z is southward, the cusp moves to the equatorial region and widens as the intensity of the *IMF* B_Z increases while for the northward direction , the cusp moves away from the equatorial region and narrow down. In our previous studies, we investigated long-range correlation and the stochastic nature of the *Dst* index[14] and proposed a cellular automata model of *Dst*

index based on self-organized criticality[15]. In the present paper, we are trying to investigate the effect of the *IMF* B_Z on the magnetic reconnection process which injects significant amount of solar wind energy into the magnetosphere and its threshold value.

2. Data

Here we used the hourly averaged *Dst* index, solar wind ion density, flow speed and B_Z component of the interplanetary magnetic field (*IMF*) data from the year 1997 to the year 2007 as extracted from NASA/GSFC's OMNI data set through OMNIWeb[16]. The *OMNI* data were obtained from the GSFC/SPDF OMNIWeb interface at http://omniweb.gsfc.nasa.gov.

3. Method

The solar wind energy can be calculated from the ion density and flow speed as:

$$dE(t) = \text{norm}\left(\frac{1}{2} \times \text{ion density} \times (\text{flow speed})^2\right) \quad \ldots \quad (1)$$

The cusp width W has been considered as a function of *IMF* B_Z obeying the following relations:

$$W(t) = 0.005\, B_Z(t) \text{ for } B_Z(t) > B_{TH} \quad \ldots \quad (2)$$

$$W(t) = B_Z(t) \text{ for } B_Z(t) < B_{TH} \quad \ldots \quad (3)$$

where B_{TH} is the threshold value of *IMF* B_Z.

The total energy input to the magnetosphere at any time t is

$$E(t) = W(t) \times dE(t) \quad \ldots \quad (4)$$

Then the value of E is averaged over 36 data using the moving average technique and termed as E_i.

E_i is a time-series representation of the amount of energy being injected into the magnetosphere. This energy then causes the Earth's horizontal magnetic field to deviate from its average value. This deviation is measured and termed as *Dst* index. Thus *Dst* index has a proportional relationship with the injected input energy. The correlation coefficient between the time series E_i and *Dst* index is estimated for a number of step shifts, ranging from 1 to 720. For each step, a value of correlation coefficient is estimated. The maximum value of the coefficient, the corresponding step shift and the associated value of B_{TH} are recorded.

Now the whole calculation is repeated for different values of B_{TH}, ranging from -40 *nT* to 40 *nT*, with an increment of 0.5 *nT*. Thus, for each year we can get the threshold value of B_{TH} for which the correlation coefficient between input energy E_i and *Dst* index is maximum. Also, the value of the step shift associated with the maximum correlation coefficient denotes the time-interval between the injection of input energy into the terrestrial magnetosphere and its effect on the horizontal magnetic field of the Earth.

4. Result and discussion

The above calculations are applied to the entire 23^{rd} solar cycle, *i.e.* to each of the years of the 11-year span of 1997 to 2007. Figure 1 shows the variation of correlation coefficient with the number of step shifts for the year 2001. It is observed that the correlation coefficient reaches its maximum value at the step shift of 16 for this year. Figure 2 shows the variation of correlation coefficient with the variation of B_{TH}, the threshold value of *IMF* B_Z, also for the year of 2001. This graph exhibits the maximum value of correlation coefficient for $B_{TH} = 4nT$. Table I shows the value of B_{TH}, maximum correlation coefficient and the associated time-interval for each of the year of entire 23^{rd} solar cycle. From the result, it is seen that for each year, the value of threshold value of *IMF* B_Z is different. Only beside the year of 2004, a low positive value of B_Z *i.e.* a low value of northward B_Z serves as the threshold value. Also, there is a time-interval of 13-18 hour between the injection energy and its effect on the horizontal magnetic field.

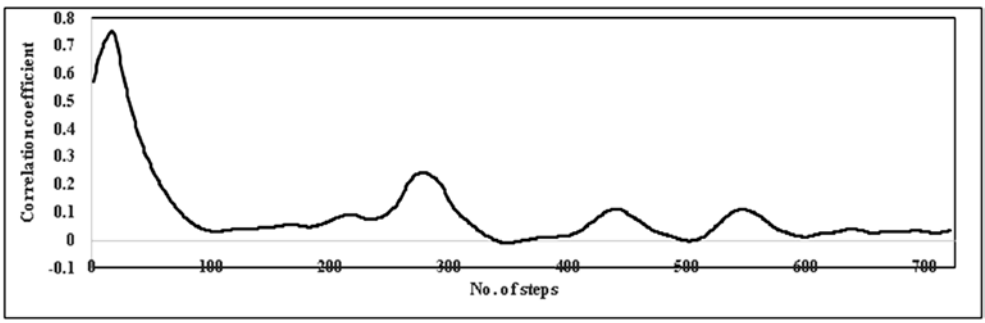

Fig. 1

Variation of correlation coefficient with the number of steps for the year 2001.

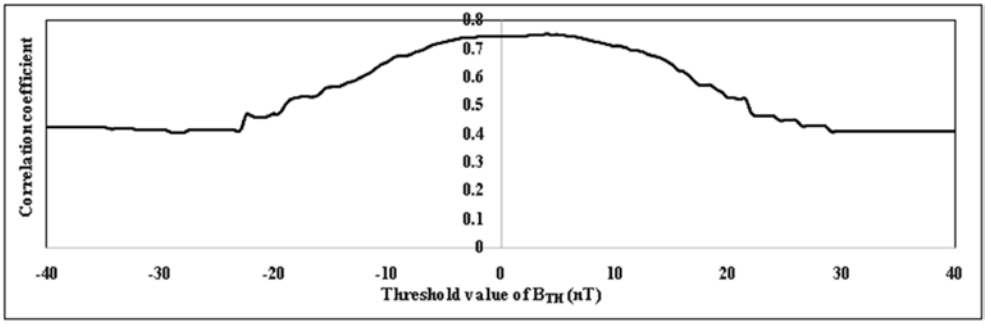

Fig. 2

Variation of correlation coefficient with variation of B_{TH}, the threshold value of *IMF* B_Z.

Table I

Value of B_{TH}, maximum correlation coefficient and the associated time-interval for each of the year of entire 23^{rd} solar cycle.

Year	B_{TH} (nT)	Step shifts	Correlation coefficient (in %)
1997	2.5	15	69.8636
1998	5	15	68.4855
1999	5	15	65.3289
2000	3.5	15	74.7755
2001	4	16	75.1322
2002	3	16	71.7233
2003	4	13	65.9140
2004	-1	13	72.2417
2005	3	17	62.9233
2006	4	16	61.3220
2007	1.5	18	51.8333

5. Conclusion

Dst index is the measurement of the net decrement of the Earth's horizontal magnetic field from its average value and thus the geomagnetic storm. This time-series is primarily controlled by the solar wind energy and

the *IMF* B_Z. The direction and intensity of *IMF* B_Z plays a crucial role in the solar wind-magnetosphere coupling and the injection of solar wind energy into the magnetosphere. In this paper, we had studied the effect of B_Z on the cusp width during the coupling process. It has been observed that the *IMF* B_Z has a specific threshold value, B_{TH} for each year. For the values greater than B_{TH}, the cusp is nearly closed whereas for the values less than B_{TH}, the cusp is open. For each of the year of the cycle 1997-2007, B_{TH} has a small value ranging from -1 *nT* to 5 *nT*. Also, the calculations shows that there is a 13-18 hours' time-interval between the injection of the input energy into the magnetosphere and its effect on the horizontal magnetic field of the Earth.

This is a first-order study of the effect of B_Z on the solar wind-magnetosphere coupling process and the width of the cusp. Future work can be aimed to analyze the exact mathematical relations between *IMF* B_Z and the coupling process.

References

1. Sugiura, M. − Hourly values of equatorial Dst for IGY. In: Annals of the International Geophysical Year, **Vol. 35**, pp. 945–948, Pergamon Press, Oxford (1964).
2. Wanliss, J. A. and Showalter, K. M. − High-resolution global storm index: Dst versus SYM-H, J. Geophys. Res., **111**, A02202 (2006), doi:10.1029/2005JA011034.
3. Kappenman, J.G., Zanetti, L.J. and Radasky, W.A. − Geomagnetic storms can threaten electric power grid, American Geophysical Union: Earth in Space, **9**, No.7, pp. 9-11 March, (1997).
4. 'Geomagnetic Storms,' CENTRA Technology, Inc. report (14 January 2011) prepared for the Office of Risk Management and Analysis, United States Department of Homeland Security.
5. Halloween Space Weather Storms of 2003, NOAA Technical Memorandum OAR SEC-88, Space Environment Centre, Boulder, Colorado, June (2004).
6. Severe Space Weather Events − Understanding Societal and Economic Impacts – Workshop Report, National Research Council of the National Academies, The National Academies Press, Washington, D. C. (2008).
7. Burton, R. K., McPherron, R. L. and Russell, C. T. − An empirical relationship between interplanetary conditions and Dst, J. Geophys. Res., **80**(31), 4204–4214 (1975), doi:10.1029/JA080i031p04204.
8. Akasofu, S.I. − Relationship between the AE and Dst indices during geomagnetic storms, J.Geophys. Res., **86**, 4820 (1981).

9. Moon, G.-H., Ahn, B.H. and Sun, W. − Estimation of the Dst index based on the AL index. Adv. Space Res., **37**(6), 1148–1151 (2006).
10. Murayama, T. − Coupling function between the solar wind and the Dst index, in Solar Wind-Magnetosphere Coupling, edited by Y. Kamide and J. A. Slavin, p. 119, Terra Sci., Tokyo (1986).
11. Park, Y.K. and Ahn, B.H. − Dst prediction based on solar wind parameters, J. Astron. Space Sci., **26**(4), 425-438 (2009).
12. Saba, M., Gonzalez, W.D. and Gonzalez, A.L.C. − Relationship between the Dst, ap, and AEindices. Adv. Space Res., **14**, 435-438 (1994).
13. Lu, J. Y., Liu, Z.-Q., Kabin, K., Jing, H., Zhao, M. X. and Wang, Y. − The IMF dependence of the magnetopause from global MHD simulations, J. Geophys. Res. Space Physics, **118**, (2013), doi:10.1002/jgra.50324.
14. Banerjee, A., Bej, A. and Chatterjee, T. N. − Astrophys Space Sci., 337: **23** (2012) doi:10.1007/s10509-011-0836-1.
15. Banerjee, A., Bej, A. and Chatterjee, T. N. − A cellular automata-based model of Earth' smagnetosphere in relation with Dst index, Space Weather, **13**, 259–270 (2015), doi:10.1002/2014SW001138.
16. King, J.H. and Papitashvili, N.E. − Solar wind spatial scales in and comparisons of hourly Wind and ACE plasma and magnetic field data, J. Geophys. Res., A02104, **110**, (2005).

INDIAN JOURNAL OF THEORETICAL PHYSICS, VOL. 65, NOS. 3 & 4, 2017

Propagation of ion acoustic solitary waves with high relativistic thermal ions and non-thermal electrons and thermal positrons in plasma

R. Das

Department of Mathematics, Arya Vidyapeeth College,
Guwahati-781016, Assam, India
e-mail : ranjan2367@gmail.com

[**Abstract :** In this investigation both compressive and rarefactive solitons are shown to exist in electron-positron-ion plasma consisting of high relativistic thermal ions, nonthermal electrons and thermal positrons. The compressive and rarefactive Korteweg-de Vries (*KdV*) solitons of small amplitude are shown to exist only for fast ion-acoustic mode. It has been found that the inclusion of variable temperature of the ion species not only significantly modifies the basic features (amplitude and width) of the ion-acoustic solitons but also introduces a new regime for the existence of solitons. Further, the increase in ion to electron temperature ratio results in decrease in soliton amplitude. Also increase in relativistic factor increases the soliton amplitude.]

Keywords: KdV**,** High relativistic, Nonthermal electrons, Thermal positrons, Ion acoustic, Soliton

PACS Nos.: 52.27.Ny; 52.35.Fp; 52.35.Sb

1. Introduction

The study of linear and nonlinear wave motions in electron–positron–ion plasmas[1-17] has been a great deal of interest due to the occurrence of such type plasmas in Van Allen radiation belts[18-22], active galactic nuclei[23], quasars and pulsar magnetosphere[24, 25], semiconductor plasmas[26], intense laser fields[27], centre of our galaxy[28], the early universe[29, 30], neutron stars[31], and white dwarfs[32, 33], intense laser-solid matter interaction experiments[34], solar atmosphere[35] and also produced in some laboratory environments[36-39]. It has been found that the presence of positrons in the plasma have important roles on the different phenomena in astrophysical plasma[5, 26].

The propagation of ion acoustic waves in collisionless plasma can be described by the *KdV* equation using perturbation method[40]. The ion-

acoustic solitons in electron-positron and ion plasmas is investigated by Popel, et al.[5]. In their investigation, they have reported that the presence of positron reduces ion acoustic amplitude. Ferdousi, et al.[41] studied the ion acoustic *KdV*, *mKdV*, and Gardner solitons in an unmagnetized electron-positron-ion plasma with non-extensive electrons and positrons. Ferdousi, et al.[42] have investigated the properties of obliquely propagating ion-acoustic solitary waves in the presence of ambient magnetic field in an electron-positron-ion non-thermal plasma through Korteweg-de Vries (*KdV*) and modified *KdV* (*mKdV*) equations. They have found that the electron and positron non-extensivity and external magnetic field (obliqueness) have significant effects on the characteristics of solitary waves. Chatterjee, et al.[43] studied the existence of ion acoustic solitary waves in magnetized dense electron-positron-ion plasma by using Sagdeev potential method. The effect of ion temperature on the formation of solitary waves is studied, and the ranges of parameters for which solitary waves and double layers exist are also studied. Salahuddin, et al.[44] studied the ion-acoustic envelope solitons in a collisionless unmagnetized electron-positron-ion plasma by Krylov-Bogoliubov-Mitropolsky perturbative technique. They have shown that the electron-positron plasmas become richer in linear and nonlinear wave dynamics.

However, most of these studies are focused on non-relativistic plasmas, but when the particle velocities are comparable to the speed of light, the characteristics of solitons are shown to be significantly influenced by relativistic effect[45-49]. In space observations, the high speed streaming ions and electrons are found to play a major role in the physical mechanism of the non linear structure. This type of plasma occurs in space plasma phenomena such as plasma sheet boundary layer of earth's magnetosphere[50,51] and in laser-plasma interaction[52,53]. Also relativistic plasma can be found in many practical situations *e.g.* in space plasma phenomena[50], Van Allen radiation belts[54] and laser plasma interaction experiments[55]. The relativistic motion in plasma is reported to exist during the early period of evolution of the Universe[56]. Shah and Saeed[57] studied the effects of various plasma parameters on the nonlinear propagation of ion acoustic waves in relativistic electron-positron-ion plasma. Gill, et al.[58]

studied the dynamics of ion acoustic solitons in a weakly relativistic electron-positron-ion plasma. Saeed, et al.[59] investigated the nonlinear propagation of ion-acoustic solitons in relativistic electron-positron-ion plasma comprising of Boltzmannian electrons, positrons, and relativistic thermal ions. They found that the increase in the relativistic streaming factor causes the soliton amplitude to thrive and its width to shrink. The soliton amplitude and width are found to decline as the ion to electron temperature ratio is increased. The increase in positron concentration results in reduction of soliton amplitude. The soliton amplitude enhances as the electron to positron temperature ratio increases. Shah, et al.[60] investigated electrostatic ion acoustic solitary waves in a plasma system comprising of relativistic ions, kappa distributed electrons, and positrons. They reported that increase in the relativistic streaming factor and positron and electron kappa parameters cause the soliton amplitude to thrive. But the soliton amplitude diminishes as the positron concentration is increased in the system. Hafez and Talukder[61] have investigated the weakly relativistic effects on ion acoustic solitary waves by considering nonextensive electrons and isothermal positrons. Recently, Hafez, et al.[62] have studied the weakly relativistic effects on the electrostatic ion acoustic solitons of positive as well as negative potentials with nonextensive electrons and positrons. Javidan and Saadatmand[63] have studied the effect of high relativistic nonthermal ions and nonthermal electrons in electron-ion-positron plasma system. They have obtained the maximum amplitude of the solitary wave and its width as functions of plasma parameters. Javidan and Pakzad[64] have investigated the propagation of ion acoustic waves in plasmas containing superthermal electrons, thermal positrons and high relativistic ions. In their investigation, the effects of relativistic ions and superthermal electrons on the soliton identifications are discussed.

In this paper, we have investigated the influences of positron concentration, electron to positron temperature ratio, ion to electron temperature ratio, and relativistic streaming factor on the nonlinear propagation of ion acoustic solitary waves in unmagnetized plasmas, whose constituents are high relativistic thermal ions, nonthermal electrons, and thermal positrons. The paper is organized as follows. First in Sec. II, we present the governing equations for nonlinear ion acoustic waves in

electron-positron-ion plasma and then using the fluid model, derived the *KdV* equation. In Sec. III, condition for existence of solitons and in Sec. IV, Solitary wave solution is discussed. Finally, a brief summary and discussion of our results are given in the last Sec. V.

2. Basic equations and derivation of KdV equation

We consider an unmagnetized plasma consisting of relativistic positive ions, nonthermal electrons and thermal positrons. The fluid equations of motion governing the collision less plasma in one dimension are:

$$\frac{\partial n_i}{\partial t}+\frac{\partial}{\partial x}(n_i v_i)=0 \qquad \ldots \quad (1)$$

$$\left(\frac{\partial}{\partial t}+v_i\frac{\partial}{\partial x}\right)\gamma v_i+\frac{\partial \phi}{\partial x}+\frac{\alpha}{n_i}\frac{\partial p_i}{\partial x}=0 \qquad \ldots \quad (2)$$

$$\left(\frac{\partial}{\partial t}+v_i\frac{\partial}{\partial x}\right)p_i+3p_i\frac{\partial}{\partial x}(\gamma v_i)=0 \qquad \ldots \quad (3)$$

$$n_e=\left(1-\beta\phi+\beta\phi^2\right)e^{\phi} \qquad \ldots \quad (4)$$

$$n_p=\delta e^{-\sigma\phi} \qquad \ldots \quad (5)$$

$$\frac{\partial^2\phi}{\partial x^2}=n_e-n_i-n_p \qquad \ldots \quad (6)$$

where, $\gamma=\left(1-\frac{v_i^2}{c^2}\right)^{-\frac{1}{2}}=1+\frac{v_i^2}{2c^2}+\frac{3v_i^4}{8c^4}$, $\alpha=\frac{T_i}{T_e}$ (= ion to electron temperature ratio), $\beta=\frac{4r}{1+3r}$ (r is the parameter that determines the population of nonthermal (fast) electrons (Kalita and Kalia[65]), $\sigma=\frac{T_e}{T_p}$ (= electron to positron temperature ratio) and $\delta=\frac{n_{p0}}{n_{e0}}$ represents the relative positron concentration in electron-positron-ion plasma.

In equations (1) – (6), densities n_i, n_e, n_p are normalized by the unperturbed electron density n_{e0}, time t by the inverse of the characteristic ion plasma frequency *i.e.*, $\omega_{pi}^{-1} = \left(\frac{m_i}{4\pi\, n_{e0} e^2} \right)^{\frac{1}{2}}$, distance x by the electron Debye length $\lambda_{De} = \left(\frac{T_e}{4\pi\, n_{e0} e^2} \right)^{\frac{1}{2}}$, ion velocity v_i by the ion-acoustic speed $C_s = \left(\frac{T_e}{m_i} \right)^{\frac{1}{2}}$, pressure p_i by $n_{e0} T_i$ and the potential ϕ by $\frac{T_e}{e}$.

In presence of non-thermal electrons, the variation in ion density with relativistic effects is negligible in comparison to the relativistic variation in its mass. So the Lorentz factor γ is not considered in equation (1) as in the references[45-67]. The massive and thermal ions are assumed to be relativistic, so the plasma composition is dominated by the relativistic ion species. At the same time, from the behavioural point of view, ions and positrons are positively charged. Due to relativistic effect of the dominant ions, the bulk of non-thermal electrons are separated into two parts, the greater part is left as nonthermal electrons and a small part is turned into positrons due to negligible collision with ions.

The reductive perturbation method can be used for investigating the behaviour of nonlinear ion acoustic waves. The stretched variables are defined as follows

$$\xi = \varepsilon^{\frac{1}{2}} (x - Ut), \quad \tau = \varepsilon^{\frac{3}{2}} t \qquad \ldots \quad (7)$$

where ε is a small dimensionless parameter which characterizes the strength of the nonlinearity and U is the phase velocity of the ion-acoustic wave in (x, t)space. Thus, the space and time derivatives are replaced by

$\frac{\partial}{\partial x}=\varepsilon^{\frac{1}{2}}\frac{\partial}{\partial \xi}$ and $\frac{\partial}{\partial t}=\varepsilon^{\frac{1}{2}}\left(\varepsilon\frac{\partial}{\partial \tau}-U\frac{\partial}{\partial \xi}\right)$ respectively. Dependent variables are expanded as follows

$$\begin{aligned} n_i &= 1-\delta+\varepsilon n_{i1}+\varepsilon^2 n_{i2}+\ldots \\ n_e &= 1+\varepsilon n_{e1}+\varepsilon^2 n_{e2}+\ldots \\ n_p &= \delta+\varepsilon n_{p1}+\varepsilon^2 n_{p2}+\ldots \\ v_i &= v_0+\varepsilon v_{i1}+\varepsilon^2 v_{i2}+\ldots \\ p_i &= 1+\varepsilon p_{i1}+\varepsilon^2 p_{i2}+\ldots \\ \phi &= \varepsilon\phi_1+\varepsilon^2\phi_2+\ldots \end{aligned} \quad \ldots \quad (8)$$

With the use of the transformations (7) and the expansions (8) in the normalized set of equations (1) – (6) subject to the boundary conditions,

$$n_{i1}=n_{e1}=0,\ v_{i1}=0,\ \ \phi_1=0, \text{ at } |\xi|\to\infty,$$

we get from ε order equations, the following quantities :

$$n_{i1}=\frac{(1-\delta)^2\phi_1}{\gamma_0\left\{(1-\delta)(U-v_0)^2-3\alpha\right\}},\ n_{e1}=(1-\beta)\phi_1,\ n_{p1}=-\delta\sigma\phi_1,$$

$$v_{i1}=\frac{(1-\delta)(U-v_0)\phi_1}{\gamma_0\left\{(1-\delta)(U-v_0)^2-3\alpha\right\}},\ p_{i1}=\frac{3(1-\delta)\phi_1}{(1-\delta)(U-v_0)^2-3\alpha},\ n_{e1}-n_{i1}-n_{p1}=0 \quad \ldots \quad (9)$$

where $\gamma_0=1+\frac{v_0^2}{2c^2}+\frac{8v_0^4}{15c^4}$.

Using the values of n_{i1}, n_{e1} and n_{p1} in the last equation of (9), we obtain the phase velocity equation for the nonlinear waves

$$(U-v_0)^2=\frac{1-\delta}{\gamma_0(1-\beta+\sigma\delta)}+\frac{3\alpha}{1-\delta} \quad \ldots \quad (10)$$

This gives the expressions of the phase velocity of Javidan and Saadatmand[63] for $\alpha=0$ and Gill, et al.[56] for $\alpha=0,\ \beta=0$.

This gives $U=v_0\pm\sqrt{\frac{(1-\delta)^2+3\alpha\gamma_0(1-\beta+\delta\sigma)}{\gamma_0(1-\delta)(1-\beta+\delta\sigma)}}$

Using the relation (10) in the set of ε^2 - order equations obtained from equations (1) – (6), we have the *KdV* equation as,

$$\frac{\partial \phi_1}{\partial \tau} + A\phi_1 \frac{\partial \phi_1}{\partial \xi} + B\frac{\partial^3 \phi_1}{\partial \xi^3} = 0 \qquad \ldots \quad (11)$$

where

$$A = \frac{(U-v_0)^2\left\{5\gamma_0 - 2 - \left(\frac{3v_0}{c} - \frac{15v_0^2}{2c^4}\right)U + \frac{15v_0^4}{4c^4}\right\} + \frac{9\alpha v_0 U}{c^2} + 3\alpha\left(3\gamma_0^2 - 4\gamma_0 + 2\right)}{2\gamma_0^2(U-v_0)\left\{(U-v_0)^2 - 3\alpha\right\}}$$

$$- \frac{\gamma_0\left\{(U-v_0)^2 - 3\alpha\right\}^2\left(1-\delta\sigma^2\right)}{2(1-\delta)(U-v_0)} \quad \text{and} \quad B = \frac{\gamma_0\left\{(U-v_0)^2 - 3\alpha\right\}^2}{2(1-\delta)(U-v_0)}$$

3. Condition for the existence of solitons and solitary wave solution

From the expression for phase velocity (10), we have $(U-v_0)^2 > 3\alpha$ (assuming $1 > \delta > \frac{\beta - 1}{\sigma}$)

Therefore $U > v_0 + \sqrt{3\alpha}$ or $U < v_0 - \sqrt{3\alpha}$

Also from (10), irrespective of δ, $\alpha > -\frac{(1-\delta)^2}{3\gamma_0(1-\beta+\sigma\delta)}$, which is possible as $\alpha = \frac{T_i}{T_e} > 0$.

Using the transformation $\chi = \xi - V\tau$, the *KdV* equation (11) can be simplified to give the solitary wave solution as

$$\phi_1 = \frac{3V}{A}\sec h^2\left(\frac{1}{2}\sqrt{\frac{V}{B}}\chi\right)$$

where *V* is the velocity with which the solitary waves travel to the right.

Thus, the wave amplitude of the soliton is given by $\phi_0 = \frac{3V}{A}$ and the corresponding width by $\Delta = 2\sqrt{\frac{B}{V}}$.

4. Discussion and results

In this model of electron-positron-ion plasma, ion to electron temperature ratio is found to play a very significant role in the formation of *KdV* solitons. Only fast ion-acoustic mode is found to exist in our investigation

under the sound mathematical condition $\alpha > -\frac{(1-\delta)^2}{3\gamma_0(1-\beta+\sigma\delta)}$. The coefficients of *KdV* equation depend on the relative positron concentration (δ), electron to positron temperature ratio (σ), ion to electron temperature ratio (α), nonthermal parameter (β) and relativistic factor $\eta\left(=\frac{v_0}{c}\right)$. From figure 1, it is clear that the coefficient A tends to zero for some particular set of parameters. Further, A is negative at $\beta = 0.7$. In this situation one can study the *mKdV* (modified Korteweg de-Vries) soliton. But in the investigation of Gill et al.[58] investigated dynamics of ion-acoustic solitons in cold electron-positron-ion plasmas with weakly relativistic effect and without nonthermal particles and found that A is always positive for all ranges of the parameters indicating that no double layers are possible. In figure 2, corresponding to the nonlinear thermal parameter $\beta = 0.7$, the value of A is negative for η smaller than 0.6 (different from the conclusion of Gill et al.[58]) which admits rarefactive soliton in small range of β. Figure 1 may be comparable with the figure 2 of Javidan and Saadatmand[63]. The patterns of growths of A in figures 1 and 2, based on various values of β are mostly quite different against the temperature ratios $\alpha = 0.0, 0.05$. For higher $\beta = 0.65, 0.70$, increase in A is much faster (Fig. 2) than that in figure 1 though it decreases slowly for β = 0.65. In the cases of β = 0.55 and 0.60 in Fig. 2, as η is increased, A decreases at first for the lower range of η and then increases for the higher range of η. On the other hand, in the corresponding cases (β = 0.55 and 0.60) in Fig. 1, A decreases for the entire range of η and the decrease in A is very rapid compared with the decrease in A for the lower range of η in Fig. 2. From the comparison of the figures 3 (α = 0.0) and 4 (α = 0.05), it clear that B decreases when α increases. Figure 4 reflects the same pattern of figure 3 but for α = 0.05 and the values of B are smaller than those for α = 0, otherwise B decreases as α increases. Interestingly, coefficients A and B of Javidan and Saadatmand[63] can be obtained (with some modification) by putting α = 0 and of Kaur et al.[66] by putting α = 0, δ = 0 ; that of Gill, et al.[58] (for weak relativistic effect) by putting δ = 0 and β = 0. Computation work shows that increase in ion to electron temperature ratio (α) results in decrease in soliton amplitude. However, increase in relativistic factor

increases the soliton amplitude. Figure 5(*a*) shows that the amplitude of soliton increases as relativistic factor increases. The decrease (increase) in soliton amplitude is dependent on increase (decrease) in the coefficient *A*. Also the corresponding widths [(Fig. 5(*b*)] are seen to decrease with the increase of relativistic factor (η) attaining higher values. Figure 6(*a*) shows the growth of soliton amplitude for $\alpha = 0.05$ which differs from that of the figure 5. The corresponding width [Fig. 6(*b*)] decreases with increase of η for $\alpha = 0.05$. In cases of higher ion temperature, the increase in the streaming ion velocity v_0, η causes the increase in the ion mass $m = \frac{m_0}{\sqrt{1-\frac{v^2}{c^2}}}$. Furthermore, the increase in the ion mass causes the decrease in the amplitude. In both the figures 5(*b*) and 6(*b*), the magnitude of width decreases with the increase of relative positron concentration δ. From figures 5 and 6, it is clear that ion to electron temperature ratio affects the amplitudes and widths. Figure 7 show the uniform but relatively non-linear decrease of magnitude of B with α for fixed $V = .0075$, $\eta = 0.2$, $\sigma = 0.20$ and $\delta = 0.40$. The above results can be compared with the results obtained by Kalita and Das[67].

The present work is different from the work of Javidan and Saadatmand[63], because in their investigation, the *KdV* equation has been derived for solitary waves in relativistic isothermal ions and without pressure variation equation. In our investigation we have shown the effect of ion to electron variable temperature ratio which significantly modifies the soliton behaviour and propagation properties in this electron-positron-ion plasma.

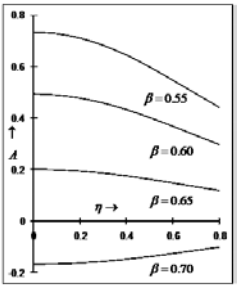

Fig. 1

The parameter *A* as a function of relativistic parameter η for different values of β for fixed $V = .0075$, $\sigma = 0$, $\alpha = 0$ and $\delta = 0.40$.

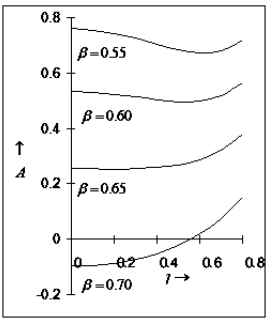

Fig. 2

The parameter A as a function of relativistic parameter η for different values of β for fixed V = .0075, σ = 0.20, α = 0.05 and δ = 0.40.

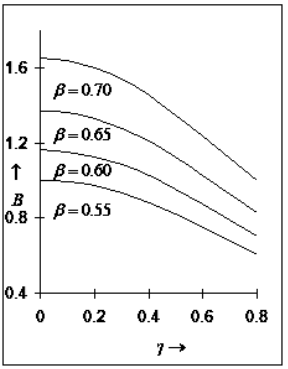

Fig. 3

The parameter B as a function of relativistic parameter η for different values of β for fixed V = .0075, α = 0, σ = 0.20 and δ = 0.40.

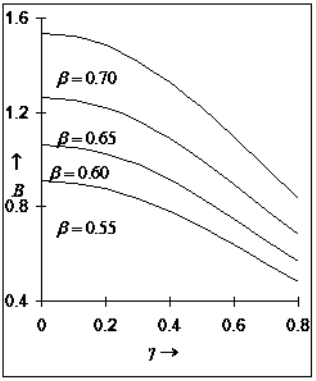

Fig. 4

The parameter B as a function of relativistic parameter η for different values of β for fixed V = .0075, α = 0.05, σ = 0.20 and δ = 0.40.

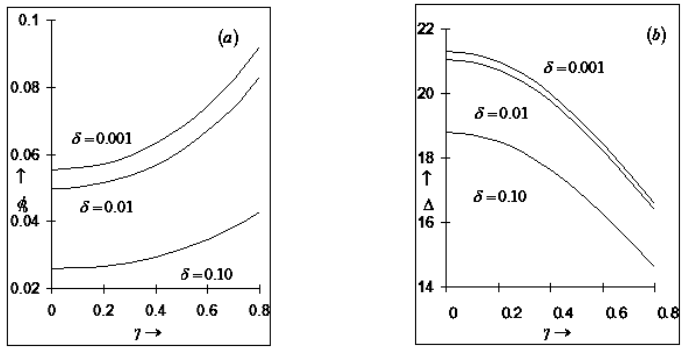

Fig. 5

Amplitudes (*a*) and widths (*b*) of compressive ion-acoustic solitons versus η for different values of δ for fixed $V = .0075$, $\alpha = 0$, $\sigma = 1$ and $\beta = 0.30$.

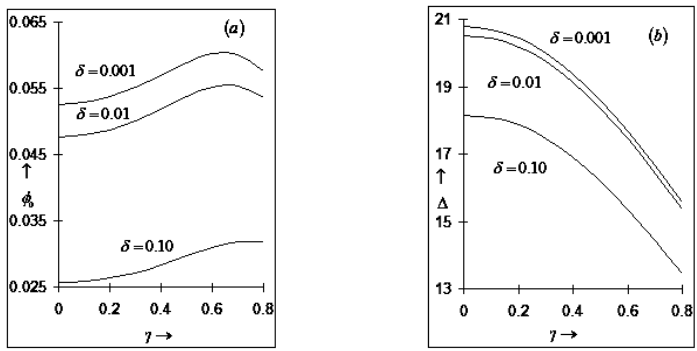

Fig. 6

Amplitudes (*a*) and widths (*b*) of compressive ion-acoustic solitons versus η for different values of δ for fixed $V = .0075$, $\alpha = 0.05$, $\sigma = 1$ and $\beta = 0.30$.

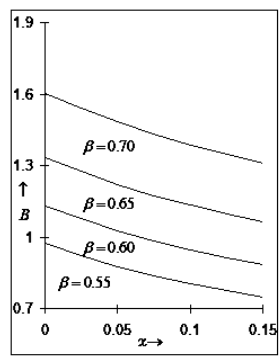

Fig. 7

The parameter B as a function of temperature ratio α for different values of β for fixed $V = .0075$, $\eta = 0.2$, $\sigma = 0.20$ and $\delta = 0.40$.

Acknowledgements

The author is grateful to the reviewer for various suggestions and helpful comments in bringing the manuscript to the present form. Also the author thanks Retired Professor B. C. Kalita, Gauhati University, India (Assam), for very fruitful discussions..

References

1. Sakai, J. and Kawata, T. − J. Phys. Sot. Jpn., **49**, 753 (1980).
2. Chain , A. C. L. and Kennel, C. E. − Astrophys. Space Sci., **97**, 9 (1983).
3. Mikhailovski, A. B. Onishchenko, O. G. and Tatarinov, E. G. − Plasma Phys. Controlled Fusion, **27**, 527 (1985).
4. Shukla, P. K., Mamun, A. A. and Stenflo, L. − Phys. Scr., **68**, 295 (2003).
5. Popel, S. I., Vladimirov, S. V. and Shukla, P. K. − Phys. Plasmas, **2**, 716 (1995).
6. Nejoh, Y. N. − Phys. Plasmas, **3**, 1447 (1996).
7. Mishra, M., Arora, A. K. and Chabbra, R. S. − Phys. Rev. E, **66**, 46402 (2002).
8. Ghosh, S. and Bharuthram, R. − Astrophys. Space Sci., **314**, 121(2008).
9. Pakzad, H. R. − Astrophys. Space Sci., **323**, 345 (2009).
10. Verheest, F., Helberg, M. A., Gary, G. J. and Mace, R. l. − Astrophys. Space Sci., **239**, 125 (1996).
11. Mushtaq, A. and Shah, H. A. − Phys. Plasmas, **12**, 072306 (2005).
12. Salahuddin, M., Saleem, H. and Siddiq, M. − Phys. Rev., E **66**, 036407 (2002).
13. Hasegawa, H., Irie, S., Usami, S. and Ohsawa, Y. − Phys. Plasmas, **9**, 2549 (2002).
14. Mahmood, S. and Akhtar, N. − Eur. Phys. J., D **49**, 217 (2008).
15. Pakzad, H. R. and Tribeche, M. −Journal of Fusion Energy, **32**, 171 (2013).
16. Hafez, M. G. and Talukder, M. R. − Astrophys. Space Sci., **359**, 27 (2015).
17. Hafez, M. G., Talukder, M. R. and Sakthivel, R. − Indian J. Phys., **90**, 603 (2016).
18. Michel, F. C. − Rev. Mod. Phys., **54**, 1 (1982).
19. Orosz, J. A., Remillard, R. A., Bailyn, C. D. and Mc Clintock, J. E. − Astrophys. J. Lett., **L83**, 478 (1997).
20. Goldreich, P. and Julian, W. H. − Astrophys. J., **157**, 869 (1969).
21. Daniel, J. and Tajima, T. − Astrophys. J., **498**, 296 (1998).
22. Tsintsadze, N. L., Rasheed, A., Shah, H. A. and Murtaza, G. − Phys. Plasmas, **16**, 112307 (2009).
23. Miller, H. R. and Witta, P.J. − Active Galactic Nuclei, P.202 Springer Berlin (1978).
24. Reynolds, C. S., Fabian, A. C., Celotti, A. and Rees, M. J. − Mon. Not. R. Astron. Soc., **283**, 873 (1996).
25. Hirotani, K., Iguchi, S., Kimura, M. and Wajima, K. − Publ. Astron. Soc., Jpn., **51**, 263 (1999).
26. Shukla, P. K., Rao, N. N., Yu, M. Y. and Tsintsadze, N. L. − Phys. Rep., **138**, 1 (1986).

27. Berezhiani, V., Tskhakaya, D. D. and Shukla, P. K. − Phys. Rev., A **46**, 6608 (1992).
28. Barns, M. I. − Positron electron pairs in Astrophysics, New York: American Institute of Physics, (1983).
29. Weinberg, S. − Gravitation and Cosmology, Wiley, New York, (1972).
30. Rees, M. J., Gibbons, G. W., Hawking, S. W. and Siklaseds, S. − The Early Universe, Cambridge University Press, Cambridge, (1983).
31. Yu, M.Y., Shukla, P. K. and Stenflo, L. − Astrophys. J., **309**, L63 (1986).
32. Ali, S., Moslem, W. M., Shukla, P. K. and Schlickeiser, R. − Phys. Plasmas, **14**, 082307(2007).
33. Harding, A. K. and Lai, D. − Rep. Prog. Phys., **69**, 2631 (2006).
34. Berezhiani, V. I., Tskhakaya, D. D. and Shukla, P. K. − Phys. Rev., A **46**, 6608 (1992).
35. Hanssen, E. T. and Emslie, A. G. − The physics of solar Flares, Cambridge University Press, Cambridge, 124 (1988).
36. Surko, C. M., Leventhal, M. and Passner, A. − Positron Plasma in the Laboratory, Phys. Rev. Lett., **62**, 901(1989).
37. Bochmer, H., Adams, M. and Rynn, N. − Phys. Plasmas, **2**, 4369 (1995).
38. E. P. Liang , S. C. Wilks, and Tabak, M. − Pair Production by Ultraintense Lasers, Phys. Rev. Lett., **81**, 4887(1998).
39. Helander, P. and Ward, D. J. − Phys. Rev. Lett., **90**, 135004 (2003).
40. Washimi, H. and Tanuiti, T. − Phys. Rev. Lett., **17**, 996 (1966).
41. Ferdousi, M., Yasmin, S., Ashraf, S. and Mamun, A. A. − Astrophys. Space. Sci., **352**, 579 (2014).
42. Ferdousi, M., Sultana, S. and Mamun, A. A. − Phys. Plasma, **22,** 032117 (2015).
43. Chatterjee, P., Saha, T., Muniandy, S. V., Wong, C. S. and Roychoudhury, R. − Phys. Plasma, **17**, 012106 (2010).
44. Salahuddin, M., Saleem, H. and Saddiq, M. − Phys. Rev., E **66**, 036407 (2002).
45. Kalita, B. C., Das, R. and Sarmah, H. K. − Phys. Plasmas, **18**, 012304 (2011).
46. Kalita, B. C., Das, R. and Sarmah, H. K. − Can. J. Phys., **88**, 157 (2010).
47. Singh, K. and Kumar, V. − Phys. Plasmas, **12**, 052103 (2005).
48. Gill, T. S., Bains, A. S. and Saini, N. S. − Can. J. Phys., **87**, 861–866 (2009).
49. Masood, W. and Rizvi, H. − Phys. Plasmas, **17**, 052314 (2010).
50. Grabbe, C. − Geophys. Res., **94**, 17299 (1989).
51. Vette, J. I. − Summary of Particle Population in the Magnetosphere, Reidel, Dordrecht, p. 305 (1970).
52. Shen, B. and Meyer-ter-Vehn, J. − Phys. Rev., E **65**, 016405 (2001).
53. Liang, E. P., Wilks, S. C. and Tabak, M. − Phys. Rev. Lett., **81**, 4887 (1998).
54. Ikezi, H. − Phys. Fluids, **16**, 1668 (1973).
55. Marklund, M. and Shukla, P. K. − Rev. Mod. Phys., **78**, 591 (2006).
56. Holcomb, K. A. and Tajima, T. − Phys. Rev., **40**, 3809 (1989).

57. Shah, A. and Saeed, R. − Phys. Lett., A **373**, 4164 (2009).
58. Gill, T. S., Singh, A., Kaur, H., Saini, N. S. and Bala, P. − Phys. Lett., A **361**, 364 (2007).
59. Saeed, R., Shah, A. and Muhammad Noaman-ul-Haq, − Phys. Plasmas, **17**, 102301 (2010).
60. Shah, A., Mahmood, S. and Haque, Q. − Phys. Plasmas, **18**, 114501 (2011).
61. Hafez, M. G. and Talukder, M. R. − Astrophys. Space Sci., **359**, 1 (2015).
62. Hafez, M. G., Talukder, M. R. and Sakthivel, R. − Indian J. Phys., **90**, 603 (2016).
63. Javidan, K. and Saadatmand, D. − Astrophys Space Sci., **333**, 471 (2011).
64. Javidan, K. and Pakzad, H. R. − Indian J. Phys., **86**, 1037 (2012).
65. Kalita, B. C. and Kalita, R. − Commun. Theor. Phys., **63**, 761 (2015).
66. Kaur, H., Gill, T. S. and Saini, N. S. − Chaos Soliton Fractals, **42**, 1638 (2009).
67. Kalita, B. C. and Das, R. – Phys. Plasmas, **14**, 072108 (2007).

INDIAN JOURNAL OF THEORETICAL PHYSICS, VOL. 65, NOS. 3 & 4, 2017

Stability of equilibrium position of a cable-connected satellites system under several influences : Elliptical orbit and Liapunov's Theorem

Sangam Kumar

P.G. Department of Physics, L. S. College,
B. R. A. Bihar University, Muzaffarpur-842001, Bihar, India
Mobile No.: +91-9905222295
E-mail: kumarsangam.phy@gmail

[**Abstract :** The present paper deals with the study of stability of equilibrium position of the motion of a system of two artificial satellites connected by a light, flexible, inextensible and non-conducting cable under the influence of earth's magnetic field, solar radiation pressure, shadow of the earth and air resistance. We discuss the case of elliptical orbit of centre of mass of the system. In non-linear oscillations of the system, one equilibrium position exists when all the perturbations mentioned above act on the system simultaneously. We apply Liapunov's theorem to test the stability of the equilibrium position. We find that the equilibrium position is unstable in the sense of Liapunov.]

Key-words: Cable-connected satellites, Equilibrium position, Elliptical orbit, Stability, Liapunov's theorem.

1. Introduction

The two pioneer workers Beletsky and Novikova[1] and Beletsky[2] studied the motion of a system of two cable-connected artificial satellites in the central gravitational field of force relative to its centre of mass. The present work is an attempt towards the generalisation of work done by them. In fact, the present work is a physical and mathematical idealisation of real space system. Singh and Demin[3] and Singh[4] investigated the problem in two and three dimensional cases. Das et al.[5] studied the effect of magnetic force on the motion of a system of two cable-connected artificial satellites in orbit. Kumar and Bhattacharya[6] studied the stability of equilibrium positions of two cable-connected artificial satellites under the influence of solar radiation pressure, earth's oblateness and earth's magnetic field. Kumar, et al.[7]

obtained the equations of motion of a system of two cable-connected artificial satellites under the influence of solar radiation pressure, earth's oblateness and shadow of the earth. Prasad and Kumar[8] obtained the equations of motion of a system of two cable-connected artificial satellites under the influence of earth's magnetic field, earth's shadow, solar radiation pressure and earth's oblateness.

Stability of equilibrium position of the motion of a system of two cable-connected artificial satellites under the influence of earth's magnetic field, solar radiation pressure, shadow of the earth and air resistance in elliptical orbit is studied. Shadow of the earth is taken to be cylindrical and the system is allowed to pass through the shadow beam. The string connecting the two satellites is light, flexible, inextensible and non-conducting. Central attractive force of the earth will be the main force and all other forces, being small enough are considered here as perturbing forces. The satellites are taken as charged material particles. Charges have been assumed to be small so that interaction between them may be neglected. Since masses of the satellites are small and distances between the satellites and other celestial bodies are very large, the gravitational forces of attraction between the satellites and other celestial bodies including the sun have been neglected.

2. The treatment of the problem

A set of equations for motion of the system in rotating frame of reference is written as Kumar[9]

$$X''-2Y'-\frac{3X}{\left(1-e^2\right)^{1/2}}=\beta\frac{\left(2+3e^2\right)}{2\left(1-e^2\right)^{7/2}}X-A\cos i+\left(\frac{B_1}{m_1}-\frac{B_2}{m_2}\right).\frac{\cos\in\cos\alpha\sin\theta_2}{\pi}$$

and

$$Y''+2X'=\beta\frac{\left(2+3e^2\right)}{2\left(1-e^2\right)^{7/2}}Y+\left(\frac{B_1}{m_1}-\frac{B_2}{m_2}\right).\frac{\sin\alpha\cos\in\sin\theta_2}{\pi}-\frac{f}{\left(1-e^2\right)^{3/2}} \quad \ldots \quad (1)$$

With the condition of constraint

$$X^2+Y^2\le\left(1+\frac{1}{2}e^2\right) \quad \ldots \quad (2)$$

Also

$$\rho = \frac{1}{(1+e\cos\nu)},$$

$$\lambda_a = \frac{p^3\rho^4}{\mu}\left(\frac{m_1+m_2}{m_1m_2}\right)\lambda = \rho^4\beta,$$

$$\beta = \frac{p^3}{\mu}\left(\frac{m_1+m_2}{m_1m_2}\right)\lambda,\ A = \left(\frac{m_1}{m_1+m_2}\right)\left(\frac{Q_1}{m_1}-\frac{Q_2}{m_2}\right)\frac{\mu_E}{\sqrt{\mu\rho}}$$

$$f = \frac{a_1p^3}{\sqrt{\mu p}},\ a_1 = \rho_a R'(c_2-c_1)\left(\frac{m_1}{m_1+m_2}\right) \qquad \ldots \quad (3)$$

m_1 and m_2 are masses of the two satellites. B_1 and B_2 are the absolute values of the forces due to the direct solar pressure on m_1 and m_2 respectively and are small. Q_1 and Q_2 are the charges of the two satellites. μE is the magnitude of magnetic moment of the earth's dipole. p is the focal parameter. μ is the product of mass of the earth and gravitational constant. λ is undermined Lagrange's multiplier. g_e is the force of gravity. e is ecentricity of the orbit of the centre of mass. v is the true anomaly of the centre of mass of the system. $\in$ is inclination of the oscillatory plane of the masses m_1 and m_2 with the orbital plane of the centre of mass of the system. α is the inclination of the ray. γ is a shadow function which depends on the illumination of the system of satellites by the sun rays. If γ is equal to zero, then the system is affected by the shadow of the earth. If γ is equal to one, then the system is not within the said shadow. R is the modulus of position vector of the centre of mass of the system. c_1 and c_2 are the Ballistic co-efficients. ρ_a is the average density of the atmosphere. i is inclination of the orbit with the equatorial plane. θ_2 is the angle between the axis of the cylindrical shadow beam and the line joining the centre of the earth and the end point of the orbit of the centre of mass within the earth's shadow, considering the positive direction towards the motion of the system. Prime denotes differentiation with respect to v.

We see that the equations (1) do not contain the time explicity. Therefore, Jacobian integral of the problem exists as Kumar[6].

Multiplying the first and second equations of (1) by X' and Y' respectively and adding them and then integrating the final equation so obtained, we get the Jacobian integral in the form

$$X'^2+Y'^2-\frac{3}{\left(1-e^2\right)^{1/2}}X^2=\beta\frac{\left(2+3e^2\right)}{2\left(1-e^2\right)^{7/2}}\left(X^2+Y^2\right)-2AX\cos i+\frac{2}{\pi}\left(\frac{B_1}{m_1}-\frac{B_2}{m_2}\right)$$

$$.\cos\in\sin\theta_2\left(X\cos\propto+Y\sin\propto\right)-\frac{2fY}{\left(1-e^2\right)^{3/2}}+h \qquad \ldots \quad (4)$$

where θ_2 is taken to be constant. *h* is the constant of integration.

3. Equilibrium solution of the problem

The equilibrium positions of the system are given by the constant values of the co-ordinates in the rotating frame of reference.

Let $X=X_1$ =constant, $Y=Y_1$ =constant $\qquad \ldots \quad (5)$

give the equilibrium positions.

With the help of (5), we write the set of equations (1) as

$$\frac{3X_1}{\left(1-e^2\right)^{1/2}}+\frac{\beta}{2}\frac{\left(2+3e^2\right)}{\left(1-e^2\right)^{7/2}}X_1=A\cos i-\left(\frac{B_1}{m_1}-\frac{B_2}{m_2}\right)\frac{\cos\in\cos\propto\sin\theta_2}{\pi}$$

and

$$\frac{\beta}{2}\frac{\left(2+3e^2\right)}{\left(1-e^2\right)^{7/2}}Y_1-\frac{f}{\left(1-e^2\right)^{3/2}}=-\left(\frac{B_1}{m_1}-\frac{B_2}{m_2}\right)\frac{\sin\alpha\cos\in\sin\theta_2}{\pi} \qquad \ldots \quad (6)$$

The presence of the perturbative term due to solar pressure clearly indicates that none of the co-ordinates of the equilibrium point may be taken to be zero unless $\left(\frac{B_1}{m_1}-\frac{B_2}{m_2}\right)$ or $\theta_2=0$. But these parameters cannot be zero. In addition to this, we are interested only to get the maximum effect of the earth's shadow on the motion of the system. Therefore, we put $\in=0$ and $\alpha=0$ in equation (6). By doing so, we get

$$\frac{3X_1}{\left(1-e^2\right)^{1/2}}+\frac{\beta}{2}\frac{\left(2+3e^2\right)}{\left(1-e^2\right)^{7/2}}X_1=A\cos i-\left(\frac{B_1}{m_1}-\frac{B_2}{m_2}\right).\frac{\sin\theta_2}{\pi}$$

and

$$\frac{\beta}{2}\frac{\left(2+3e^2\right)}{\left(1-e^2\right)^{7/2}}Y_1=\frac{f}{\left(1-e^2\right)^{3/2}} \qquad \ldots \quad (7)$$

All the two equations in (7) are independent of each other.

From (7), we get the equilibrium position as

$$[X_1,Y_1]=\left[\frac{A\cos i-\frac{1}{\pi}\left(\frac{B_1}{m_1}-\frac{B_2}{m_2}\right).\sin\theta_2}{\frac{\beta}{2}\frac{\left(2+3e^2\right)}{\left(1-e^2\right)^{7/2}}+\frac{3}{\left(1-e^2\right)^{1/2}}},\frac{2f}{\beta}\frac{\left(1-e^2\right)^2}{\left(2+3e^2\right)}\right] \qquad \ldots \quad (8)$$

4. Stability of the equilibrium position

Liapunov's theorem[10] is applied to test the stability of the equilibrium position given by (8).

Let us assume that there are small variations in the co-ordinates at the given equilibrium position denoted by δ_1 and δ_2, then

$$\begin{aligned} X &= X_0+\delta_1, & Y &= Y_0+\delta_2 \\ \therefore X' &= \delta_1' & Y' &= \delta_2' \\ \therefore X'' &= \delta_1'' & Y'' &= \delta_2'' \end{aligned} \qquad \ldots \quad (9)$$

Using (9) in the equations (1), a set of variational equations comes to the form

$$\delta_1''-2\delta_2'-\left(X_0+\delta_1\right)\left[\frac{3}{\left(1-e^2\right)^{1/2}}+\frac{\beta\left(2+3e^2\right)}{2\left(1-e^2\right)^{7/2}}\right]=\left(\frac{B_1}{m_1}-\frac{B_2}{m_2}\right).\frac{\sin\theta_2}{\pi}-A\cos i$$

and

$$\delta_2''+2\delta_1'-\beta\left(Y_0+\delta_2\right)\frac{\left(2+3e^2\right)}{2\left(1-e^2\right)^{7/2}}=-\frac{f}{\left(1-e^2\right)^{3/2}} \qquad \ldots \quad (10)$$

where $\in=0$ and $\propto=0$.

As the original equations (1) admit Jacobian integral, the variational equations of motion (10) will also admit Jacobian integral.

Multiplying the first and second equations of (10) by $2\delta_1'$ and $2\delta_2'$ respectively, adding them and then integrating the final equation, we get the Jacobian integral at the equilibrium position as

$$\delta_1'^2+\delta_2'^2+\delta_1^2\left[\frac{-3}{\left(1-e^2\right)^{1/2}}-\frac{\beta}{2}\frac{\left(2+3e^2\right)}{\left(1-e^2\right)^{7/2}}\right]+\delta_2^2\left[-\frac{\beta}{2}\frac{\left(2+3e^2\right)}{\left(1-e^2\right)^{7/2}}\right]$$

$$+\delta_1\left[2\left\{A\cos i-\left(\frac{B_1}{m_1}-\frac{B_2}{m_2}\right).\frac{\sin\theta_2}{\pi}-\frac{3X_0}{\left(1-e^2\right)^{1/2}}-\frac{\beta X_0}{2}\frac{\left(2+3e^2\right)}{\left(1-e^2\right)^{7/2}}\right\}\right]$$

$$+\delta_2\left[2\left\{\frac{f}{\left(1-e^2\right)^{3/2}}-\frac{\beta Y_0}{2}\frac{\left(2+3e^2\right)}{\left(1-e^2\right)^{7/2}}\right\}\right]=h_1 \qquad \ldots \quad (11)$$

h_1 is the constant of integration at the equilibrium position.

To test the stability in the sense of Liapunov[7], Jacobian integral is taken as Liapunov's function

$L\left(\delta_1',\delta_2',\delta_1,\delta_2\right)$ as

$$L\left(\delta_1',\delta_2',\delta_1,\delta_2\right)=\delta_1'^2+\delta_2'^2+\delta_1^2\left[\frac{-3}{\left(1-e^2\right)^{1/2}}-\frac{\beta}{2}\frac{\left(2+3e^2\right)}{\left(1-e^2\right)^{7/2}}\right]+\delta_2^2\left[-\frac{\beta}{2}\frac{\left(2+3e^2\right)}{\left(1-e^2\right)^{7/2}}\right]$$

$$+\delta_1\left[2\left\{A\cos i-\left(\frac{B_1}{m_1}-\frac{B_2}{m_2}\right).\frac{\sin\theta_2}{\pi}-\frac{3X_0}{\left(1-e^2\right)^{1/2}}-\frac{\beta X_0}{2}\frac{\left(2+3e^2\right)}{\left(1-e^2\right)^{7/2}}\right\}\right]$$

$$+\delta_2\left[2\left\{\frac{f}{\left(1-e^2\right)^{3/2}}-\frac{\beta Y_0}{2}\frac{\left(2+3e^2\right)}{\left(1-e^2\right)^{7/2}}\right\}\right] \qquad \ldots \quad (12)$$

5. Results and discussion

We take L as Liapunov's function. As L is the integral of the system of variational equations (10), its differential taken along the trajectory of the system must vanish identically. Hence, only condition that the unperturbed position be stable in the sense of Liapunov is that L must be positive definite. For making the function (12), a positive definite function, it is necessary that the function does not have terms of first order in the variables whereas the terms of the second order must satisfy the Sylvestor's conditions for positive definiteness of quadrative forms. Hence, the sufficient conditions for the stability of the system at the equilibrium position are

$$(i)\quad -\left[\frac{12\mu k_2}{R^5}\left(\frac{m_1+m_2}{m_1}\right)\frac{1}{(1-e^2)^{1/2}}+\frac{p^3}{2\mu}\left(\frac{m_1+m_2}{m_1m_2}\right)\frac{(2+3e^2)}{(1-e^2)^{7/2}}+\frac{3}{(1-e^2)^{1/2}}\right]>0$$

$$(ii)\quad \left[\frac{3\mu k_2}{R^5}\left(\frac{m_1+m_2}{m_1}\right)\frac{1}{(1-e^2)^{1/2}}-\frac{p^3}{\mu}\left(\frac{m_1+m_2}{m_1m_2}\right)\frac{(2+3e^2)}{2(1-e^2)^{7/2}}\right]>0$$

$$(iii)\quad \left[2A\cos i-2\left(\frac{B_1}{m_1}-\frac{B_2}{m_2}\right)\frac{\sin\theta_2}{\pi}-\frac{24\mu k_2}{R^5}\left(\frac{m_1+m_2}{m_1}\right)\cdot\frac{1}{(1-e^2)^{1/2}}X_1\right.$$
$$\left.-\frac{p^3}{\mu}\left(\frac{m_1+m_2}{m_1m_2}\right)\frac{(2+3e^2)}{(1-e^2)^{7/2}}X_1-\frac{6}{(1-e^2)^{1/2}}X_1\right]=0 \qquad \ldots \quad (13)$$

6. Conclusion

Conditions (13) are analyzed separately. Here, all the three conditions for stability of the equilibrium position are not identically satisfied simultaneously. Hence, the equilibrium position is unstable in the sense of Liapunov.

Acknowledgements

I am thankful to U. G. C. Kolkata for providing me the Research Project with Sanction Letter No. F. PSB-005/15-16, dated 15.11.2016. I am also thankful to Prof. R. K. Sharma from Thiruvanathapuram for his encouragement.

References

1. Beletsky, V. V. and Novikova, E. T. − Kosmicheskie Issledovania, **7 (6)**, pp. 377 - 384 (1969).
2. Beletsky, V. V. − Kosmicheskie Issledovania, **7 (6)**, pp. 827-840 (1969).
3. Singh, R. B. and Demin, V. G. − Cel. Mech., **06**, pp. 268-277 (1972).
4. Singh, R. B. − Astronau. Acta, **18**, pp. 301-308 (1973).
5. Das, S. K., Bhattacharya, P. K. and Singh, R. B. − Proc. Nat. Acad. Sci. India, **46**, pp. 287- 299 (1976).
6. Kumar, S. and Bhattacharya, P. K. − Proc. Workshop on Spa. Dyn. and Cel. Mech., Muz., India, Eds. K.B. Bhatnagar and B. Ishwar, pp. 71-74 (1995).
7. Kumar, S., Srivastava, U. K. and Bhattacharya, P. K. − Proc. Math. Soc. B. H. U., **21**, pp. 51- 61 (2005).
8. Prasad, J. D. and Kumar, S. − Jour. Pur. Acad. Sci. Jaunpur, India, **17 (Phy. Sci.)**, pp. 27-34 (2011).
9. Kumar, S. − Indian Jour. of Theo. Phys., **65,** Nos.1& 2, pp. 49-56 (2017).
10. Liapunov, A. M. − Sabrania Sachimeiviya, Moscow (Russian), **2N**, pp. 327-335 (1959).

INDIAN JOURNAL OF THEORETICAL PHYSICS, VOL. 65, NOS. 3 & 4, 2017

Gravitation and cosmology in Finsler spacetime

S. S. De

Department of Applied Mathematics,
University of Calcutta
e-mail : ssddadai08@rediffmail.com

[**Abstract :** Gravitation and cosmology have been considered in an anisotropic spacetime which is (α, β) – Finsler spacetime. In this background spacetime of our universe, the modified Einstein field equations have been constructed and these equations are found to be insensitive to the different connections of Finsler space. From the barotropic equation of state, with an introduction of a pressure from the anisotropic pressure components and anisotropic force, the equation for the scale factor of the expanding universe has been obtained. The late-time accelerated expansion of our universe has been obtained as the solution of this equation without introducing any dark energy.]

1. Introduction

One of the recent cosmological observations is the accelerated expansion of our universe. The standard model of cosmology, the *ΛCDM* cosmological model, which incorporates the cosmological constant Λ with the cold dark matter can successfully resolve this phenomenon. But it suffers from two major difficulties, namely, the cosmological constant problem and the cosmic coincidence problem. The first one is regarding extremely small current value of vacuum energy density $\left(\rho_{\wedge} = c^2 \wedge \Big/ 8\pi G \approx 10^{-47}\, GeV^4\right)$ in the scenario of field theory or string theory. On the other hand, the second problem is about too much closeness of density of matter with the vacuum energy density. Other alternative theories also include more peculiar dark energies (*DE*) but they suffer with similar difficulties[1]. With the modifications of Einstein – Hilbert action other modified gravity theories, such as, *f*(*R*) gravity, *f*(*T*) gravity, scalar tensor theories, Gauss-Bonnet

gravity, Hoŗava – Lifshitz gravity, nonlinear massive gravity, etc.[2] have been proposed to resolve the phenomenon of accelerated expansion of the universe, but these models have no physical foundation, or, contain too many parameters.

The standard model (ΛCDM model) is based on the important assumption which states that our universe is homogeneous and isotropic in character in the large scale apart from the said introduction of *DE*. But recent observational data of Planck Collaboration[3] indicate some anomalous phenomena which are not in consistent with the basic assumption of ΛCDM model (isotropy of spacetime). Some of these data which are particularly important point out hemispherical asymmetry and parity asymmetry. Also, other astronomical observations[4] show a preferred direction in the galactic coordinate system for the maximum acceleration of the universe, and also, variation of fine structure constant at large scales. All these observational facts clearly indicate that our universe has a preferred direction which means that the background spacetime of the universe is anisotropic in nature. Therefore, gravitational behavior and cosmology should be considered in a spacetime which is inherently anisotropic.

Finsler spacetime is a spacetime that breaks the isotropic symmetry of the Riemannian spacetime or that of *FRW* background spacetime in the case of cosmological consideration. Finsler geometry is a generalization of Riemannian geometry and it was, in fact, suggested by Riemann himself[5] in 1854. It was later developed by Paul Finsler[6] in 1918. Presently, cosmology in a particular Finsler spacetime will be explored by constructing gravitational field equations in that spacetime, without introducing any *DE*.

This paper is organized as follows. In section 2, we shall give a brief introduction of Finsler geometry. In section 3, a particularly relevant Finsler space is introduced as the background spacetime of the universe. The killing equation in this Finsler space has been obtained by using isometric transformation of structure. It was shown there that the symmetry of Riemannian space has been broken in this spacetime. In the subsequent sections 4 and 5, gravitational field equations in Finsler spacetime have

been obtained. With an equation of state, the solution for the scale factor which can explain the accelerated expansion of the universe has been found. In section 6, some concluding remarks have been made.

2. Finsler space

In 1854, Riemann[5] suggested that the positive nth root of a nth order differential form might serve as a metric function. In particular, the positive 4th root of a 4th order differential form can be taken as the distance element between two neighboring points, *i.e.*,

$$ds^4 = g(x)_{\mu\nu\rho\sigma}\, dx^\mu dx^\nu dx^\rho dx^\sigma \qquad \ldots \quad (1)$$

Now, for the displacement along the connecting curve $\gamma(s)$ with tangent $y^\mu = \frac{dx^\mu}{ds}$, one can write Eq. (1) as

$$F^4_{(4)} = g(x)_{\mu\nu\rho\sigma}\, y^\mu y^\nu y^\rho y^\sigma \qquad \ldots \quad (2)$$

where $F^4_{(4)}$ is homogeneous of fourth order in y^μ's.

From (2), it follows that

$$F^4_{(4)} = G_{\mu\nu}(x, y)\, y^\mu\, y^\nu$$

where $G_{\mu\nu}(x, y) = g(x)_{\mu\nu\rho\sigma}\, y^\rho\, y^\nu$ is now a homogeneous function of second order in y^μ,s, and if it is written as $G_{\mu\nu}(x, y) = g_{\mu\nu}(x, y)\, F_{(2)}(x, y)$ where $F_{(2)}(x, y)$ is homogeneous of second order and $g_{\mu\nu}(x, y)$ is a zero order homogeneous function in y^μ; we have

$$\frac{F^4_{(4)}}{F_{(2)}} \equiv F^2(x, y) = g_{\mu\nu}(x, y)\, y^\mu\, y^\nu \qquad \ldots \quad (3)$$

where $F(x, y)$ is now homogeneous of first order in y^μ,s. In this way we arrive at the fundamental function $F(x, y)$ representing Finsler structure. Its dependence on the position coordinates x^μ and to the fiber coordinates y^μ indicates that the geometry of Finsler space is a geometry on the tangent bundle *TM*. The position dependence of Riemannian geometry is here replaced by the pair (x^μ, y^μ), known as element of support, x^μ being the coordinates of base manifold *M*. In physical applications, the fiber

coordinates y^μ are interpreted as internal variable, cosmic flow line, velocity of the observer etc.

The above $g_{\mu\nu}(x, y)$ is not, in general, the Finsler metric tensor, but simply represents a homogeneous tensor of degree zero for defining F. In fact, the metric tensor of Finsler space is defined as

$$g_{\mu\nu}(x, y) = \frac{1}{2}\frac{\partial^2 F^2}{\partial y^\mu \partial y^\nu}, \quad y^\mu \neq 0 \qquad \ldots \quad (4)$$

and, we can then arrive at the relation (3) for the Finsler structure F having the property :

$$F(x, \lambda y) = \lambda F(x, y) \text{ for all } \lambda > 0 \qquad \ldots \quad (5)$$

It should be noted that the distance element ds is given by

$$ds = F(x, dx) \qquad \ldots \quad (6)$$

Consequently, the distance traversed on the base manifold along a direction y^μ is given by the integral

$$I = \int F(x, y)\, ds \qquad \ldots \quad (7)$$

and geodesic equation for Finsler space can be obtained by applying the principle of least action on this integral. It is given by

$$\frac{d^2 x^\mu}{ds^2} + 2G^\mu = 0 \qquad \ldots \quad (8)$$

where G^μ is called spray coefficients of Finsler space, is given by[7]

$$G^\mu = \frac{1}{4} g^{\mu\nu}\left(\frac{\partial^2 F^2}{\partial x^\lambda \partial y^\nu} y^\lambda - \frac{\partial F^2}{\partial x^\nu}\right) \qquad \ldots \quad (9)$$

The geodesic equation (8) ensures that the Finslerian structure F is constant along the geodesic.

3. A Finsler space as background spacetime of universe

We here introduce the following Finslerian structure F for the background spacetime of our universe.

$$F^2 = y^t y^t - R^2(t)\, y^r y^r - r^2 R^2(t)\, \bar{F}^2(\theta, \phi, y^\theta, y^\phi) \qquad \ldots \quad (10)$$

Here, $\bar{F}^2$ is proposed to be of the form :

$$\bar{F}^2 = y^\theta y^\theta + f(\theta, \phi)\, y^\phi y^\phi \qquad \ldots \quad (11)$$

$\overline{F}$ can be regarded as the Finsler structure of the two dimensional Finsler space. The metric tensors for the Finsler space[8] are given by

$$\bar{g}_{ij} = diag\,(1,\, f(\theta,\phi)) \quad \text{and} \quad \bar{g}^{ij} = diag\left(1, \frac{1}{f(\theta,\phi)}\right) \qquad \ldots \quad (12)$$

[$i, j = 2, 3$ or, θ, ϕ]

The geodesic spray coefficients calculated from the Finsler structure $\overline{F}$ are

$$G^2 = -\frac{1}{4}\frac{\partial f}{\partial \theta}\, y^{\phi}\, y^{\phi} \qquad \ldots \quad (13a)$$

$$G^3 = \frac{1}{4f}\left(2\frac{\partial f}{\partial \theta}\, y^{\theta}\, y^{\phi} + \frac{\partial f}{\partial \phi}\, y^{\phi}\, y^{\phi}\right) \qquad \ldots \quad (13b)$$

In order to consider gravitation, we require a geometrical quantity which is the Ricci scalar. In Finsler geometry there is geometrically invariant Ricci scalar. This is given by[7]

$$Ric \equiv R^{\mu}_{\mu} = \frac{1}{F^2}\left(2\frac{\partial G^{\mu}}{\partial x^{\mu}} - y^{\lambda}\frac{\partial^2 G^{\mu}}{\partial x^{\lambda}\partial y^{\mu}} + 2G^{\lambda}\frac{\partial^2 G^{\mu}}{\partial y^{\lambda}\partial y^{\mu}} - \frac{\partial G^{\mu}}{\partial y^{\lambda}}\frac{\partial G^{\lambda}}{\partial y^{\mu}}\right) \qquad \ldots \quad (14)$$

where

$$R^{\mu}_{\upsilon} = R^{\mu}_{\lambda\upsilon\rho}\, y^{\lambda}\, y^{\rho} \Big/ F^2 \qquad \ldots \quad (15)$$

It is to be noted that although $R^{\mu}_{\lambda\upsilon\rho}$ depends on connections, R^{μ}_{υ} does not. Consequently, the Ricci scalar depends only on the Finsler structure F, and is insensitive to connections, such as Chern connection, Cartan connection, ect. In fact, in Finsler gravity the vacuum field equation is given by $Ric = 0$.

Now, for Finsler structure $\overline{F}$, the Ricci scalar $\overline{Ric}$ can be found as

$$\overline{F}^2\,\overline{Ric} = \left\{-\frac{1}{2f}\frac{\partial^2 f}{\partial \theta^2} + \frac{1}{4f^2}\left(\frac{\partial f}{\partial \theta}\right)^2\right\}\left(y^{\theta}\, y^{\theta} + f\, y^{\phi}\, y^{\phi}\right) + y^{\theta}\, y^{\phi}\left(\frac{1}{f^2}\frac{\partial f}{\partial \theta}\frac{\partial f}{\partial \phi}\right) \qquad \ldots \quad (16)$$

The coefficient of $y^{\theta}y^{\phi}$ is zero if f is independent of ϕ, *i.e.*,

$$f(\theta, \phi) = f(\theta) \qquad \ldots \quad (17)$$

We have in this case,

$$\overline{Ric} = -\frac{1}{2f}\frac{\partial^2 f}{\partial \theta^2} + \frac{1}{4f^2}\left(\frac{\partial f}{\partial \theta}\right)^2 \qquad \ldots \quad (18)$$

For the constant flag curvature, that is, for $\overline{Ric} = \lambda$, where λ is a constant, we have the following equation for specification of the function :

$$-\frac{1}{2f}\frac{\partial^2 f}{\partial \theta^2} + \frac{1}{4f^2}\left(\frac{\partial f}{\partial \theta}\right)^2 = \lambda \qquad \ldots \quad (19)$$

In more general case λ may be taken as a function of θ. For $\overline{Ric} = \lambda$, one can find the Finsler structure $\overline{F}$ as

$$\overline{F}^2 = \begin{cases} y^\theta y^\theta + A \sin^2\left(\sqrt{\lambda}\theta\right) y^\phi y^\phi, & \text{if } \lambda > 0 \\ y^\theta y^\theta + A\theta^2 y^\phi y^\phi, & \text{if } \lambda = 0 \\ y^\theta y^\theta + A \sinh^2\left(\sqrt{-\lambda}\theta\right) y^\phi y^\phi, & \text{if } \lambda < 0 \end{cases} \qquad \ldots \quad (20)$$

The constant A may be taken as unity without any loss of generality.

Thus, for the case of $\lambda > 0$, we have following form of the Finsler structure (10) :

$$F^2 = \alpha^2 + r^2 R^2(t)\, \chi(\theta)\, y^\phi y^\phi \qquad \ldots \quad (21)$$

where $\chi(\theta) = \sin^2\theta - \sin^2\left(\sqrt{\lambda}\theta\right)$ $\qquad \ldots \quad (22)$

and α is a Riemannian metric, which is given by

$$\alpha^2 = y^t y^t - R^2(t)\, y^r y^r - r^2 R^2(t)\,(y^\theta y^\theta + \sin^2\theta y^\phi y^\phi) \qquad \ldots \quad (23)$$

We can also write the Finsler structure (21) as

$$F = \alpha\, \phi(s), \qquad \phi(s) = \sqrt{1+s^2} \qquad \ldots \quad (24)$$

where $$s = \frac{\left(b_\phi\, y^\phi\right)}{\alpha} = \frac{\beta}{\alpha} \qquad \ldots \quad (25)$$

with $b_\mu = (0, 0, 0, b_\phi), \qquad b_\phi = r\, R(t)\, \sqrt{\chi(\theta)}$

$\beta = b_\mu y^\mu = b_\phi y^\phi$ is an one form.

The relation (24) shows that F is the metric function of (α, β)-Finsler space.

We, now, write the Killing equation $K_V(F) = 0$ in Finsler space by using isometric transformations of Finsler structure as[9]

$$\left(\phi(s) - s\frac{\partial\phi(s)}{\partial s}\right)K_V(\alpha) + \frac{\partial\phi(s)}{\partial s}K_V(\beta) = 0 \qquad \ldots \quad (26)$$

where $$K_V(\alpha) = \frac{1}{2\alpha}\left(V_{\mu/\upsilon} + V_{\upsilon/\mu}\right)y^\mu\, y^\upsilon \qquad \ldots \quad (27)$$

$$K_V(\beta) = \left(V^\mu\frac{\partial b_\upsilon}{\partial x^\mu} + b_\mu\frac{\partial V^\mu}{\partial x^\upsilon}\right)y^\upsilon \qquad \ldots \quad (28)$$

The symbol "$|$" means the covariant derivative with respect to the Riemannian metric α. From these equations it follows that

$$K_V(\alpha) + s\,K_V(\beta) = 0 \quad \text{or,} \quad \alpha K_V(\alpha) + \beta K_V(\beta) = 0.$$

Consequently, we have

$$K_V(\alpha) = 0 \quad \text{and} \quad K_V(\beta) = 0 \qquad \ldots \quad (29)$$

or,

$$V_{\mu/\upsilon} + V_{\upsilon/\mu} = 0 \qquad \ldots \quad (30)$$

and $$V^\mu\frac{\partial b_\upsilon}{\partial x^\mu} + b_\mu\frac{\partial V^\mu}{\partial x^\upsilon} = 0 \qquad \ldots \quad (31)$$

Here, the second Killing equation constrains the first one which is the Killing equation of the Riemannian space. This is responsible for breaking the symmetry (isometric) of the Riemannian space.

It is here to be noted that the present Finsler space (for the case F^2 as quadric in y^θ and y^ϕ) can be obtained from a Riemannian manifold (M, $g_{\mu\upsilon}(x)$) as we have

$$F(x, y) = \sqrt{g_{\mu\upsilon}(x)\, y^\mu\, y^\upsilon} \qquad \ldots \quad (32)$$

4. Gravitational field equations

We have pointed out that the two dimensional Finsler space $\overline{F}$ has been specified as a constant flag curvature space as it was assumed $\overline{Ric} = \lambda$. This flag curvature of Finsler space is, in fact, the generalization of the sectional curvature of Riemannian space. However, for more general case, the Finsler space is specified by θ-dependent flag curvature. But presently our Finsler space (10) is specified with the real valued constant flag curvature λ. For the case $\lambda = 1$ we get the usual *FRW* universe.

The geodesic spray coefficients for the present Finsler space can be found as

$$G^t = \frac{1}{4} a' \left[r^2 \, \overline{F}^2 + y^r \, y^r \right] \quad \ldots \quad (33)$$

[Here, we write $R^2 = a$ for convenience, and prime indicates the derivative with respect to time]

$$G^r = \frac{1}{2a} \left[a' \, y^r \, y^t - r \, a \, \overline{F}^2 \right] \quad \ldots \quad (34)$$

$$G^\theta = \overline{G}^\theta + y^\theta \left[\frac{1}{r} y^r + \frac{a'}{2a} y^t \right] \quad \ldots \quad (35)$$

$$G^\phi = \overline{G}^\phi + y^\phi \left[\frac{1}{r} y^r + \frac{a'}{2a} y^t \right] \quad \ldots \quad (36)$$

With these spray coefficients, the Ricci scalar can be computed as

$$F^2 Ric = \overline{F}^2 \left\{ \overline{Ric} - 1 + \frac{r^2}{2} \left(a'' + \frac{(a')^2}{2a} \right) \right\} + \frac{1}{2} y^r \, y^r \left(a'' + \frac{(a')^2}{2a} \right) - \frac{3}{2} y^t \, y^t \left(\frac{a''}{a} - \frac{(a')^2}{2a^2} \right) \quad \ldots \quad (37)$$

As there are different types of connections in Finsler geometry compared to only one torsion free connection in Riemannian geometry (the Christoffel connection), different approaches are prevalent in constructing gravitational field equations in Finsler space. As the result, these equations are not equivalent to each other. But we shall here follow the notion of Ricci tensor

in Finsler geometry, that was first introduced by Akbar-Zadeh[10], and construct the field equations in Finsler space following Li Xin, et al[8]. In these, Ricci tensor is constructed from the Ricci scalar, Ric, which is insensitive to connections. It is given by

$$Ric_{\mu\nu} = \frac{\partial^2\left(\frac{1}{2}F^2\, Ric\right)}{\partial y^\mu\, \partial y^\nu} \quad \ldots \quad (38)$$

The scalar curvature in Finsler geometry is given as

$$S = g^{\mu\nu}\, Ric_{\mu\nu} \quad \ldots \quad (39)$$

and for the present Finsler geometry, it is found to be

$$S = -\frac{3a''}{a} - \frac{2(\lambda - 1)}{r^2 a} \quad \ldots \quad (40)$$

The modified Einstein tensor in Finsler spacetime,

$$G_{\mu\nu} \equiv Ric_{\mu\nu} - \frac{1}{2} g_{\mu\nu}\, S \quad \ldots \quad (41)$$

yields

$$G_t^t = \frac{3(a')^2}{4a^2} + \frac{\lambda - 1}{r^2 a} \quad \ldots \quad (42)$$

$$G_r^r = \frac{a''}{a} - \frac{(a')^2}{4a^2} + \frac{\lambda - 1}{r^2 a} \quad \ldots \quad (43)$$

$$G_\theta^\theta = G_\phi^\phi = \frac{a''}{a} - \frac{(a')^2}{4a^2} \quad \ldots \quad (44)$$

Now, let us assume the general energy-momentum tensor

$$T_\nu^\mu = (\rho + p_t) u^\mu\, u_\nu - p_t\, g_\nu^\mu + (p_r - p_t)\eta^\mu\, \eta_\nu \quad \ldots \quad (45)$$

where $u^\mu\, y_\mu = -\eta^\mu\, \eta_\mu = 1$, p_r, p_t are respectively denote the pressures of the anisotropic fluid in the radial and transversal directions. Consequently, the modified gravitational field equations in Finsler spacetime are obtained (in terms of scale factor $R(t)$) as

$$8\pi_F G\rho = \frac{3\dot{R}^2}{R^2} + \frac{\lambda - 1}{r^2 R^2} \quad \ldots \quad (46)$$

$$8\pi_F G p_r = -\frac{2\ddot{R}}{R} - \frac{\dot{R}^2}{R^2} - \frac{\lambda - 1}{r^2 R^2} \quad \ldots \quad (47)$$

$$8\pi_F G p_r = -\frac{2\ddot{R}}{R} - \frac{\dot{R}^2}{R^2} \quad \ldots \quad (48)$$

It should be noted that for $\lambda = 1$, $p_r = p_t$, and we recover the gravitational field equations for flat *FRW* universe. On the other hand, if we put $p_r = p_t$ in the above field equations, we readily find $\lambda = 1$. Hence, we find $\lambda = 1$ corresponds *FRW* universe and vice versa. Here, to denote the volume of $\overline{F}$ we have used[7] $4\pi_F$. Also, in deducing the above gravitational field equations in Finsler spacetime, we have used the following proposal by Li, et al[8]. It is given by

$$\left(G_\upsilon^\mu - 8\pi G_F T_\upsilon^\mu\right)_{/M} = 0 \quad \ldots \quad (49)$$

where '$|M$' means that the gravitational field equation (49) restricted to base space *M*. It was argued there that the above field equation is insensitive to connections. Also, this field equation could be derived approximately from the formation of Pfeifer, et al[11], who have constructed gravitational dynamics for Finsler spacetimes in terms of an action integral on the unit tangent bundle. The base manifold of the Finsler space, thus, regulates the gravitational field equation in Finsler space, and the fiber coordinates y^μ play the role of the velocities of the cosmic components, that is, the fluid velocities in the energy momentum tensor. Again, as pointed out earlier, our Finsler spacetime can be regarded as a Riemannian manifold with metric (32). Therefore, one can proceed to find the Einstein gravitational field equations using the usual Christoffel connection of Riemann geometry. The metric $g_{\mu\upsilon}$ is given as

$$g_{\mu\upsilon} = diag\,(1, -R^2(t), -r^2 R^2(t) \sin^2 \sqrt{\lambda}\theta) \quad \ldots \quad (50)$$

The field equations obtained in this usual way can be found to be the same as those given in (46), (47) and (48). Thus, in our case of background spacetime of the universe, the gravitational field equations are exact.

5. Accelerating universe

We propose a pressure P composed from the pressure components p_r, p_t and an anisotropic pressure due to the anisotropic force r^3F_a where $F_a = \dfrac{2(p_t - p_r)}{r}$. With this pressure P, we can impose barotropic equation of state

$$P = \omega\rho \qquad \ldots \quad (51)$$

where the pressure P is taken as

$$P = (1+\omega)\, p_t - \omega\, p_r + \frac{m^2 r^3}{2} F_a \qquad \ldots \quad (52)$$

Here, m is an arbitrary constant whose dimension is that of mass (in the natural unit $c = \hbar = 1$). We can take m = 1, or in the case of no contribution of anisotropic force to the pressure, it can take the value zero, *i.e.*, m = 0. Regarding the pressure P as given in (52), we can say that a pressure for an imperfect fluid is defined as the negative of average of the normal stresses in three orthogonal directions. As the pressure in a direction is the negative of the normal stress in that direction, we have

$$P = \frac{1}{3}(p_r + p_t + p_t) = \frac{1}{3}\, p_r + \frac{2}{3}\, p_t \qquad \ldots \quad (53)$$

This pressure is, in fact, a special case for the pressure in the relation (52), with $\omega = -\dfrac{1}{3}$, m = 0. By using the field equations (46), (47) and (48), this pressure in (53) gives rise to the usual energy conservation equation for the homogeneous and isotropic universe, that is

$$\frac{\partial\rho}{\partial t} + 3H\,(\rho + P) = 0 \qquad \ldots \quad (54)$$

together with a relation

$$\frac{\partial\rho}{\partial r} = -F_a \qquad \ldots \quad (55)$$

Obviously the pressure P plays the role of an effective pressure. These two equations (54) and (55) give the energy conservation equation as

$$d\,(\rho\, V) = -P\, dV - V\, F_a\, dr \qquad \ldots \quad (56)$$

The general expression for the pressure in (52) consists of the weighted average of the pressure components p_t and p_r, and the contribution from the anisotropic force

Now, by using the barotropic equation of state (51) with pressure in (52), we have from the field equations (46), (47), (48) of Finsler spacetime, the following equation for the scale factor *R(t)* :

$$\ddot{R}+\frac{1+3\omega}{2}\frac{\dot{R}^2}{R}-\frac{m^2(\lambda-1)}{2R}=0 \qquad \ldots \quad (57)$$

It is to be noted that the term λ plays a crucial role in the field equations in Finsler space and, in fact, it arises from the anisotropic nature of the Finsler geometry itself.

We can find the solution for the scale factor *R(t)* for different values of ω. For the dust case ($\omega = 0$) of the universe, a solution of the equation (57) can be found as

$$R(t) = At \qquad \ldots \quad (58)$$

where *A* is a constant. This scale factor corresponds to the mild inflation as considered by De[11] for the very early universe in its particle creation era. On the other hand for $\omega = -1$, the above equation (57) becomes

$$\ddot{R}=\frac{1}{R}\left\{\dot{R}^2+C\right\} \qquad \ldots \quad (59)$$

where

$$C=\frac{m^2(\lambda-1)}{2}$$

The solution can readily found to be as follows :

$$R(t)=R(0)\cosh\ kt+\frac{\dot{R}(0)}{k}\sinh kt \qquad \ldots \quad (60)$$

where

$$k^2=\frac{\dot{R}^2(0)+\dfrac{m^2(\lambda-1)}{2}}{R^2(0)} \qquad \ldots \quad (61)$$

Here, $R(0)$ and $\dot{R}(0)$ are uncorrelated initial values of $R(t)$ and $\dot{R}(t)$ respectively. At late times $\left(t >> \frac{1}{k} \right)$, we have

$$R(t) = \frac{1}{2}\left\{ R(0) + \frac{\dot{R}(0)}{k} \right\} e^{kt} \, \alpha \, e^{kt} \qquad \ldots \quad (62)$$

which leads to accelerated expansion of the universe.

6. Concluding remarks

We have considered here the gravitation and cosmology in an anisotropic spacetime which is a special type of Finsler space. The modified Einstein field equations have constructed and these equations are insensitive to the connections of Finsler geometry. In constructing them, we have followed the proposal of Li, et al[8] for the gravitational field equations restricted to the base space. There it was shown that such consideration is an approximation of the general formalion of Pfeifer, et al[10]. But, in our cases these equations are exact as they can be derived from the Riemannian spacetime equivalent to the special type (α, β)-Finsler space for the background spacetime of our universe.

The noteworthy fact is that a parameter λ arises in the gravitational field equations as well as in the equation which determines the scale factor for expansion of the universe. This parameter can be regarded as the measure of anisotropy of the Finsler spacetime which is anisotropic in nature. This parameter plays an important role in determining the "late time" when universe can have accelerated expansion. Also, there are solutions of the equation (57), which represent nonsingular universe. Presently, we have found an accelerated universe expansion without introducing any dark energy.

References

1. Caldwell, R.R., Dave, R. and Steinhardt, P.J. − Phys. Rev. Lett., **80**, 1582 (1988); Peebles, P.J. and Ratra, B. − Rev. Mod. Phys., **75**, 559, (2003); Padmanabhan, T. − Phys. Rept., **380**, 235, (2003); Saridakis, E.N. − Nucl. Phys., B**819**, 116, (2009); Cai, Y. – F., Saridakis, E.N., Setare, M.R. and Xia, J. − Q. Phys. Rept., **493**, 1-60, (2010).
2. Dvali, G., Gabadaze, G. and Porrati, M. − Phys. Lett., B**485**, 208, (2000); Starobinsky, A.A. − JETP Lett., **86**, 157, (2007); Pereira, S.H., Bessa, C.H.G. and

Lima, J.A.S. − Phys. Lett., B**690**, 103, (2010); Bengochea, G.R. and Ferraro, R. − Phys. Rev. D, **79**, 124019, (2009); Ferraro, R. and Fiorini, F. − Phys. Rev., D**75**, 084031, (2007); Chen, S.H., Dent, J.B., Dutta, S. and Saridakis, E.N. − Phy. Rev., D**83**, 023508, (2011); Fuji, Y. and Maeda, K. − The Scalar – Tensor Theory of Gravitation, Cambridge University Press (2003); Bauer, F., Sota, J. Stefan$\bar{c}$ic$'$, H. − Phys. Lett., B**688**, 269, (2010); Saridakis, E.N. − Eur. Phys. J.C. **67**, 229, (2010); Saridakis, E.N. − Class. Quant. Grav., **30**, 075003, (2013).

3. Planck Collaboration, arXiv : 1303.5062.
4. Antoniou, I. and Perivolaropoulos, L. − JCAP, **1012**, 012, (2012); Webb, J.K. et al., − Phys. Rev. Lett., **107**, 191101, (2011).
5. Riemann, G.F.B. − Uber die Hypothesen welche der Grunde leigen. Habilitation Thesis, University of Göttingen, (1854).
6. Finsler, P. − Uber Kurven und Flächen in Allgeneinen Räumen. Dessertation, University of Göttingen, (1918).
7. Li, X. and Chang, Z. − Phys. Rev. D **90**, 064049, (2014).
8. Li, X., Wang, S. and Chang, Z. − Comm. Theor. Phys., **61**, 111, (2013), (arXiv : 1309.1758).
9. Akbar-Zadeh, H. − Acad. Roy. Belg. Bull. Cl. Sci. (5) **74**, 281, (1988).
10. Pfeifer, C. and Wohlfarth, M.N.R. − Phys. Rev. D**85**, 064009, (2012).
11. De, S.S. − Int. Jour. Theor. Phys., **38**, 2419, (1999); De, S.S. − Int. Jour. Theor. Phys., **41**, 137, (2002); De, S.S. and Rahaman, F. − Finsler Geometry of Hadrons and Lyra Geometry : Cosmological Aspects, Lambert Academic Publishing, Germany, (2012).

INDIAN JOURNAL OF THEORETICAL PHYSICS, VOL. 65, NOS. 3 & 4, 2017

Self-preserving solutions for the kinetic energy spectrum in a particle-ladden homogeneous isotropic turbulent flow

S. K. Saha

Chaki Centre for Mathematics and Mathemetical Sciences,
Kolkata-700025
E-mail: sksaha30@gmail.com

and

H. P. Mazumdar

Honorary Visiting Professor, Indian Statistical Institute,
Kolkata-700108
E-mail: hpmi2003@yahoo.com

[**Abstract**: Self-preserving solutions of spectral equation governing the decay of turbulence energy spectrum in a particle- ladden homogeneous isotropic turbulent flow are obtained for the case of large Reynolds number. Asymptotic behaviour of such solutions for small and large values of wave number *k* are discussed.]

1. Introduction

In recent times much attention is paid to the prediction of particle-ladden turbulent flows as they occur in many technologically important areas. Research interest in these flows are generally two–fold *e.g.*, Islam and Mazumdar[1] considered the effect of turbulence on the particle concentration field and the modification of turbulence by the particles. We shall be concerned here with certain aspect of the problem how turbulence is modified by the particles when they are present in the flow in large enough concentration (Squares and Eaton[2]).

Theoretical investigations were carried out in this area by Tchen[3], Meck and Jones[4], Reeks[5], Nir and Pismen[6] and others. Most of these works involve studies of the influence of particle inertia on the turbulent dispersion

process. General confirmations of the conclusions made in these studies, were obtained from the experiments (Wells and Stock[7], Snyder and Lumley[8]). Reeks[9], Elghobashi and Truesdell[10], Yeung and Pope[11] and Squares and Eaton[2] have carried out numerical simulation of particle-ladden turbulent flows. It is difficult to make proper interpretations of the experimental data as they are valid only for the conditions of the experiment and can not be generalized (Elghobashi and Truesdell[12]). For example, when fine droplets (or particles) of diameters $\leq 250\mu$ are injected in a free turbulent jet, the turbulent intensity decreases, lowering the spreading rate of the half width of the jet, whereas the addition of the large particles of diameters $\geq 500\mu$ causes an increase in the turbulent intensity. Hardalupas, et al[13] observed opposite phenomena in their experimental investigation on a particle-ladden turbulent flow.

Rao[14] studied the final period decay of energy spectrum of a particle-ladden homogeneous isotropic turbulence by a similarity process. In the present paper an attempt is made to examine the similarity features of the decay of turbulence kinetic energy spectrum in a particle-ladden homogeneous isotropic turbulent flow. We shall assume that the size of the particles is sufficiently large so that the turbulence is attenuated by the dispersed phase.

2. Formulation of the problem

The spectral equation governing the decay of turbulence kinetic energy in a particle-ladden homogeneous isotropic turbulent flow, is given by (Baw and Peskin[15], Tsuji[16])

$$\frac{\partial}{\partial t}\mathrm{E(k,\,t)} = \mathrm{T(k,\,t)} - 2\nu k^2\mathrm{E(k,\,t)} - 2\beta\frac{\nu k^2}{\frac{1}{\tau}+\nu k^2}\mathrm{E(k,\,t)}, \qquad \ldots \quad (1)$$

where k is the wave number, ν is the kinematic viscosity, τ is the characteristic time $= \frac{2}{9}\frac{\rho_s\sigma^2}{\mu}$, ρ_s is the density of the solid material , σ is the radius of the particle, μ is the co-efficient of viscosity, $\beta = \frac{\rho_p}{\rho\tau}$, ρ_p is the volume concentration of the solid phase in the flow, ρ is the density of the gas.

$E(k, t) = 2\pi k^2 \varphi_{ii}(k, t)$, $\varphi_{ij}(k, t)$ being the Fourier transform of $\overline{v_i v_j'}$, the correlation between the fluctuating gas velocity components v_i and v_j' pertaining to the points $P(\vec{X})$ and $P'(\vec{X})$ inside the flow field;

$T(k, t) = 2\pi k^2 \Gamma_{ii}(k, t)$, $\Gamma_{ij}(k, t)$ is the Fourier transform of $\frac{\partial}{\partial r_k}(\overline{v_i v_k v_j'} - \overline{v_i v_j' v_k'})$, $\vec{r} = \overrightarrow{X'} - \vec{X}$.

The term on the left hand side of (1), describes the rate at which turbulence kinetic energy changes. The first term on the right hand side of (1) represents the transfer of kinetic energy at the wave number k due to turbulence self interactions. The second term describes the dissipation of turbulence kinetic energy due to the effects of molecular viscosity. The third term takes account of the effect due to the presence of particles, which are so massive that they are unaffected by the gas turbulent fluctuations (Wallace[17]). In the next section we seek self-preserving solution of equation (1).

3. Self-preserving solution for the turbulence energy spectrum

In order to solve equation (1), the energy transfer spectrum $T(k, t)$ is to be modeled. We accept the local form for $T(k, t)$, as suggested by A. M. Obukhov[18], *e.g.*,

$$T(k, t) = -2\gamma_2 \frac{d}{dk}\left[\int_k^\infty E(k,t)\, dk_1 \left\{\int_0^k k_2^2 E(k_2, t)\, dk_2\right\}^{1/2}\right], \quad \ldots \quad (2)$$

where γ_2 is a non-dimensional constant.

Substituting (2) in (1) we obtain

$$\frac{\partial}{\partial t}E(k, t) = -2\gamma_2 \frac{d}{dk}\left[\int_k^\infty E(k,t)\, dk_1 \left\{\int_0^k k_2^2 E(k_2, t)\, dk_2\right\}^{1/2}\right] - 2\nu k^2 E(k, t) - 2\beta \frac{\nu k^2}{\frac{1}{\tau}+\nu k^2} E(k, t). \quad \ldots \quad (3)$$

Based on the assumption that particles are essentially unaffected by the turbulence fluctuations, we may set

$$\frac{1}{\tau} << \nu k^2. \quad \ldots \quad (4)$$

It is to be remarked that when the condition (4) is satisfied, for every high frequency fluctuations of gas, gas-solid velocity correlations are negligible as the response time of the particle is sufficiently long (Wallace[17]).

In view of the relation (4), the equation (3) is reducible to

$$\frac{\partial}{\partial t}\mathrm{E(k,t)} = -2\gamma_2 \frac{d}{dk}\left[\int_k^\infty E(k,t)\,dk_1\left\{\int_0^k k_2^2 \mathrm{E}(k_2,\mathrm{t})\,\mathrm{d}k_2\right\}^{1/2}\right]$$

$$-2\nu k^2 \mathrm{E(k,t)} - 2\beta \mathrm{E(k,t)}. \qquad \ldots \quad (5)$$

We seek a general type of self-preserving solution of (5) in the form (Sen[19])

$$\mathrm{E(k,t)} = \frac{1}{\alpha^2 k_0^3 t_0^2}\frac{s^3}{\tau^2}\mathrm{f}\left(\frac{sk}{k_0}\right), \qquad \ldots \quad (6)$$

where α, k_0 , t_0 are constants, $\tau = \frac{t}{t_0}$.

Substituting (6) in (5) we obtain after simplifications

$$(3\mathrm{c}-2)\mathrm{f(x)} + \mathrm{cxf'(x)} = -\frac{2\gamma_2}{\alpha}\frac{d}{dx}\left[\int_x^\infty f(x_1)\,dx_1\left\{\int_0^x x_2^2 f(x_2)\,\mathrm{d}x_2\right\}^{1/2}\right]$$

$$-\frac{2}{Re}x^2\mathrm{f(x)} - 2\beta\,\mathrm{t\,f(x)}, \qquad \ldots \quad (7)$$

where

$$x = \frac{sk}{k_0},\ Re = \text{Reynolds number} = \frac{1}{\nu k_0^2 t_0},\ C = \frac{\tau s_\tau}{s},\ S_\tau = \frac{\partial s}{\partial \tau}.$$

If we take $c = \frac{1}{2}$, the equation (7) is transformed to

$$(3\mathrm{c}-2)\mathrm{f(x)} + \mathrm{cxf'(x)} = -\frac{2\gamma_2}{\alpha}\frac{d}{dx}\left[\int_x^\infty f(x_1)\,dx_1\left\{\int_0^x x_2^2 f(x_2)\,\mathrm{d}x_2\right\}^{1/2}\right]$$

$$-\frac{2}{Re}x^2\mathrm{f(x)} - 2\mathrm{MA}\sqrt{\mathrm{R}}\mathrm{f(x)}, \qquad \ldots \quad (8)$$

where

$$\mathrm{R} = \frac{\varepsilon t^2}{\nu},\ \mathrm{M} = \frac{\rho_p}{\rho} = \left(\frac{\rho_p}{\tau\rho}\right).\tau = \beta\tau,\ \mathrm{A} = \frac{1}{\tau}\sqrt{\frac{\nu}{\varepsilon}}.$$

Clearly equation (8) may admit self-preserving solution for different choices of MA if $R = \frac{\varepsilon t^2}{\nu}$ remains constant during decay process. Usually, R = constant applies to the wave number range of the energy containing eddies and it need not apply to equilibrium range of wave number. In order to describe the self-preserving features of the turbulence energy spectrum, Heisenberg[20] assumed that the energy containing eddies would be in quasi-equilibrium, so that we may consider them as if they are in equilibrium as far as possible in view of their finite rate of decay (Hinze[21]). We accept this

premise for our analysis of the present case. Let us discuss asymptotic behaviour of $f(x)$ for the cases (i) $x \to 0$ and (ii) $x \to \infty$, when turbulence is characterized by very large Reynolds number $Re \to \infty$.

Case I: Let

$$f(x) \sim Bx^n \text{ as } x \to 0; \quad \ldots (9)$$

B is a non-zero constant and $n > 0$.

Substituting (9) in equation (8), we obtain, after some calculation,

$$[(3c - 2) + nc + 2MA\sqrt{R}]x^n - \frac{\gamma_2\sqrt{B}}{\alpha(n+1)\sqrt{(n+3)}}(3n + 5)\, x^{\frac{3n+3}{2}} = 0. \quad \ldots (10)$$

As $n>0$ and $x \to 0$, it is easily seen that the first term of (10) is significant. Equating to zero the co-efficient of x^n, we obtain

$$n = \frac{2-3c}{c} - \frac{2MA\sqrt{R}}{c}, \text{ for } MA\sqrt{R} < \frac{2-3c}{2}. \quad \ldots (11)$$

The family of solutions given in (6) have the asymptotic behavior

$$f(x) \sim x^{\frac{2-3c}{c} - \frac{2MA\sqrt{R}}{c}}, (x \to 0), \text{ for } MA\sqrt{R} < \frac{2-3c}{2}. \quad \ldots (12)$$

For $c = \frac{1}{2}$, (12) gives

$$f(x) \sim x^{1-4MA\sqrt{R}}, (x \to 0), \text{ for } MA\sqrt{R} < \frac{1}{4}, \quad \ldots (13)$$

which correspondsto the Heisenberg's type sprectrum law

$$E(k, t) \sim k^{1-4MA\sqrt{R}}, (k \to 0), \text{ for } MA\sqrt{R} < \frac{1}{4}. \quad \ldots (14)$$

For $c = \frac{2}{5}$, (12) gives

$$f(x) \sim x^{2-5MA\sqrt{R}}, (x \to 0), \text{ for } MA\sqrt{R} < \frac{2}{5}, \quad \ldots (15)$$

which corresponds to the sprectrum law

$$E(k, t) \sim k^{2-5MA\sqrt{R}}, (k \to 0), \text{ for } MA\sqrt{R} < \frac{2}{5}. \quad \ldots (16)$$

Again for $c = \frac{1}{3}$, (12) gives

$$f(x) \sim x^{3-6MA\sqrt{R}}, (x \to 0), \text{ for } MA\sqrt{R} < \frac{1}{2}, \quad \ldots (17)$$

which corresponds to the sprectrum law

$$E(k, t) \sim k^{3-6MA\sqrt{R}}, (k \to 0), \text{ for } MA\sqrt{R} < \frac{1}{2}. \quad \ldots (18)$$

Further if we put $c = \frac{2}{7}$, in (12) we obtain

$$f(x) \sim x^{4-7MA\sqrt{R}}, (x\to 0), \text{ for } MA\sqrt{R} < \frac{4}{7}, \quad \ldots \quad (19)$$

which corresponds to the Loitsiansky type sprectrum law

$$E(k, t) \sim k^{4-7MA\sqrt{R}}, (k\to 0), \text{ for } MA\sqrt{R} < \frac{4}{7}. \quad \ldots \quad (20)$$

The constant of proportionality being Loitsiansky's constant if $MA = 0$ (cf. Loitsiansky[22], Lin[23] and Batcheler[24]).

Case II: Let

$$f(x) \sim B' x^{-n} \text{ as } x \to \infty; \quad \ldots \quad (21)$$

B' is a non-zero constant and $n > 0$.

Taking (21) into account, equation (8) is reducible to

$$[(3c-2) - nc + 2MA\sqrt{R}]x^{-n} - \frac{\gamma_{2\sqrt{B'}}}{\alpha(1-n)\sqrt{(3-n)}}(5-3n)x^{\frac{-3n+3}{2}} = 0. \quad \ldots \quad (22)$$

It can be easily seen that the second term on the left hand side of (22) is predominant if $n < 3$ and $n \neq 1$. Accepting this we equate the co-efficient of $x^{\frac{3(1-n)}{2}}$ to zero and obtain $n = \frac{5}{3}$. Thus in the case when the turbulence is characterised by sufficiently large Reynolds number the asymptotic behaviour of $f(x)$ as $x\to \infty$ is given by

$$f(x) \sim x^{-\frac{5}{3}}. \quad \ldots \quad (23)$$

This gives

$$E(k, t) \sim k^{-\frac{5}{3}}; (k \to \infty). \quad \ldots \quad (24)$$

4. Conclusion

In the above sections we have carried out the method on the assumption of modified Obukhov form for energy transfer through a homogeneous isotropic particle-ladden turbulent flow. It is shown that such calculations are valid for the asymptotic behaviour of energy spectrum $E(k, t)$ for wave numbers $k\to 0$ and $k\to\infty$. The results clearly show that the self-preserving solutions are admitted for different values of MA ($M = \frac{\rho_p}{\rho}$, $A = \frac{1}{\tau}\sqrt{\frac{\nu}{\varepsilon}}$) and R ($= \frac{\varepsilon t^2}{\nu}$) during the process of decay. Surprisingly it is observable that

several power laws exhibited by the energy spectra for different values of $MA\sqrt{R}$ which are in turn dependent on the choice of the parameter c and finally all the energy spectra behaving so differently for small values of $k \to 0$ ultimately merge to the energy spectrum $E(k, t) \sim k^{-\frac{5}{3}}$; $(k \to \infty)$.

References

1. Islam, N**.** and Mazumdar, H. P. − Ind. J. Theo. Phys., **44,** No. 1, 9-16 (1996).
2. Squires, K. D. and Eaton, J. K. − Phys. Fluids, **42**, 1191 (1990).
3. Tchen, C. M. − Ph. D. Dissertation , Delt, The Hague, Martinus Nijhoff (1947).
4. Meek, C. C. and Jones, B. G. − J. Atmos. Sci., **30**, 239 (1973).
5. Reeks, M. W. − J. Fluid Mech., **83**, 529 (1977).
6. Nir, A. and Pisman, L. M. − J. Fluid Mech., **94**, 369 (1979).
7. Wells , M. R. and Stock, D. E. − J. Fluid Mech., **136**, 31 (1983).
8. Snyder, W. H. and Lumbey, J. l. − J. Fluid Mech., **48**, 41 (1971).
9. Reeks, M. W. − J. Fluid Mech., **97**, 569 (1980).
10. Elghobashi, S. E. and Truesdell, G. C. − Phys. Fluids, A5, 7th Symposium on turbulent shear flows, Stanford University (1989).
11. Yeung , P. K. and Pope, S. B. − J. Fluid Mech., **207**, 531 (1989).
12. Elghobashi, S. E. and Truesdell, G. C. − Phys. Fluids, A5, 1790 (1993).
13. Hardalupus, Y. et al − Proc. Roy. Soc. London, Sec A **426**, 31 (1969).
14. Rao, C. S. − Studies in two phase gas-solids flow, Ph. D. Dissertation, University of Houston, Houston , U. S. A. (1970).
15. Baw , P. S. H. and Peskin, R. L. − Technical Report No. 188- MAE, NYO2930-31, Department of Mechanical and Aerospace Engineering, Rutgers – The state University, New Brunswick, New Jersey (1968).
16. Tsuji, Y. − In Encyclopedia of fluid Mechanics, edited by N. P. Cheremisinoff, **4**, 283 (1986).
17. Wallace, J. P. − A study of the fluid turbulence energy spectrum in a gas-solid suspension, Ph. D. Thesis, Rutgers University (1966).
18. Ellison, T. H. − The universal small scale spectrum of turbulence at high Reynolds number , Mechanique de la turbulence (coll. Intern. CNRS Marseille), Paris, 1962, 501-522 (1962).

19. Sen, N. R. − The modern theory of turbulence, Indian association for the cultivation of science, Calcutta, (1956).
20. Heisenberg, W. − Zeit Phys., **124**, 628 (1948).
21. Hinze, J. O. − Turbulence, Mc Graw-Hill, New York (1975).
22. Loitsiansky, L. G. − Rep. Centr. Aero. Hydrodyn. Ins.(Moscow), No. 440 (translated as Tech. Memor. Nat. Adv. Comm. Aero., Wash, No.1079) (1939).
23. Lin , C. G. − Proc. I. St. Symp. In Appl. Math. Amer. Soc., p. 81 (1949).
24. Batcheler, G. C. – Proc. Roy. Soc., A195, 1043, 513 (1949).

INDIAN JOURNAL OF THEORETICAL PHYSICS, VOL. 65, NOS. 3 & 4, 2017

On the evaluation of activation energy in thermoluminescence by Kirsh method for the case of temperature dependent frequency factor

A. Sarkar, I. Bhattacharyya*, S. Bhattacharyya, P. S. Majumdar
Department of Physics, Acharya Prafulla Chandra College,
New Barrackpur, West Bengal
*E-mail : indranil@apccollege.ac.in

Soumya Das
Department of Electrical Engineering,
Narula Institute of Technology, West Bengal

and

S. Dorendrajit Singh
Department of Physics, Manipur University,
Chanchipur, Imphal-795003

[**Abstract:** The accuracy of the Kirsh method when the frequency factor depends on temperature as T^a ($-2 \leq a < 2$) for the case of general order and first order thermoluminescence (*TL*) is evaluated. By considering a number of computer generated *TL* peaks it is shown that the maximum error in the determination of activation energy by Kirsh method for the case of temperature dependent frequency factor is about 10%. Finally the applicability of present findings has been assessed by considering some experimental *TL* peaks.]

Keywords: Frequency Factor, Activation Energy, Order of Kinetics, Kirsh Method.

1. Introduction

Thermoluminescence (*TL*) is a form of luminescence which is exhibited by some insulating or semiconducting solids after being irradiated with some ionizing radiations such as X-rays, γ-rays β-rays etc. *TL* has got important applications in the field of radiation dosimetry, dating and defect studies of solids[1]. In a simple kinetic order (*KO*) model the parameters such as activation energy (E), frequency factor (s) and order of kinetics (b) are used to explain the *TL* phenomenon.

In *KO* model by convention the frequency factor is considered to be independent of temperature (T) but the detailed theoretical analysis points towards the dependence of frequency factor with temperature of the type[2-4].

$$s = s_0 T^a \qquad (-2 \leq a < 2) \qquad \ldots \quad (1)$$

where S_0 is a constant and a is the temperature exponent.

Kirsh[5] suggested a method for the simultaneous determination of order of kinetics and activation energy of *TL* peak. The suitability of this method for the case of temperature independent frequency factor has been demonstrated by Karmakar et al[6]. In the present work we have assessed the acceptability of Kirsh method to determine E and b in the context of dependence of s on temperature in *TL*.

2. Methodology

By considering the temperature dependence of s in *TL* the expression for *TL* intensity as a function of absolute temperature *T* for a first order *TL* peak ($b = 1$) is given by[7]

$$I(T) = n_0 s_0 T^a exp\left[\frac{-E}{KT} - \frac{S_0}{\beta}\int_{T_0}^{T} T'^a \exp\left(\frac{-E}{KT'}dT'\right)\right] \qquad \ldots \quad (2)$$

With the corresponding maximum condition

$$\frac{E}{KT_m^2} - S_0 T_m^2 exp\,[\frac{-E}{KT_m}]\,\beta + \frac{a}{T_m} = 0 \qquad \ldots \quad (3)$$

Similarly the *TL* intensity for a non 1st order *TL* peak ($b \neq 1$) can be expressed as [7]

$$I(T) = n_0 s_0 T^a exp\frac{-E}{KT}\{[1 + [s_0\frac{b-1}{\beta}]\int_{T_0}^{T} T'^a exp[\frac{-E}{KT'}]dT']^{\frac{-b}{b-1}} \qquad \ldots \quad (4)$$

and the peak temperature T_m can be obtained from the equation

$$\frac{a}{T_m} + \frac{E}{KT_m^2} = bs_0 T_m^a exp[\frac{-E}{KT_m}]\beta[1 + [s_0\frac{b-1}{\beta}]\int_{T0}^{Tm} T'^a exp[\frac{-E}{KT'}]dT']^{-1}$$

$$\ldots \quad (5)$$

where the symbols have their usual meanings[7].

According to Kirsh[5] $\frac{\Delta \ln(I)}{\Delta \ln(n/n_0)}$ depends linearly on $\Delta \ln(1/T)$ with gradient $-(E/k)$ and intercept b. The difference between the values of any quantity such as I corresponding to two nearby points of the glow curve is denoted by Δ. So Kirsh method allows simultaneous evaluation of E and b.

3.Results and discussions

The evaluation of the integral $\int_{T_0}^{T} T^{a} \exp(-\frac{E}{KT})\, dT$ occurring in equations (2), (4) and (5) have been carried out by following the technique proposed by Singh et al[8] . The area of the *TL* peak between any two temperatures has been obtained by using Simpson 1/3rd rule[9]. In figures 1 and 2 we show some *TL* peaks with temperature dependent frequency factor as reported by Fleming[7] for $a = 2$ and $a = -2$. $\frac{I}{I_m}$ is the fractional intensity and I_m is the peak intensity. In the process of computation we have found that the value of s_0 as reported by Fleming will be 55.96 instead of 25.46 for $E = 1.303\ eV$, $a = 2$, $T_m = 595K$ and $\beta = 0.42Ks^{-1}$. It is to be noted that the symmetry factor $\mu_g = \frac{\delta}{\omega}$ [$\delta = (T_2 - T_m)$ and $\omega = (T_2 - T_1)$, T_1 and T_2 and $\omega = (T_2 - T_1)$, T_1 and T_2 are half intensity temperatures in the rising and falling sides of the peak]. For the first order *TL* peaks shown in figures $(1a)$ and $(1b)$ for $a = 2$ and $a = -2$ are respectively 0.44 and 0.45. Similarly for second order *TL* peaks shown in figures $(2a)$ and $(2b)$ for $a = 2$ and $a = -2$ μ_g values are nearly 0.52. This shows that the shape of the *TL* peaks depends weakly on temperature exponent a (Chen and Kirsh[10]).

The applicability of Kirsh method for the dependence of s with temperature has been checked by applying it to a number of computer generated *TL* peaks for the non zero values of a. The results have been presented in Table 1. The values of E and b as calculated by Kirsh method are denoted respectively by E_K and b_K. It is evident from Table 1 that the values of E_K and b_K apparently agree very well with corresponding input values of E_{in} and b_{in} of E and b respectively. This is illusory because it is not possible to estimate a from *TL* data in isolation no matter how

extensive and varied this data may be[7]. The values E_0 and b_0 of E and b have been computed for the case of zero temperature exponent of frequency factor for $a = 0$ are presented in Table 1. The values of E_0 and b_0 in different cases differ from the input values of E_{in} and b_{in} of E and b as well as from E_k and b_k by an amount less than 10%. The amount of deviation of E_0 from the input value of E agrees with the observations of Fleming[7] and Chen and Kirsh[10] for the case of peak shaped method [1].

In order to check the suitability of our findings we consider two experimental *TL* peaks analyzed by Singh[11]. These are (*i*) completely isolated 593 *K TL* peak in bluish green microcline obtained by thermally cleaning lower temperature peaks by heating up to 563 *K* [Fig. 3] (*ii*) partly isolated 476 *K TL* peak of Norwegian orthoclase obtained by thermally cleaning lower temperature peaks up to 543 *K* [Fig. 4]. We have modified the curve fitting algorithm developed by Singh, et al[12,13] including the temperature exponent a as a parameter of fitting. We have used the fitting functions suggested by Bhattacharya, et al[14] for the case of temperature dependent frequency factor. The relevant parameter of fitting for 593 K peak of bluish microcline and 476 *K* peak of Norwegian orthoclase are presented in Table 2. It is to be noted that heating rates for both the peaks are 0.42 Ks^{-1}. In Table 2 E_{cf} , $b_{cf,}$ s_{cf} and a_{cf} are curve fitted values of E, b, s and a. In Table 2 we also depict the values of E_K b_K and s_K as calculated by Kirsh method. It is evident from Table 2 that for both the peaks E_K, b_K and s_K are in good agreement with the values of the trapping parameters as calculated by the method of curve fitting.

The goodness of fitting have been checked by computing the figure of merit (*FOM*) defined by[15]

$$FOM = \frac{\sum_i [I_{exp}(T_i) - I_{fit}(T_i)]}{\sum_i I_{fit}(T_i)} \times 100\ \% \qquad \ldots \quad (6)$$

where $I_{exp}(T_i)$ and $I_{fit}(T_i)$ are respectively the experimental and fitted values of *TL* intensity I at temperature T_i. The value of frequency factor s_k as determined by Kirsh method can be evaluated by using the relation[14]

$$\frac{\beta E_K}{kT_m^2} = s_K \exp\left(-\frac{E_K}{KT_m}\right)\left[1 + (b_K - 1)\frac{2KT_m}{E_K}\right] \qquad \ldots \quad (7)$$

where k is the Boltzmann Constant and T_m is the peak temperature. s_K is the frequency factor as determined by the Kirsh method. The values of *FOM* presented in Table 2 also indicate a fairly good fit.

Table 1

Activation energies and orders of kinetics of some numerically computed peaks.

E_{in} *(eV)*	b_{in}	$(S_0)_{in}$ $(s^{-1}K^{-a})$	a	E_K	b_K	E_0	b_0
1.6	1	10^9	2	1.601	0.996	1.636	1.02
1.6	2	10^9	2	1.601	1.99	1.636	2.04
1.6	1	10^9	-2	1.600	1.03	1.564	0.98
1.6	2	10^9	-2	1.601	2.07	1.562	2.05
0.4	1	10^7	2	0.400	0.993	0.427	1.07
0.4	2	10^7	2	0.400	1.99	0.427	2.10
0.4	1	10^{11}	-2	0.400	1.02	0.384	0.96
0.4	2	10^{11}	-2	0.400	2.03	0.382	2.09
1.6	1.5	10^9	2	1.600	1.50	1.686	1.58
1.6	1.5	10^9	-2	1.600	1.52	1.518	1.57
0.4	1.5	10^7	2	0.400	1.50	0.418	1.56
0.4	1.5	10^{11}	-2	0.400	1.48	0.388	1.46

Table 2

Values of trapping parameters of some experimental *TL* peaks as calculated by the method of curve fitting and Kirsh method*.

Peak Temperature	E_{cf} (eV)	b_{cf}	s_{cf} (sec^{-1})	a_{cf}	E_K (eV)	b_K	s_K (sec^{-1})	*FOM*
593*K*	1.42	2	3.56(10)	0.0	1.40	2	3.70(10)	0.75
476*K*	1.16	2	7.6(10)	0.0	1.13	2	7.9(10)	0.82

*$A(B)$ stands for $A \times 10^B$

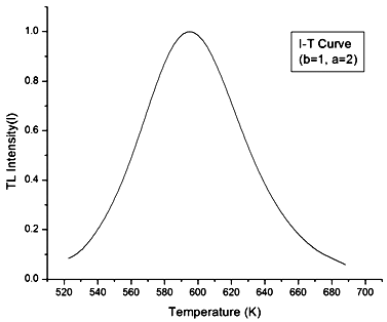

Fig. 1(a)

Computer generated TL peak for $a = 2$, $E = 0.409\ eV$, $T_m = 580K$, $b = 1$, $\beta = 0.42\ Ks^{-1}$

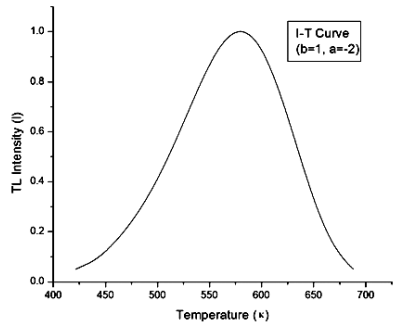

Fig 1(b)

Computer generated TL peak for $a = -2$, $E = 0.591\ eV$, $T_m = 580K$, $b = 1$, $\beta = 0.42\ Ks^{-1}$

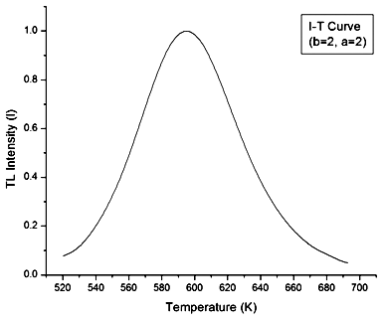

Fig. 2(a)

Computer generated TL peak for $a = 2$, $E = 1.303\ eV$, $T_m = 580K$, $b = 2$, $\beta = 0.42\ Ks^{-1}$

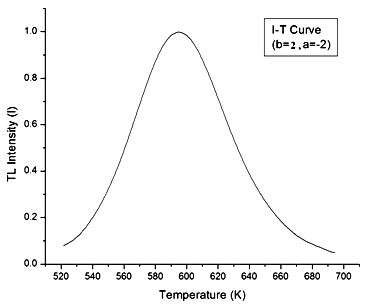

Fig. 2(b)

Computer generated TL peak for $a = -2$, $E = 1.497\ eV$, $T_m = 595K$, $b = 2$, $\beta = 0.42\ Ks^{-1}$

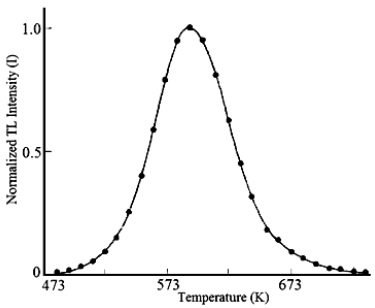

Fig. 3

Completely isolated 593 K experimental peak of Bluish Green Microclene. Solid line denotes the experimental peak. Dots denote the points corresponding to the computer generated best fit peak.

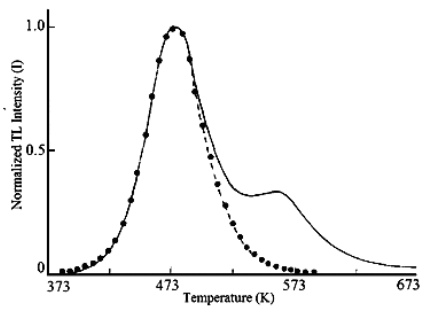

Fig. 4

Same as Fig. 3 but for partly isolated experimental 476 K peak of Norewegian orthoclase.

4. Conclusion

In the present paper the suitability of Kirsh method for the simultaneous determination of E and b has been assessed by considering some computer generated and experimental *TL* peaks. It has been found that the method can be applied to *TL* peaks with temperature dependent frequency factor. It has also been observed that the maximum error in the determination of the activation energy by Kirsh method for the case of the temperature dependent frequency factor is of the order of 10%. It is also found that for $a = 2$ the value of activation energy as calculated by Kirsh method is underestimated but for $a = -2$ it is over estimated. For the experimental *TL* peaks the errors in the activation energy as determined by Kirsh method are within the limits obtained for the computer generated peaks.

References

1 Chen, R. and McKeever, S.W.S.− Theory of Thermoluminescence and Related Phenomena, World scientific, Singapur (1997).
2 Keating, P.N. − Proc. .Phys. Soc., **78**, 1408 (1961).
3 Lax, M. − Phys. Rev., **119** , 1502 (1960).
4 Benski, G. − Phys. Rev., **111**, 1515 (1958).
5 Krish, Y. − Phys. Stat Sol (a), **129**, 15 (1992).
6 Karmakar, M., Sarkar, B., Barman, S., Majumdar, P.S., Singh, S.D. and Bhattacharya, M. – Indian J. Phys., **82**, 1495 (2008).
7 Fleming, R. J. −J. Phys., D **23,** 950 (1990).
8 Singh, S. D., Devi, W.G., Singh, A. K. M., Bhattacharya, M. and Majumdar, P.S. − J. Thermal Anal. **61**, 1013 (2000).
9 Press, W. H., Teukolsky, S. A., Vellerling, W.T. and Flannery, B. P. − Numerical methods in Fortran, Cambridge University Press, Cambridge (1992).
10 Chen, R. and Kirsh, Y. − Analysis of thermally stimulated processes, Pargamon, Oxford (1981).
11 Singh, S.J. − Ph.D. Thesis (Manipur University, India) (1992).
12 Singh, S.J., Karmakar, M., Singh, W.S. and Singh, S.D. − Physica. Scripta, **86**, 035 (2012).
13 Singh, S.J., Karmakar, M. and Singh, S.D. − Radiation effect and defects in solids, **168**, 35 (2013).
14 Bhattacharya, M., Deb, N. C., Meszane, A. Z. and Majumdar, P.S. − Phys. Stat. Sol.(a), **185,** 291 (2001).
15 Pagonis, V., Kitis, G. and Furetta, C. – Numerical and Practical Exercises in Thermoluminescence, Spriger, New York (2010).

INDIAN JOURNAL OF THEORETICAL PHYSICS, VOL. 65, NOS. 3 & 4, 2017

Effect of visco-elastic co-efficient and slip on blood flow velocity in a stenosed artery

Subhrojyoti Debnath
Brahmananda Keshab Chandra College,
111/2 B. T. Road, Bon-Hooghly, Kolkata-700108
E-mail address : subhrojyotidebnath@yahoo.in

[**Abstract** : In this investigation flow of blood is discussed in a stenosed artery. Here the stenosis is considered as mild and axially symmetric. Blood is taken as an elastico-viscous fluid, also termed as Kuvshinski type fluid. The governing equations are made considering the visco-elastic parameter (λ) and an externally applied transverse magnetic field (B_0). The problem is solved analytically by the help of appropriate boundary conditions taking the slip velocity in effect. Mainly the nature of velocity of blood is discussed here under the influence of slipparameter (α), visco-elastic parameter (λ) and the externally applied transverse magnetic field (B_0) and are depicted graphically.]

Keywords : Kuvshinski type fluid, mild stenosis, visco-elastic parameter, slip parameter.

1. Introduction

Problems regarding blood flow in a stenosed artery are interesting as well as important in physiological and clinical fields. Due to the pumping action of heart a pressure gradient arises which gives rise to a type of oscillatory flow of blood through the arteries. This oscillatory flow depends on the number of physical parameters. Many researchers studied those kind of blood flow behaviors through the human arteries, considering blood as Newtonian as well as non-Newtonian fluids.

Redaelli, A. et. al.[1] studied the pulsatile flow of blood in arteries considering finite element simulations. Jung, H. et. al.[2] considered blood as non-Newtonian fluid and discussed the flow in symmetric stenosed artery. Bhardwaj, K. et. al.[3] discussed about oscillatory flow of blood in an artery with mild stenosis. Ponalgusammy, R.[4] considered a two layered blood flow

model in an artery with stenosis and slip velocity. Sanyal, D. C. et. al.[5] studied the effect of magnetic field on pulsatile motion of blood in a circular tube in presence of periodic body acceleration. Rathod, V. P.[6] worked on pulsatility of blood flow, taking blood as a couple stress fluid in presence of periodic body acceleration and external magnetic field through a porous medium. Kumar, S.[7] studied the effect of body acceleration of blood flow when the stenosis is time dependent. Sanyal, D. C.[8] considered stenosis as axi-symmetric and studied pulsatile motion of blood in presence of external magnetic field. Varshney, N. K. et. al.[9] considered blood as couple stress *MHD* fluid in an inclined circular tube and studied pulsatile flow of blood with periodic body acceleration. Kumar, A. et. al.[10] worked on the flow of blood taking blood as an elastico-viscous fluid with porous effect and periodic body acceleration. Tanwar, V. et. al.[11] studied magnetic field effect on oscillating flow of blood in presence of mild stenosis. Mohan, V. et. al.[12] studied the effect of magnetic field taking blood as an elastic-viscous fluid in an artery with mild stenosis.

In present article the slip flow of blood in the inner wall of an artery is taken into account. Effects of slip flow, elastico-viscous parameter and externally applied magnetic field on the pulsatile motion of blood are discussed and shown graphically.

2. Mathematical formulation of the problem

At first blood is considered as an elastic-viscous (Kuvshinski type) fluid. Furthermore blood is here assumed as viscous, incompressible in nature and its flow is assumed to be unsteady and axially symmetric. The density and viscosity of blood are taken as constant. The radius of artery is chosen as constant except the stenosed portion. In the lumen of the artery the growth of stenosis is assumed to be symmetrical. Geometry of the stenosis is represented in the following figure and formulated mathematically by equation (1).

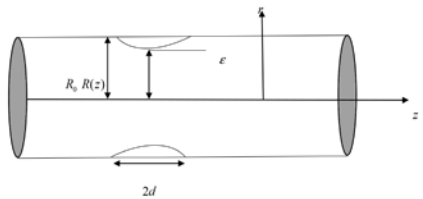

Fig. 1
Geometry of the stenosis in the inner wall of an artery.

$$\frac{R(z)}{R_0}=1-\frac{\varepsilon}{2R_0\left(1+\cos\frac{\pi z}{d}\right)} \quad \ldots \quad (1)$$

here R_0 is the radius of undisturbed portion of the artery, $R(z)$ is the radius of the artery in stenosed portion. $2d$ is the total length of the stenosis and ε is the maximum height of the stenosis in such a manner that $\frac{\varepsilon}{R_0}<<1$ *i.e.*, the stenosis is mild in nature.

The governing equations of motion within the artery can be taken as

$$\left(1+\lambda\frac{\partial}{\partial t}\right)\rho\frac{\partial u}{\partial t}=-\frac{\partial p}{\partial z}+\mu\left(\frac{\partial^2 u}{\partial r^2}+\frac{1}{r}\frac{\partial u}{\partial r}\right)-\sigma\mathrm{B}_0^2\left(1+\lambda\frac{\partial}{\partial t}\right)u \quad \ldots \quad (2)$$

where ρ is the density, p is the fluid pressure and u is the fluid velocity in the axial direction. μ is taken here as the co-efficient of viscosity, σ as electrical conductivity of the medium, B_0 as the magnitude of externally applied transverse magnetic field and λ as the visco-elastic co-efficient.

In the boundary conditions, it is assumed that a slip velocity at the inner wall of artery exists, so that

$$\left.\begin{aligned}&\bar{u}+\frac{\alpha}{R}\frac{\partial\bar{u}}{\partial r}=0 \ \text{ on } \ r=R\\&\frac{\partial\bar{u}}{\partial r}=0 \ \text{ on } \ r=0\end{aligned}\right\} \quad \ldots \quad (3)$$

3. Solution of the problem

To solve the problem analytically the governing equation and the boundary conditions are transformed by taking $y=\frac{r}{R_0}$. Thus equations (2) and (3) are changed to

$$\frac{\partial^2\bar{u}}{\partial y^2}+\frac{1}{y}\frac{\partial\bar{u}}{\partial y}-\frac{\rho\lambda R_0^2}{\mu}\frac{\partial^2\bar{u}}{\partial t^2}-\frac{\rho R_0^2}{\mu}\frac{\partial\bar{u}}{\partial t}-\frac{R_0^2\sigma\mathrm{B}_0^2\lambda}{\mu}\frac{\partial\bar{u}}{\partial t}-\frac{R_0^2\sigma\mathrm{B}_0^2}{\mu}\bar{u}=\frac{\partial p}{\partial z}\frac{R_0^2}{\mu} \quad \ldots \quad (4)$$

$$\left.\begin{aligned} &\bar{u}+\frac{\alpha}{R_0}\frac{\partial \bar{u}}{\partial y}=0 \ \text{ on } \ y=\frac{R}{R_0} \\ &\frac{\partial \bar{u}}{\partial y}=0 \ \text{ on } \ y=0 \end{aligned}\right\} \qquad \ldots \quad (5)$$

Next it is considered that

$$\left.\begin{aligned} &\bar{u}(y,t)=\bar{u}(y)e^{\text{int}} \\ &-\frac{\partial p}{\partial z}=Pe^{\text{int}} \end{aligned}\right\} \qquad \ldots \quad (6)$$

which reduces (4) as

$$\frac{\partial^2 \bar{u}}{\partial y^2}+\frac{1}{y}\frac{\partial \bar{u}}{\partial y}-\beta^2\bar{u}=-\frac{PR_0^2}{\mu} \qquad \ldots \quad (7)$$

where

$$\beta^2=\frac{in\rho R_0^2}{\mu}+\frac{in\sigma\lambda R_0^2 \mathrm{B}_0^2}{\mu}+\frac{R_0^2\sigma \mathrm{B}_0^2}{\mu}-\frac{n^2\rho\lambda R_0^2}{\mu}.$$

The solution of (7) is obtained as a series solution using Frobenius method and is given by

$$\bar{u}(y)=A\sum_{j=0}^{\infty}\frac{\beta^{2j}y^{2j}}{4^j\left(j!\right)^2}-\frac{PR_0^2}{4\mu}\sum_{j=0}^{\infty}\frac{\beta^{2j}y^{2j+2}}{4^j\left((j+1)!\right)^2} \qquad \ldots \quad (8)$$

where

$$A=\frac{PR_0^2}{4\mu}\frac{R_0\sum_{j=0}^{\infty}\frac{\beta^{2j}R^{2j+2}}{{R_0}^{2j+2}4^j\left((j+1)!\right)^2}+\alpha\sum_{j=0}^{\infty}\frac{\beta^{2j}R^{2j+1}(2j+2)}{{R_0}^{2j+1}4^j\left((j+1)!\right)^2}}{R_0\sum_{j=0}^{\infty}\frac{\beta^{2j}R^{2j}}{{R_0}^{2j}4^j\left(j!\right)^2}+\alpha\sum_{j=0}^{\infty}\frac{\beta^{2j}R^{2j-1}2j}{{R_0}^{2j-1}4^j\left(j!\right)^2}}$$

$$=\frac{PR_0^2}{4\mu}\chi \ \text{(say)} \qquad \ldots \quad (9)$$

is obtained from the boundary conditions (5).

Changing from y to r the solution can be written as

$$\bar{u}(r,t)=\left\{A\sum_{j=0}^{\infty}\frac{\beta^{2j}r^{2j}}{R_0^{\,2j}4^j\left(j!\right)^2}-\frac{PR_0^2}{4\mu}\sum_{j=0}^{\infty}\frac{\beta^{2j}r^{2j+2}}{R_0^{\,2j+2}4^j\left(\left(j+1\right)!\right)^2}\right\}e^{\text{int}} \qquad (10)$$

If $\acute{u}$ is considered as the flow velocity in the absence of stenosis, then

$$u'=\frac{R_0^2}{8\mu}\left(\frac{\partial p}{\partial z}\right)_0 \qquad \ldots \quad (11)$$

The non-dimensional form of velocity profile becomes

$$u=\frac{\bar{u}}{u'}$$

$$=\frac{\dfrac{PR_0^2}{4\mu}\left\{\chi\sum_{j=0}^{\infty}\dfrac{\beta^{2j}y^{2j}}{4^j\left(j!\right)^2}-\sum_{j=0}^{\infty}\dfrac{\beta^{2j}y^{2j+2}}{4^j\left(\left(j+1\right)!\right)^2}\right\}}{\dfrac{R_0^2}{8\mu}\left(\dfrac{\partial p}{\partial z}\right)_0}$$

$$=\frac{-2\left(\dfrac{\partial p}{\partial z}\right)}{\left(\dfrac{\partial p}{\partial z}\right)_0}\left\{\chi\sum_{j=0}^{\infty}\frac{\beta^{2j}r^{2j}}{R_0^{\,2j}4^j\left(j!\right)^2}-\sum_{j=0}^{\infty}\frac{\beta^{2j}r^{2j+2}}{R_0^{\,2j+2}4^j\left(\left(j+1\right)!\right)^2}\right\} \qquad \ldots \quad (12)$$

The volumetric flow rate is

$$Q=2\pi\int_0^R\bar{u}rdr$$

which gives here

$$Q=2\pi\left\{A\sum_{j=0}^{\infty}\frac{\beta^{2j}R^{2j+2}}{R_0^{\,2j}4^j\left(j!\right)^2\left(2j+2\right)}-\frac{\pi PR_0^2}{2\mu}\sum_{j=0}^{\infty}\frac{\beta^{2j}R^{2j+4}}{R_0^{\,2j+2}4^j\left(\left(j+1\right)!\right)^2\left(2j+4\right)}\right\}e^{\text{int}}$$

$$\ldots \quad (13)$$

If Q_0 is taken as the volumetric flow rate in the absence of stenosis, then

$$Q_0 = \frac{\pi R_0^4}{4\mu}\left(\frac{\partial p}{\partial z}\right)_0$$

In this particular case if it is considered that $\frac{Q}{Q_0} = 1$, then

$$\frac{\left(\frac{\partial p}{\partial z}\right)}{\left(\frac{\partial p}{\partial z}\right)_0} = \frac{1}{2\left\{\sum_{j=0}^{\infty}\frac{\beta^{2j}R^{2j+4}}{R_0^{\,2j+4}4^j\left((j+1)!\right)^2(2j+4)} - \chi\sum_{j=0}^{\infty}\frac{\beta^{2j}R^{2j+2}}{R_0^{\,2j+2}4^j\left(j!\right)^2(2j+2)}\right\}} \quad \ldots \quad (14)$$

Again if τ_R be the wall shear stress, then

$$\tau_R = \mu\left(\frac{\partial \bar{u}}{\partial r}\right)_{r=R}$$

$$= \mu\left\{A\sum_{j=0}^{\infty}\frac{\beta^{2j}R^{2j-1}2j}{R_0^{\,2j}4^j\left(j!\right)^2} - \frac{PR_0^2}{4\mu}\sum_{j=0}^{\infty}\frac{\beta^{2j}R^{2j+1}(2j+2)}{R_0^{\,2j}4^j\left((j+1)!\right)^2}\right\}e^{\text{int}} \quad \ldots \quad (15)$$

If τ_0 is considered as the wall shear stress in the absence of stenosis, then

$$\tau_0 = -\frac{R_0}{2}\left(\frac{\partial p}{\partial z}\right)_0$$

Then the non-dimensional form of wall shear stress can be obtained as

$$\tau = \frac{\tau_R}{\tau_0} = \frac{1}{2}\frac{\left(\frac{\partial p}{\partial z}\right)}{\left(\frac{\partial p}{\partial z}\right)_0}\left\{\chi\sum_{j=0}^{\infty}\frac{\beta^{2j}R^{2j-1}2j}{R_0^{\,2j-1}4^j\left(j!\right)^2} - \sum_{j=0}^{\infty}\frac{\beta^{2j}R^{2j+1}(2j+2)}{R_0^{\,2j+1}4^j\left((j+1)!\right)^2}\right\} \quad \ldots \quad (16)$$

4. Numerical results and discussion

In the present analysis mainly the velocity profile is discussed depending on the various parameters involved. From the obtained analytical solutions the numeric value of the velocity profile are calculated and then depicted through graphs.

In figure 2, effect of slip velocity α on the flow velocity u versus time t is shown. As the slip velocity increases the flow velocity of blood also increases with respect to time t. Graphs are drawn between flow velocity u and tube radius r in figures 3, 4 and 5. In figure 3 it is shown that the flow velocity again increases with the increasing values of slip velocity α.

From figure 4, it is evident that the visco-elastic co-efficient λ also effects the flow velocity u and velocity decreases with the increasing value of λ. In the figure 5, the effect of externally applied magnetic field B_0 in flow velocity u is shown. The flow velocity u increases with the increasing values of B_0.

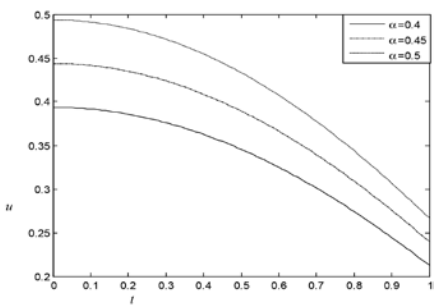

Fig. 2

u versus t for different values of α.

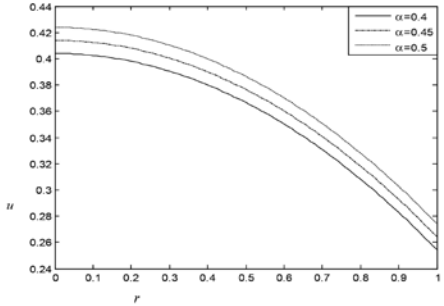

Fig. 3

u versus r for different values of α.

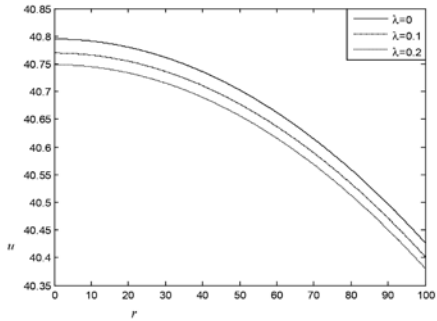

Fig. 4

u versus r for different values of λ.

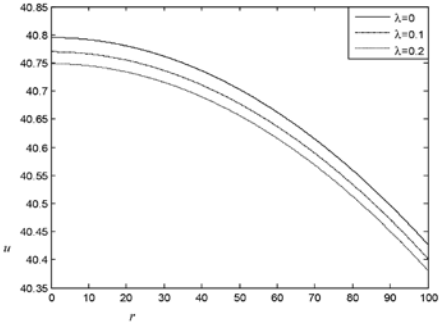

Fig. 5

u versus r for different values of B_0.

References

1. Redaelli, A., Boschetti, F. and Inzoli, F. – The assignment of velocity profile in finite element simulations of pulsatile flow in arteries, Computers in Biology and medicine, **17**, 233-247 (1997).

2. Jung, H., Choi, J. W. and Parl, C. G. – Asymmetric flow of non-Newtonian fluid in symmetric stenosed artery, Korea-Australia Rheology Journal, **16**, 101-108 (2004).
3. Bhardwaj, K. and Kanodia, K. K. – Oscillatory arterial blood flow with mild stenosis, ActaCienceaIndica, **XXXIII(1)**, 71-93 (2007).
4. Ponalgusammy, R. – Blood flow through an artery with mild stenosis. A two layered model, different shapes of stenosis and slip velocity at the wall, Journal of Applied Science, **7**, 1071-1077 (2007).
5. Sanyal, D. C., Das, K. and Debnath, S. – Effect of magnetic field on pulsatile blood flow through an inclined circular tube with periodic body acceleration, Journal of Physical Sciences, **11**, 43-56 (2007).
6. Rathod, V. P. and Tanveer, S. – Pulsatile flow of couple stress fluid through a porous medium with periodic body acceleration and magnetic field, Bull. Malays. Sci. Soc. (2), **32(2)**, 245-259 (2009).
7. Kumar, S. and Dixit, A. – Mathematical model for the effect of body acceleration on blood flow in time dependent stenosed artery, International Journal of Stability and Fluid Mechanics, **1(1)**, 103-115 (2010).
8. Sanyal, D. C. and Biswas, A. – Pulsatile motion of blood through an axi-symmetric artery in presence of magnetic field, Assam Univ. Jour. of Sci. and Tech. : Phys. Sci. and Tech., **5(11)**, 12-20 (2010).
9. Varshney, N. K. and Agarwal, A. – MHD Pulsatile flow of couple stress fluid through an inclined circular tube with periodic body acceleration, Jour. of Purvanchal Acad. of Sci., **17**, 277-293 (2011).
10. Kumar, A., Varshney, C. L. and Singh, V. P. – Mathematical modelling of blood flow in elastic-viscous fluid under periodic body acceleration with porous effect, Int. Jour. of Math. Archive, **1(3)**, 2277-9698 (2012).
11. Tanwar, V., Agarwal, R. and Varshney, N. K. – Magnetic field effect on oscillatory arterial blood flow with mild stenosis, Appl. Math. Sci., **6(120)**, 5959-5966 (2012).
12. Mohan, V., Prasad, V. and Varshney, N. K. – Analytical study of elastico-viscous fluid (blood) through an artery with mild stenosis, Int. Jour. of Math. Archive, **4(9)**, 71-76 (2013).

INDIAN JOURNAL OF THEORETICAL PHYSICS, VOL. 65, NOS. 3 & 4, 2017

Fractional order two temperature generalized thermoelasticity of an infinite medium with cylindrical cavity under three phase lag heat transfer

Nasiruddin Mondal, Md Abul Kashim Molla and Sadek Hossain Mallik*
Department of Mathematics and Statistics,
Aliah University, Kolkata-700160
*E-mail: sadek.math@aliah.ac.in

[**Abstract :** In this work a theory of fractional order two temperature generalized thermoelasticity in the context of three-phase-lag (3*PL*) heat transfer is constructed using a new consideration of Taylor's series expansion as developed by Jumarie. The theory is then applied to study the thermoelastic interactions in an isotropic infinite medium with cylindrical cavity where the internal surface of the cavity is subjected to a thermal and mechanical loading. The governing equations of the problem are solved by state space approach in Laplace transform domain. The inversion of Laplace transform of the solutions have been obtained numerically using a method based on Fourier series expansion technique. The numerical values of different thermophysical quantities are computed for copper like material and are depicted graphically to study the effect of two temperature and fractional parameters. Comparison of the results obtained for *GN* Model-III, 3*PL* model and fractional 3*PL* (*F*3*PL*) model are also shown graphically.]

Key Words and Phrases : Two-Temperature generalized thermoelasticity; Fractional Three-phase-lag model; State space approach; Cylindrical cavity
2010 Mathematics Subject Classification : 74F05

1. Introduction

The generalized theory of thermoelasticity is one of the modified versions of classical uncoupled and coupled theory of thermoelasticity and has been developed in order to remove the paradox of physical impossible phenomena of infinite velocity of thermal signals in the classical coupled

thermoelasticity. Five generalizations of the coupled theory of thermoelasticity have been investigated by Hetnarski[1,2]. The first generalization formulates the generalized thermoelasticity theory involving one thermal relaxation time which is investigated by Lord and Shulman[3]. The temperature rate-dependent thermoelasticity is developed by Green and Lindsay which includes two thermal relaxation times and does not violate the classical Fourier's law of heat conduction[4].

The third generalization of the coupled theory of thermoelasticity is developed by Hetnarski and Ignaczak and is known as low-temperature thermoelasticity. The fourth generalization to the coupled theory of thermoelasticity introduced by Green and Naghdi[5,6,7] provides a general framework within which a much wider class of heat flow problem can be modelled. The theory is further subdivided into three types based on constitutive response functions, which are known as model I, II and III. The nature of these three types of constitutive equations are such that when the respective theories are linearized, model I encompasses the classical heat conduction theory (based on Fourier law) but the linearized versions of model II and III allows propagation of thermal waves at finite speed. In Green-Naghdi model II[7], the internal rate of production of entropy is taken to be identically zero, which implies no dissipation of thermal energy. This model admits undamped thermoelastic waves in an elastic material and is known as the theory of thermoelasticity without energy dissipation. Green-Naghdi model III[6] includes the previous two models as special cases.

The fifth generalization of the coupled theory of thermoelasticity is referred to the dual-phase-lag thermoelasticity[8,9]. Tzou considered micro-structural effects in the delayed response in time in the macroscopic formulation by taking into account that increase of the lattice temperature which is delayed due to phonon-electron interactions on the macroscopic level. Tzou introduced two-phase-lag (2*PL*) model in which both the heat flux vector and the temperature gradient are considered. According to this model, classical Fourier's law, $\vec{q} = -K\vec{\nabla}\phi$ has been replaced by $\vec{q}(P, t + \tau_q) = -K\vec{\nabla}\phi(P, t + \tau_T)$ where the temperature gradient $\vec{\nabla}\phi$ at a point P of the material at time $t + \tau_T$ corresponds to the heat flux vector $\vec{q}$ at

the same point in time $t + \tau_q$. Here, K is the thermal conductivity of the material. The delay time τ_T is interpreted as that caused by the micro-structural interactions and is called the phase-lag of the temperature gradient. The other delay time τ_q is interpreted as the relaxation time due to the fast transient effects of thermal inertia and is called the phase-lag of the heat flux. Recently, the three-phase-lag (3*PL*) heat conduction equation has been introduced by Roy Choudhuri[10] in which the Fourier's law of heat conduction is replaced by an approximation to a modification of the Fourier's law with the introduction of three different phase-lags for the heat flux vector, the temperature gradient and the thermal displacement gradient. According to this model

$$\vec{q}(P, t+\tau_q) = -[K\vec{\nabla}\phi(P, t+\tau_T) + K^*\vec{\nabla}\nu(P, t+\tau_\nu)] \qquad \cdots \quad (1)$$

where, $\vec{\nabla}\nu(\dot{\nu} = \phi)$ is the thermal displacement gradient and K^* is the additional material constant and τ_ν is the phase-lag for the thermal displacement gradient.

Gurtin and William[11,12], Chen and Gurtin[13] and Chen, et al.[14] have formulated a theory of heat conduction in deformable bodies, which depends on two distinct temperatures; the conductive temperature φ and the thermodynamic temperature θ. The first is due to thermal processes and the second is due to the mechanical processes inherent between the particles and the layers of the elastic materials. The presence of the material parameter a ($\geq$ 0), known as the temperature discrepancy, in two temperature thermoelasticity makes it different from the one temperature thermoelasticity. In particular, if a = 0 then $\varphi = \theta$ and the governing equations of classical theory can be obtained from the two-temperature thermoelasticity theories. The linearized version of the two temperature theory has been studied by many authors. Warren and Chen[15] have investigated the wave propagation in the two-temperature thermoelasticity.

Youssef has developed the two temperature generalized thermoelasticity theory using Lord- Shulman model[16] as well as Green Nagdhi model II[17]. Uniqueness and growth of solutions in two temperature generalized thermoelastic theories have been studied by Magañe and Quintanilla[18].

Fractional calculus is a branch of mathematical analysis that focuses on the study of differential operators of arbitrary order. Firstly, Abel[19] has applied fractional calculus in the solution of an integral equation that gave the first application of fractional derivatives which arose in the formulation of the tautochrone problem. A brief history of the development of fractional calculus can be found in Ross[20]. Caputo[21] gave the definition of fractional derivatives of order $0 < \alpha \leq 1$ of continuous function. Caputo and Mainardi[22] and Caputo[23] have employed the fractional order derivatives for the description of viscoelasticity materials and they have successfully established the connection between fractional derivatives and the theory of linear viscoelasticity and found a good agreement with the experimental results. Among the few works devoted to applications of fractional calculus to thermoelasticity, we can refer to the works of Povstenko[24,25,26] who introduced a fractional heat conduction law and found the associated thermal stresses. Sherief, et al.[27], Youssef and Al-Lehaibi[28] and Ezzat[29,30] introduced new models of thermoelasticity using a fractional heat conduction equation. Recently, Ezzat, et al.[31] proposed a new model of thermoelasticity with three-phase-lag heat conduction in the context of a new consideration of time-fractional order Fourier's law of heat conduction and also proved uniqueness and reciprocity theorems. They solved one-dimensional problem for an elastic half-space in the presence of heat sources. Mondal, et al.[32] solved a one dimensional problem using dual phase Lag model in the context of fractional calculus for variable thermal conductive material.

The main object of this paper is to study thermoelastic disturbances in a homogeneous isotropic infinite elastic medium with cylindrical cavity. The study has been carried out in the context of time-fractional two-temperature generalized thermoelasticity for three phase lag (3*PL*) heat transfer. The method of Laplace transform in time domain has been applied to the governing equations and the resulting equations have been solved in that transform domain using state space approach. Finally, Laplace inversion has been carried out numerically by a method based on Fourier series expansion technique[33]. Numerical results for the thermal displacement, thermodynamic temperature, conductive temperature, thermal strain and thermal stress in

physical space-time domain have been obtained for a copper like material and presented graphically for the models *GN-III*, fractional three-phase-lag (*F*3*PL*) and 3*PL*. Some comparisons of the said thermophysical quantities are shown in figures to study the effects of two-temperature and fractional parameters.

2. The mathematical model

We have constructed fractional order theory of heat conduction for two-temperature generalized thermoelasticity with three-phase-lag heat transfer by taking a new Taylor's series expansion of time-fractional order α[1] on both sides of equation (1) and retaining terms up to α-order in τ_T and τ_v and terms up to 2α-order in τq as follows

$$\left(1+\frac{\tau_q^{\alpha}}{\alpha!}\frac{\partial^{\alpha}}{\partial t^{\alpha}}+\frac{\tau_q^{2\alpha}}{(2\alpha)!}\frac{\partial^{2\alpha}}{\partial t^{2\alpha}}\right)\vec{q}=-\left(K^{*}+\tau_{\nu}^{*}\frac{\partial}{\partial t}+K\frac{\tau_T^{\alpha}}{\alpha!}\frac{\partial^{\alpha+1}}{\partial t^{\alpha+1}}\right)\vec{\nabla}\phi, \quad \ldots (2)$$

where

$$\tau_{\nu}^{*}=K+K^{*}\frac{\tau_{\nu}^{\alpha}}{\alpha!}\frac{\partial^{\alpha-1}}{\partial t^{\alpha-1}}, 0<\alpha\leq 1.$$

In the context of the thermoelasticity theory, the energy equation for a homogenous isotropic thermoelastic solid is given as

$$-\mathrm{div}\vec{q}=\rho c_E\dot{\theta}+\gamma T_0\dot{e}_{ii}. \quad \ldots (3)$$

Eliminating $\vec{q}$ from (2) and (3), we get

$$\left[K^{*}\left(1+\frac{\tau_{\nu}^{\alpha}}{\alpha!}\frac{\partial^{\alpha}}{\partial t^{\alpha}}\right)+K\frac{\partial}{\partial t}\left(1+\frac{\tau_T^{\alpha}}{\alpha!}\frac{\partial^{\alpha}}{\partial t^{\alpha}}\right)\right]\nabla^2\phi=\left(1+\frac{\tau_q^{\alpha}}{\alpha!}\frac{\partial^{\alpha}}{\partial t^{\alpha}}+\frac{\tau_q^{2\alpha}}{(2\alpha)!}\frac{\partial^{2\alpha}}{\partial t^{2\alpha}}\right)$$
$$\times\left(\rho c_E\frac{\partial^2\theta}{\partial t^2}+\gamma T_0\frac{\partial^2 e}{\partial t^2}\right), \quad 0<\alpha\leq 1.$$

3. Formulation of the problem

We consider an infinite isotropic thermoelastic medium with a cylindrical cavity of radius *R*. Let the body be referred to cylindrical co-ordinate system (r, ϑ, z) with the z axis lying along the axis of the cylindrical cavity, so that the body occupies the region $R \leq r < \infty$. The surface of the cavity is under the mechanical loading, which is enough to

prevent the cubical dilatation and is under the thermal shock. Considering the axisymmetric plane strain problem, the displacement and temperatures can be taken as the function of r and t only. It follows that the displacement vector $\vec{u}$, the thermodynamic temperature θ, and the conductive temperature φ have following forms

$$\vec{u} = (u(r,t), 0, 0),\ \theta = \theta(r,t),\ \phi = \phi(r,t).$$

The non-zero strain components are given by

$$e_{rr} = \frac{\partial u}{\partial r}, e_{\vartheta\vartheta} = \frac{u}{r}.$$

The cubical dilatation e is given by

$$e = e_{ii} = e_{rr} + e_{\vartheta\vartheta} + e_{zz} = \frac{\partial u}{\partial r} + \frac{u}{r} = \frac{1}{r}\frac{\partial (ru)}{\partial r}. \quad \ldots (4)$$

The non-zero stress-strain-temperature relations in the present problem are

$$\sigma_{rr} = (\lambda + 2\mu)\frac{\partial u}{\partial r} + \lambda\frac{u}{r} - \gamma\theta, \quad \ldots (5)$$

$$\sigma_{\vartheta\vartheta} = (\lambda + 2\mu)\frac{u}{r} + \lambda\frac{\partial u}{\partial r} - \gamma\theta, \quad \ldots (6)$$

where, λ and μ are Lame's constants, and $\gamma = (3\lambda + 2\mu)\overline{\alpha}t$ where, $\overline{\alpha}t$ is the coefficient of the linear thermal expansion. The equation of motion without body force is given by

$$(\lambda + 2\mu)\frac{\partial e}{\partial r} - \gamma\frac{\partial \theta}{\partial r} = \rho\frac{\partial^2 u}{\partial t^2}. \quad \ldots (7)$$

In absence of heat source, the fractional heat equation corresponding to two temperature generalized thermoelasticity based on three-phase-lag model is

$$\left[K^*\left(1 + \frac{\tau_\nu^\alpha}{\alpha!}\frac{\partial^\alpha}{\partial t^\alpha}\right) + K\frac{\partial}{\partial t}\left(1 + \frac{\tau_T^\alpha}{\alpha!}\frac{\partial^\alpha}{\partial t^\alpha}\right)\right]\nabla^2\phi = \left(1 + \frac{\tau_q^\alpha}{\alpha!}\frac{\partial^\alpha}{\partial t^\alpha} + \frac{\tau_q^{2\alpha}}{(2\alpha)!}\frac{\partial^{2\alpha}}{\partial t^{2\alpha}}\right)$$
$$\times \left(\rho c_E\frac{\partial^2\theta}{\partial t^2} + \gamma T_0\frac{\partial^2 e}{\partial t^2}\right), 0 < \alpha \leq 1. \quad \ldots (8)$$

where, ρ is the density, K is the thermal conductivity, K^* is the material constant for the Green-Naghdi (GN) models, T_0 is the reference temperature, c_E is the specific heat at the constant strain, τ_T and τ_q are the phase-lags of

the temperature gradient and the heat flux respectively, Δ^2 is the Laplacian given, in our case, by

$$\nabla^2 = \frac{1}{r}\frac{\partial}{\partial r}\left(r\frac{\partial}{\partial r}\right).$$

The thermodynamic temperature θ and conductive temperature φ are related by

$$\phi - \theta = a\nabla^2\phi, \qquad \ldots \quad (9)$$

where $a(>0)$ is the two temperature parameter.

Introducing the following non-dimensional variables

$$r' = c_0\eta r, u' = c_0\eta u, t' = c_0^2\eta t, \tau_T' = c_0^2\eta\tau_T, \tau_q' = c_0^2\eta\tau_q,$$
$$\tau_\nu' = c_0^2\eta\tau_\nu, \theta' = \frac{\theta}{T_0}, \phi' = \frac{\phi}{T_0}, \sigma_{ij}' = \frac{\sigma_{ij}}{\lambda+2\mu}, e' = e,$$

Equations (5)-(9) can be obtained in non-dimensional form (after dropping the primes) as follows

$$\sigma_{rr} = \frac{\partial u}{\partial r} + \gamma^2\frac{u}{r} - \alpha_1\theta, \qquad \ldots \quad (10)$$

$$\sigma_{\vartheta\vartheta} = \frac{u}{r} + \gamma^2\frac{\partial u}{\partial r} - \alpha_1\theta, \qquad \ldots \quad (11)$$

$$\frac{\partial e}{\partial r} - \alpha_1\frac{\partial\theta}{\partial r} = \frac{\partial^2 u}{\partial t^2}, \qquad \ldots \quad (12)$$

$$\left(1 + \frac{\tau_q^\alpha}{\alpha!}\frac{\partial^\alpha}{\partial t^\alpha} + \frac{\tau_q^{2\alpha}}{(2\alpha)!}\frac{\partial^{2\alpha}}{\partial t^{2\alpha}}\right)\left(\frac{\partial^2\theta}{\partial t^2} + \varepsilon\frac{\partial^2 e}{\partial t^2}\right) = \left[C_T^2\left(1 + \frac{\tau_\nu^\alpha}{\alpha!}\frac{\partial^\alpha}{\partial t^\alpha}\right)\right.$$
$$\left. + \frac{\partial}{\partial t}\left(1 + \frac{\tau_T^\alpha}{\alpha!}\frac{\partial^\alpha}{\partial t^\alpha}\right)\right]\nabla^2\phi, \qquad \ldots \quad (13)$$

$$\phi - \theta = \omega\nabla^2\phi, \qquad \ldots \quad (14)$$

where

$$\varepsilon = \frac{\gamma}{\rho c_E}, \omega = ac_0^2\eta^2, \alpha_1 = \frac{\gamma T_0}{\lambda+2\mu}, \gamma^2 = \frac{\lambda}{\lambda+2\mu}, C_T = \sqrt{\frac{K^*}{\rho C_E c_0^2}},$$

where $c_0^2 = \frac{\lambda+2\mu}{\rho}$ and $\eta = \frac{\rho c_E}{k}$.

Now we can write (12) in the following form

$$\frac{\partial^2 e}{\partial t^2} = \nabla^2 e - \alpha_1 \nabla^2 \theta. \qquad \ldots \quad (15)$$

The initial and regularity conditions for the problem are given by

$$u = \theta = \phi = 0 \text{ at } t = 0 \text{ for } r \geq R,$$

$$\frac{\partial u}{\partial t} = \frac{\partial \theta}{\partial t} = \frac{\partial \phi}{\partial t} = 0 \text{ at } t = 0 \text{ for } r \geq R,$$

$$u = \theta = \phi = 0 \text{ as } r \longrightarrow \infty.$$

The problem is to solve the equations (13)-(15) subjected to the following boundary conditions :

(*i*) ***Thermal boundary condition :***

The internal surface r = R is subjected to the thermal shock given by

$$\phi(R, t) = \phi_R F(t), \qquad \ldots \quad (16)$$

where $F(t) = \phi_0,\ t > 0$

$= 0,\ t < 0.$

(ii) Mechanical boundary condition :

On the internal surface $r = R$, there is no cubical dilatation, *i.e.*,

$e(R, t) = eR = 0.$ … (17)

4. Method of solution

For the solution of the problem we apply Laplace transform defined by

$$\overline{f}(r, s) = \int_0^\infty f(r, t) e^{-st} dt, \quad Re(s) > 0$$

to the equations (10), (11), (13), (14) and (15) we get

$$\overline{\sigma}_{rr} = \frac{\partial \overline{u}}{\partial r} + \gamma^2 \frac{\overline{u}}{r} - \alpha_1 \overline{\theta}, \qquad \ldots \quad (18)$$

$$\overline{\sigma}_{\vartheta\vartheta} = \frac{\overline{u}}{r} + \gamma^2 \frac{\partial \overline{u}}{\partial r} - \alpha_1 \overline{\theta}, \qquad \ldots \quad (19)$$

$$\left(1 + \frac{\tau_q^\alpha}{\alpha!} s^\alpha + \frac{\tau_q^{2\alpha}}{(2\alpha)!} s^{2\alpha}\right)\left(s^2 \overline{\theta} + \varepsilon s^2 \overline{e}\right) = \left[C_T^2 \left(1 + \frac{\tau_\nu^\alpha}{\alpha!} s^\alpha\right) + s\left(1 + \frac{\tau_T^\alpha}{\alpha!} s^\alpha\right)\right] \nabla^2 \overline{\phi}, \qquad \ldots \quad (20)$$

$$\overline{\phi} - \overline{\theta} = \omega \nabla^2 \overline{\phi}, \qquad \ldots \quad (21)$$

$$\nabla^2 \overline{e} = s^2 \overline{e} + \alpha_1 \nabla^2 \overline{\theta}. \qquad \ldots \quad (22)$$

The boundary conditions (16) and (17) in the transformed domain take the forms

$$\overline{\phi}(R,s) = \overline{F}(s) = \frac{\phi_0}{s}, \quad \ldots \quad (23)$$

$$\overline{e}(R,s) = \overline{e} = 0. \quad \ldots \quad (24)$$

From (20) and (21), we get where

$$\overline{\theta} = (1 - wm)\overline{\phi} - \omega m \epsilon \overline{e}, \quad \ldots \quad (25)$$

where

$$m = \frac{\left(1 + \frac{\tau_q^\alpha}{\alpha!}s^\alpha + \frac{\tau_q^{2\alpha}}{(2\alpha)!}s^{2\alpha}\right)s^2}{C_T^2\left(1 + \frac{\tau_\nu^\alpha}{\alpha!}s^\alpha\right) + s\left(1 + \frac{\tau_T^\alpha}{\alpha!}s^\alpha\right) + \omega s^2\left(1 + \frac{\tau_q^\alpha}{\alpha!}s^\alpha + \frac{\tau_q^{2\alpha}}{(2\alpha)!}s^{2\alpha}\right)}.$$

Substituting $\overline{\theta}$ from (25) into (20), we obtain

$$\nabla^2\overline{\phi} = m\overline{\phi} + m\varepsilon\overline{e}. \quad \ldots \quad (26)$$

Putting the value of $\overline{\theta}$ in (22) and using equation (26) we have

$$\nabla^2\overline{e} = M_1\overline{e} + M_2\overline{\phi}, \quad \ldots \quad (27)$$

where

$$M_1 = \frac{s^2 + \alpha_1\varepsilon(1 - \omega m)m}{1 + \alpha_1\omega m\varepsilon}, M_2 = \frac{\alpha_1(1 - \omega m)m}{1 + \alpha_1\omega m\varepsilon}.$$

Equations (26), (27) can be written in the form of a vector-matrix differential equation as follows

$$\nabla^2\overline{V}(r,s) = A(s)\overline{V}(r,s), \quad \ldots \quad (28)$$

where

$$\overline{V}(r,s) = \begin{pmatrix} \overline{\phi}(r,s) \\ \overline{e}(r,s) \end{pmatrix},$$

and

$$A(s) = \begin{pmatrix} m & \varepsilon m \\ M_2 & M_1 \end{pmatrix}.$$

5. State space approach

The solution of the system (28) can be written in the following form

$$\overline{V}(r,s) = \frac{R}{r}e^{-\sqrt{A(s)}(r-R)}\overline{V}(R,s), \quad \ldots \quad (29)$$

where

$$\overline{V}(R,s) = \begin{pmatrix} \overline{\phi}(R,s) \\ \overline{e}(R,s) \end{pmatrix}.$$

To find the matrix $\sqrt{A(s)}$, $A(s)$, we use the spectral decomposition of $A(s)$ given by

$$A(s) = \lambda_1 E_1 + \lambda_2 E_2, \quad \ldots \quad (30)$$

where λ_1 and λ_2 are the eigenvalues of the matrix $A(s)$ and E_1, E_2 are projections on eigenspaces corresponding to λ_1, λ_2, given by

$$E_1 = \frac{1}{\lambda_1 - \lambda_2} \begin{pmatrix} m - \lambda_2 & \varepsilon m \\ -\frac{(\lambda_1 - m)(\lambda_2 - m)}{m\varepsilon} & \lambda_1 - m \end{pmatrix},$$

$$E_2 = \frac{1}{\lambda_1 - \lambda_2} \begin{pmatrix} \lambda_1 - m & -\varepsilon m \\ \frac{(\lambda_1 - m)(\lambda_2 - m)}{m\varepsilon} & m - \lambda_2 \end{pmatrix}.$$

Thus, we get

$$\begin{aligned} B(s) = \sqrt{A(s)} &= \sqrt{\lambda_1} E_1 + \sqrt{\lambda_2} E_2 \\ &= \frac{1}{\sqrt{\lambda_1} + \sqrt{\lambda_2}} \begin{pmatrix} m + \sqrt{\lambda_1 \lambda_2} & \varepsilon m \\ M_2 & M_1 + \sqrt{\lambda_1 \lambda_2} \end{pmatrix}. \quad \ldots \quad (31) \end{aligned}$$

Now, the solution (29) can be written as

$$\overline{V}(r,s) = \frac{R}{r} e^{-B(s)(r-R)} \overline{V}(R,s). \quad \ldots \quad (32)$$

Using Cayley-Hamilton theorem the matrix exponential $\exp(-B(s)(r-R))$ in equation (32) can be expressed as

$$\exp(-B(s)(r-R)) = b_0(r,s)\, I + b_1(r,s) B(s), \quad \ldots \quad (33)$$

where b_0, b_1 are the coefficients depending on s, r to be determined from the equations

$$\exp(-P_1(r-R)) = b_0 + b_1 P_1, \quad \ldots \quad (34)$$

$$\exp(-P_2(r-R)) = b_0 + b_1 P_2; \quad \ldots \quad (35)$$

P_1, P_2 being the eigen values of the matrix $B(s)$, *i.e.* the roots of the characteristic equation of the matrix $B(s)$ obtained as follows

$$\lambda^2 - \lambda(\sqrt{\lambda_1} + \sqrt{\lambda_2}) + \sqrt{\lambda_1}\sqrt{\lambda_2} = 0. \quad \ldots \quad (36)$$

Solving (34) and (35), we get b_0 and b_1 as follows

$$b_0 = \frac{P_1 e^{-P_2(r-R)} - P_2 e^{-P_1(r-R)}}{P_1 - P_2}; \quad \ldots \quad (37)$$

$$b_1 = \frac{e^{-P_1(r-R)} - e^{-P_2(r-R)}}{P_1 - P_2}. \quad \ldots \quad (38)$$

Hence, (33) can be written as

$$\exp(-B(s)(r-R)) = L(r,s) = (l_{ij}(r,s)), i,j = 1,2 \quad \ldots \quad (39)$$

where

$$l_{11} = \frac{(P_1^2 - m)e^{-P_2(r-R)} - (P_2^2 - m)e^{-P_1(r-R)}}{P_1^2 - P_2^2}, \quad \ldots \quad (40)$$

$$l_{12} = \frac{\varepsilon m(e^{-P_1(r-R)} - e^{-P_2(r-R)})}{P_1^2 - P_2^2}, \quad \ldots \quad (41)$$

$$l_{21} = \frac{M_2(e^{-P_1(r-R)} - e^{-P_2(r-R)})}{P_1^2 - P_2^2}, \quad \ldots \quad (42)$$

$$l_{22} = \frac{(P_1^2 - M_1)e^{-P_2(r-R)} - (P_2^2 - M_1)e^{-P_1(r-R)}}{P_1^2 - P_2^2}. \quad \ldots \quad (43)$$

Hence, from (32) and (39), we get

$$\overline{V}(r,s) = \frac{R}{r}(l_{ij}(r,s))\overline{V}(R,s). \quad \ldots \quad (44)$$

Then, the solutions for $\overline{\phi}$ and $\overline{e}$ can be obtained from (44) by using the boundary conditions (23) and (24) as follows

$$\overline{\phi}(r,s) = \frac{R\overline{F}(s)}{r(P_1^2 - P_2^2)}((P_1^2 - m)e^{-P_2(r-R)} - (P_2^2 - m)e^{-P_1(r-R)}), \quad (45)$$

$$\overline{e}(r,s) = \frac{RM_2\overline{F}(s)}{r(P_1^2 - P_2^2)}(e^{-P_1(r-R)} - e^{-P_2(r-R)}). \quad \ldots \quad (46)$$

Substituting (45) and (46) into (25) we get $\overline{\theta}$ in the following form

$$\overline{\theta}(r,s) = \frac{R\overline{F}(s)}{r(P_1^2 - P_2^2)}(\theta_1 e^{-P_2(r-R)} - \theta_2 e^{-P_1(r-R)}), \quad \ldots \quad (47)$$

where

$$\theta_1 = (1-\omega m)(P_1^2 - m) - M_2 \omega m \varepsilon, \quad \theta_2 = (1-\omega m)(P_2^2 - m) - M_2 \omega m \varepsilon.$$

Integrating (46) we get $\overline{u}$ as follows

$$\overline{u}(r,s) = \frac{RM_2\overline{F}(s)}{rP_1P_2(P_1^2 - P_2^2)}(P_2 e^{-P_1(r-R)} - P_1 e^{-P_2(r-R)}). \qquad \ldots \quad (48)$$

Using (48) in (18) we get $\overline{\sigma}_{rr}$ as follows

$$\overline{\sigma}_{rr}(r,s) = \frac{R\overline{F}(s)}{r^2P_1P_2(P_1^2 - P_2^2)}[\{(\gamma^2 - 1) + \alpha_1 r P_1 \theta_2\}P_2 e^{-P_1(r-R)}$$

$$- \{(\gamma^2 - 1) + \alpha_1 r P_2 \theta_1\}P_1 e^{-P_2(r-R)}]. \qquad \ldots \quad (49)$$

Equations (45)-(49) give complete solutions to the thermal shock problem in the Laplace transform domain..

5. Numerical results and discussion

In order to invert the Laplace transform in the above equations, we adopt a numerical inversion method based on a Fourier series expansion[33]. The numerical code has been prepared using Fortran 77 programming language. For computational purpose, copper like material has been taken into consideration. The values of the material constants are taken as Roy Choudhuri and Dutta[35]

$$\alpha_t = 1.78 \times 10^{-5} K^{-1}, \; c_v = 383.1 m^2/K, \; \eta = 8,886.73 m/s^2,$$

$$\mu = 3.86 \times 10^{10} N/m^2, \; \lambda = 7.76 \times 10^{10} N/m^2, \; \rho = 8,954 g/m^3,$$

$$T_0 = 293K, \; \epsilon = 1.608, \; \alpha_1 = 0.0104, \; \gamma = 0.501,$$

and the hypothetical values of relaxation time parameters are taken as :

$$\tau_q = 0.001, \; \tau_v = 0.025, \; \tau_T = 0.015.$$

Also, for the computational purpose we have taken :

$$C_T = 2.0, \; \varphi_0 = 1.0, \; R = 1.0.$$

The computations were carried out for t = 0.4. The displacement, thermodynamic temperature, conductive temperature, the thermal stress and the thermal strain distributions are represented graphically for dierent values of r for weak conductivity (α = 0:7) and normal conductivity (α = 1:0) for both one-temperature (ω = 0:0) and two-temperatures (ω= 0:2) respectively.

Throughout the figures (1-5), the curves without marker represent the results corresponding to model *F*3*PL* (fractional three-phase-lag) and the curves with marker (square) represent the results corresponding to model 3*PL* (three-phase-lag).

Figures 1-5, are drawn for comparative study of two models (*F*3*PL* and 3*PL*) in one-temperature theory (1*TT*) as well as two-temperature theory (2*TT*). Figures 6-10 are drawn for comparative study of three models (*F*3*PL*, 3*PL* and *GN-III*) in two-temperature theory whereas figures 11-15 are drawn for comparative study of three models (*F*3*PL*, 3*PL* and *GN-III*) in one-temperature theory.

Figures 1-5 represent dierent thermophysical quantities, *viz*., thermal displacement (u), thermodynamic temperature (θ), conductive temperature (ϕ), thermal stress (σ_{rr}), thermal strain (e_{rr}) versus the space variable r respectively for t = 0:4 in one-temperature as well as two temperature theory. From figure 1, we see that, the maximum magnitude of displacement appears at the boundary of the cavity. In both types of conductivities (α = 0:7; 1:0), the magnitude of displacement is greater in 1*TT* in comparison to 2*TT* and the effect of fractional parameter is more prominent on 1*TT*. From figure 2, we observe that the thermodynamic temperature becomes negative at a larger distance from the inner surface of the cavity in 1*TT* than 2*TT*. In the region $1.0 \leq r \leq 1.2$ (approx.), the magnitude of the thermodynamic temperature is smaller for one temperature case and they are positive. The effect of two temperature parameter as well as fractional parameter are prominent in the region $1.2 < r \leq 4.0$ (approx.), after which all the curves coincide and gradually tend to vanish. From figure 3, it is clear that the conductive temperature satisfies our assumed boundary condition in all cases. Likewise the thermodynamic temperature, the conductive temperature becomes negative at a larger distance from the inner surface of the cavity in 1*TT* than 2*TT*. The magnitude of the conductive temperature is greater for one temperature case and they are positive in the region $1.0 \leq r \leq 1.3$ (approx.). The effect of two temperature parameter as well as fractional parameter are prominent in the region $1.3 < r \leq 4.6$ (approx.), after which all the curves coincide and they gradually tend to vanish.

From figure 4, we see that the radial stress is compressive in nature throughout the body. The maximum magnitude of the radial stress is attained at the surface of the cavity for both types of conductivities. In the region $1.0 \leq r \leq 2.5$ (approx.), the magnitude corresponding to 2*TT* is greater in comparison to 1*TT*. In the region $r > 2.5$, all the curves coincide and they tend to vanish.

From figure 5, we see that the effect of conductivity parameter appears for 1*TT* but no effect of conductivity parameter appears for 2*TT*. The magnitude of strain in 2*TT* are more or less identical for weak and normal conductivity, whereas for 1*TT*, the magnitude is greater in normal conductivity.

Figures 6-10 represent the different thermophysical quantities, *viz*., thermal displacement (u), thermodynamic temperature (θ), conductive temperature (ϕ), thermal stress (σ_{rr}), thermal strain (e_{rr}) versus the space variable r respectively for $t = 0.4$ for two temperature theory. From figure 6, we see that throughout the region the magnitude of displacement corresponding to *F*3*PL* is largest among the three models (*F*3*PL*, 3*PL*, *GN-III*). It is also observe that at the nearer region of the surface of the cavity, the magnitude corresponding to the *GN-III* model is smaller than the magnitude corresponding to 3*PL* models.

From figure 7, we see that the magnitude of the thermodynamic temperature (θ), are almost identical at the surface of the cavity and in the region $r \geq 4.1$ (approx.), the difference of magnitude for three considerations are prominent in the region $1.1 \leq r \leq 4.1$ (approx.).

From figure 8, we see that the conductive temperature (ϕ) satisfies our assumed boundary condition in all cases. We also observe that the conductive temperature is positive at the surface of the cavity in all considerations. For *F*3*PL* model the conductive temperature becomes negative for smaller value of r with respect to the other two models.

From figure 9, it is clear that the radial stress is compressive throughout the body. The rate of decay for *GN-III* model is faster than other two models. Figure 10 indicates that the surface of the cavity is strain-free *i.e* it satisfies our assumed boundary condition. The maximum magnitude of strain is due to the *GN-III* model. After $r \geq 3.5$ the strain in all cases is negative and then it tends to vanish.

Figures 11-14 represent the different thermophysical quantities, *viz*., thermal displacement (u), thermodynamic temperature (θ), thermal stress (σ_{rr}), thermal strain (e_{rr}) versus the space variable r respectively for t = 0.4 for one temperature theory. From figure 11, we see that the internal surface of the cavity gets maximum displacement for all models. For $r \geq 3.5$ the displacement becomes positive and then they tend to vanish. From figure 12, we see that the magnitude of the thermodynamic temperature (θ), are almost identical at the surface of the cavity and in the region $r \geq 4.2$ (approx.), the difference of magnitude for three considerations are prominent in the region $1.1 \leq r \leq 4.2$ (approx.). Figure 13 shows that the radial stress is compressive in the region $1.0 \leq r \leq 2.75$ (approx.). Also the rate of decay of the magnitude of the radial stress is faster for *GN-III* model like 2*TT*. From figure 14, we see that the strain satisfies our assumed boundary condition. The strain is positive in the region $1.0 \leq r \leq 3.2$ (approx.), after that it becomes negative and then tends to vanish.

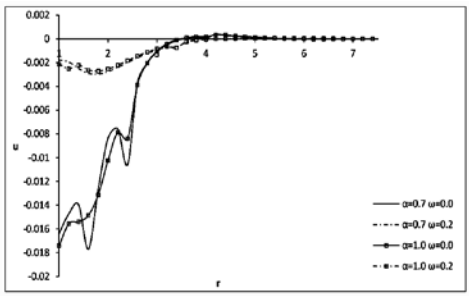

Fig. 1
Variation of displacement u with r for different ω and α.

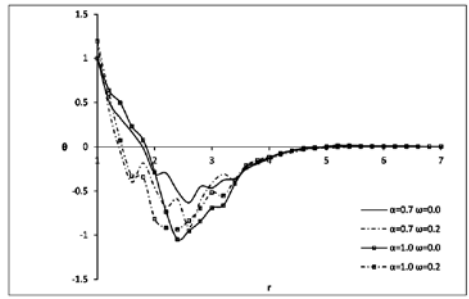

Fig. 2
Variation of thermodynamic temperature θ with r for different ω and α.

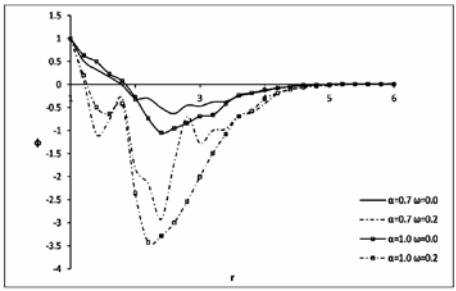

Fig. 3
Variation of conductive temperature ϕ with r for different ω and α.

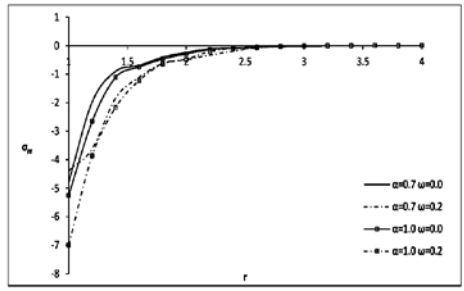

Fig. 4
Variation of stress $\sigma_{r\,r}$ with r for different ω and α.

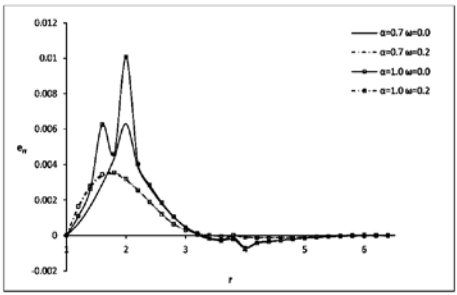

Fig. 5
Variation of strain $e_{r\,r}$ with r for different ω and α.

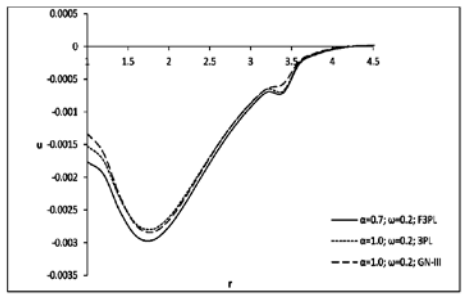

Fig. 6
Variation of displacement u with r for ω= 0.2.

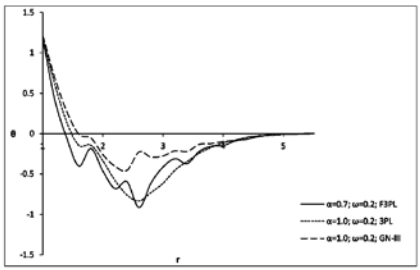

Fig. 7
Variation of thermodynamic temperature θ with r for ω= 0.2.

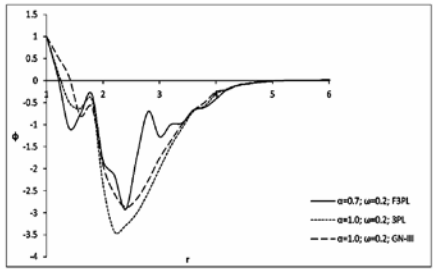

Fig. 8
Variation of conductive temperature ϕ with r for ω= 0.2.

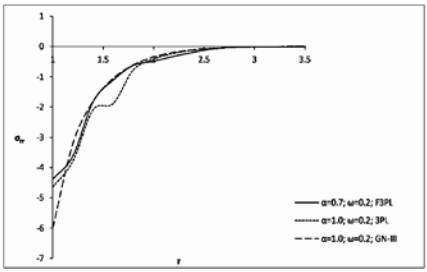

Fig. 9
Variation of stress $\sigma_{r\,r}$ with r for ω= 0.2.

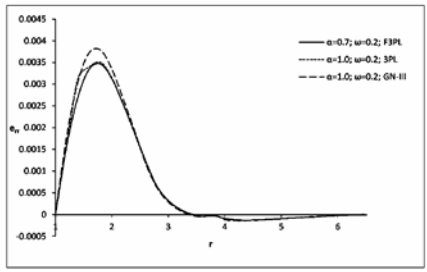

Fig. 10
Variation of strain $e_{r\,r}$ with r for ω= 0.2.

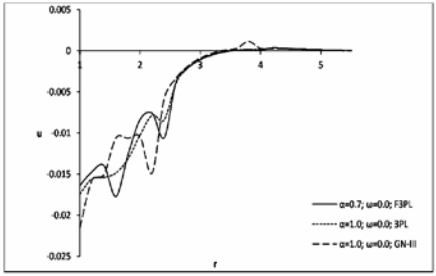

Fig. 11
Variation of displacement u with r for ω= 0.0.

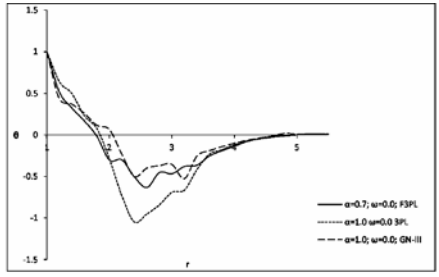

Fig. 12
Variation of thermodynamic temperature θ with r for ω= 0.0.

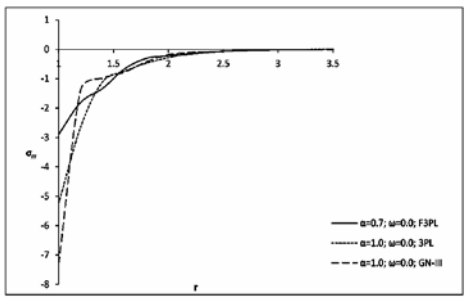

Fig. 13
Variation of stress $\sigma_{r\,r}$ with r for ω= 0.0

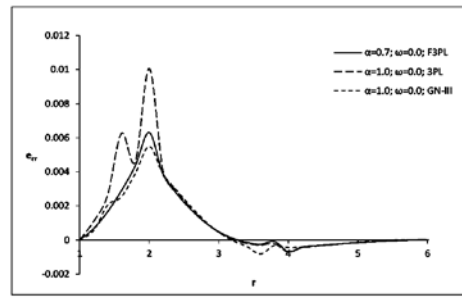

Fig. 14
Variation of strain $e_{r\,r}$ with r for ω= 0.0

References

1. Jumarie, G.− Derivation and solutions of some fractional Black Scholes equations in coarse-grained space and time, application to Mertons optimal portfolio, Comput. Math. Appl., **59**, pp. 1142-1164 (2010).
2. Hetnarski, R. B. and Ignaczak, J. − Generalized Thermoelasticity, J. Therm. stresses, **22**, pp. 451-476 (1999).
3. Lord, H. W. and Shulman, Y. − A generalized dynamical theory of thermoelasticity, J. Mech. Phys. Solids, **15**, pp. 299-309 (1967).
4. Green, A. E. and Lindsay, K. A. − Thermoelasticity, Journal of Elasticity, **2**, pp. 1-7, (1972).
5. Green, A. E. and Naghdi, P. M. − A re-examination of the basic results of thermomechanics, Proc. Roy. Soc. London. Ser. A, **432**, pp. 171-194 (1991).
6. Green, A. E. and Naghdi, P. M. − On undamped heat waves in an elastic solid, J. Therm. Stresses, **15**, pp. 252-264 (1992).
7. Green, A. E. and Naghdi, P. M. −Thermoelasticity without energy dissipation, J. Elasticity, **31**, pp. 189-208 (1993).
8. Chandrasekharaiah, D. − Hyperbolic thermoelasticity, A review of recent literature, J. Appl. Mech. Rev., **51**, pp.705-729 (1998).
9. Tzou, D. − A unified field approach for heat conduction from macroto micro-scales, J. ASME J. Heat Transfer, **117,** pp. 8-16 (1995).
10. Roy Choudhuri, S. K. − On a thermoelastic three-phase-lag model, J. Therm. Stresses, **30**, pp. 231-238 (2007).
11. Gurtin, M. E. and Williams, W. O.−On the Clausius-Duhem inequality, Z. Angew. Math. Phys., **17**, pp. 626-633 (1966).
12. Gurtin, M. E. and Williams, W. O.−An axiomatic foundation for continuum thermodynamics, Arch. Ration. Mech. Anal., **26**, pp. 83-117 (1967).
13. Chen, P. J. and Gurtin, M. E. − On a theory of heat conduction involving two temperatures, Z. Angew. Math. Phys., **19**, pp. 614-627 (1968).
14. Chen, P. J., Gurtin, M. E. and Williams, W. O.−On the thermodynamics of non-simple elastic materials with two-temperatures, Z. Angew. Math. Phys., **20**, pp. 107-112 (1969).
15. Warren, W. E. and Chen, P. J. − Wave propagation in two temperatures theory of thermoelasticity, Acta Mech., **16**, pp. 83-117 (1973).

16. Youssef, H. M. −Theory of two-temperature generalized thermoelasticity, IMA J. Appl. Math., **71**, pp. 1-8 (2006).
17. Youssef, H. M. − Theory of two-temperature thermoelasticity without energy dissipation, J. Therm. Stresses, **2**, pp. 138-146 (2011).
18. Magañe, A. and Quintanilla, R. − Uniqueness and growth of solutions in two-temperature generalized thermoelastic theories, J. Math. Mech. Solids, **14**, pp. 622-634 (2009).
19. Abel, N. H. − Solution de quelques problèmes à l'aide d'intégrales défines, Oeuvres complètes, nouvelle éd, 1, Christiania, Grondahl & Sons, pp. 11-27, (1881). (Edition de Holmboe).
20. Ross, B. −The development of fractional calculus 1695-1900, Historia Mathematica, **1**, pp. 75-89 (1977).
21. Caputo, M. − Linear model of dissipation whose Q is always frequency independent, J. Geophysical Journal of the Royal Astronomical Society, **13**, pp. 529-539 (1967).
22. Caputo, M. and Mainardi, F.− A new dissipation model based on memory mechanism, J. Pure and Applied Geophysics, **91**, pp. 134-147 (1971).
23. Caputo, M. and Mainardi, F. − Linear model of dissipation in an elastic solids, J. Rivista del Nuovo Cimento, **1**, pp. 161-198 (1971).
24. Povstenko, Y. Z. − Fractional heat conductive and associated thermal stress, J. Therm. Stresses, **28**, pp. 83-102 (2004).
25. Povstenko, Y. Z. − Fractional Catteneo-type equations and generalized thermoelasticity, J. Therm. Stresses, **34**, pp. 94-114 (2011).
26. Povstenko, Y. Z. − Thermoelasticity that uses fractional heat conduction equation, J. Math. Stresses, **162**, pp. 296-305 (2009).
27. Sherief, H. H., El-Said, A. and Abd El-Latief, A. − Fractional order theory of thermoelasticity, Int. J. Solids Struct., **47**, pp. 269-275 (2010).
28. Youssef, H. M. and Al-Lehaibi, E. A. − State-space approach of two-temperature generalized thermoelasticity of one dimensional problem, Int. J. Solids Struct, **5**, pp. 1550-1562 (2007).
29. Ezzat, M. A. − Theory of fractional order in generalized thermoelectric MHD, Applied Mathematical Modelling, **35**, pp. 4965-4978 (2011).
30. Ezzat, M. A. − Magneto-thermoelasticity with thermoelectric properties and fractional derivative heat transfer, J. Physica B,. **406**, pp. 30-35 (2011).
31. Ezzat, M A., Elkaramany, A. and Fayik, M. − Fractional order theory in thermoelastic solid with three-phase lag heat transfer, J. Arch Appl. Mech., **82**, pp. 557-572 (2012).
32. Mondal, S., Mallik, S. H. and Kanoria, M. − Fractional order two-temperature dual-phase-lag thermoelasticity with variable thermal conductivity, International Scholarly Research Notices, **1**, pp. 1-13 (2014).
33. Honig, G. and Hirdes, U. − A method for the numerical inversion of the Laplace transform, J. Comp. Appl. Math., **10**, pp. 113-132 (1984).
34. Bahar, L. Y. and Hetnarski, R. B. − State space approach to thermoelasticity, J. Therm. Stresses, **1**, pp. 135-145 (1978).
35. Roy Choudhuri, S. K. and Dutta, P. S. − Thermoelastic interaction without energy dissipation in an infinite solid with distributed periodically varying heat sources, Int. J. Solids Struct., **42**, pp. 4192-4203 (2005).

ISSN : 0019-5693

INDIAN JOURNAL
OF
THEORETICAL PHYSICS

[Founder President : Late Prof. K. C. Kar, D.Sc.]

VOLUME 65

2017

Published by the

CALCUTTA INSTITUTE OF THEORETICAL PHYSICS
(Formerly, INSTITUTE OF THEORETICAL PHYSICS)
"BIGNAN KUTIR"
4/1, MOHAN BAGAN LANE, KOLKATA-700 004

(UGC approved and refereed Journal)

INFORMATION TO AUTHORS

Manuscripts should represent results of original works on theoretical physics or experimental physics with theoretical background or on applied mathematics. Letters to the Editor and Review articles in emerging areas are also published. Submission of the manuscript will be deemed to imply that it has not been published previously and is not under consideration for publication elsewhere (either partly or wholly) and further that, if accepted, it will not be published elsewhere. It is the right of the Editorial Board to accept or to reject the paper after taking into consideration the opinions of the referees.

Manuscripts may be submitted in pdf/MS word format to **admin@citphy.org or susil_vcsarkar@yahoo.co.in** Online submission of the paper through our **website: www.citphy.org** is also accepted. The file should be prepared with 2.5 cm margin on all sides and a line spacing of 1.5.

The title of the paper should be short and self-explanatory. All the papers must have an abstract of not more than 200 words, the abstract page must not be a part of the main file. Abstract should be self-contained. It should be clear, concise and informative giving the scope of the research and significant results reported in the paper. Below the abstract four to six key words must be provided for indexing and infornjation retrieval.

The main file should be divided into sections (and sub-sections, if necessary) starting preferably with introduction and ending with conclusion. Displayed formula must be clearly typed (with symbols defmed) each on a separate /'ine and well-separated from the adjacent text. Equations should be numbered with on the right-hand side consecutively throughout the text. Figures and Tables with captions should be numbered in Arabic numerals in the order of occurrence in the text and these should be embedded at appropriate places in the text. Associated symbols must invariably follow SI practice.

References should be cited in the text by the Arabic numerals as superscript. All the references to the published papers should be numbered serially by Arabic numerals and given at the end of the paper. Each reference should include the author's name, title, abbreviated name of the journal, volume number, year of publication, page numbers, as in the simple citation given below :

For Periodicals : Sen, N.R. - On decay of energy spectrum of Isotopic Turbulence, 1. Appl. Phys. **28,** No. l0, l09-110 (1999).

1. Mikhilin, S. G. - Integral Equations, Pergamon Press, New York (1964).
2. Hinze, A. K. - Turbulence Study of Distributed Turbulent Boundary Layer Flow, Ph.D, Thesis, Rorke University (1970).

The corresponding author will receive page proof, typically as a pdf file. The proof should be checked carefully and returned to the editorial office within two or three days. Corrections to the proof should be restricted to printing errors and made according to standard practice. At this stage any modifications (if any) made in the text should be highlighted.

To support the cost of publication of the journal, the authors (or their Institutions) are requested to pay publication charge Rs.200/- per printed page for authors of Indian Institutes and US$ 20 for others. Publication charges to be sent directly to **CALCUTTA INSTITUTE OF THEORETICAL PHYSICS, 'BIGNAN KUTIR', 4/1, MOHAN BAGAN LANE, KOLKATA-700 004, INDIA.**

A pdf of the final publisher's version of the paper will be sent to the corresponding author shortly after print publication by our Co-publisher, **Wilcox Books & Periodicals Co. (wilcoxbooks@gmail.com)**

All communications are to be sent to the Secretary, Calcutta Institute of Theoretical Physics, 'Bignan Kutir', 4/1, Mohan Bagan Lane, Kolkata-700 004.

Indian Journal of Theoretical Physics is in the list of Journals approved by UGC.

For details please visit our website www.citphy.org

INDIAN JOURNAL OF THEORETICAL PHYSICS

International Board of Editorial Advisors

B. Das Gupta, (*USA*)
Nao-Aki Noda, (*Japan*)
D. S. Roy, (*India*)
A. Sen, (*India*)
A. Roy Chaudhury, (*India*)
S. Raha, (*India*)
A. H. Siddiqi, (*India*)
N. K. Gupta, (*India*)
K. Ghatak, (*India*)
O. P. Agarwal, (*USA*)
Ching-Kong Chao, (*Taiwan*)
M. R. Islami, (*Iran*)
Halina Egner, (*Poland*)
K. C. Deshmukh, (*India*)
A. Kundu, (*India*)
B. Chakraborty, (*India*)
A. N. Sekhar Iyengar, (*India*)

BOARD OF EDITORS

D. K. Basu
C. Dutta
S. K. Biswas
R. K. Bera
D. Syam
I. Bose
M. Kanoria
P. R. Ghosh
Rita Chaudhuri
S. K. Sarkar
D. C. Sanyal
P. K. Chaudhuri
D. Sarkar
A. Sanyal
J. Mukhopadhyay
A. K. Ghosh

***Editorial Secretary* : D. C. Sanyal**

CALCUTTA INSTITUTE OF THEORETICAL PHYSICS

(Formerly, Institute of Theoretical Physics)

[Established in 1953 by Late Prof. K. C. Kar, D.Sc.]

***Director* : D. K. Basu** ***Secretary* : S. K. Sarkar**
***Registrar* : C. Dutta** ***Asst. Secretary* : P. S. Majumdar**
***Members* : P. R. Ghosh, A. Roy, D. C. Sanyal, J. Mukhopadhyay, M. Chakraborti**

PUBLICATIONS
OF
CALCUTTA INSTITUTE OF THEORETICAL PHYSICS

"BIGNAN KUTIR"
4/1, Mohan Bagan Lane, Kolkata - 700 004, India
Phone: +91-33-25555726

INDIAN JOURNAL OF THEORETICAL PHYSICS (lSSN : 0019-5693)

Research Journal containing Original Papers, Review Articles and Letters to the Editor is published quarterly in March, June, September and December and circulated all over the world.

Subscription Rates

₹ 1500 per volume (for Bonafide Indian Party)
US $ 350 (for Foreign Party)

Back Volume Rates

₹ 1500 per volume (for Bonafide Indian Party)
US $ 350 per volume or Equivalent Pounds per volume

Books Written by Prof. K. C. Kar, D. Sc.

- **INTRODUCTION TO THEORETICAL PHYSICS**
  [Vol. I and Vol. II (Accoustics)]
  Useful to students of higher physics
  Price : ₹ 60 or US $ 10 per volume
- **WAVE STATISTICS : Its principles and Applications**
  [Vol. I and Vol. II]
  Useful to Post Graduate and Research students
  Price : ₹ 80 or US $ 12
- **STATISTICAL MECHANICS : Principles and applications**
  [Vol. I and Vol. II]
  Useful to Advanced students of Theoretical Physics
  Price : ₹ 120 or US $ 15
- **A NEW APPROACH TO THE THEORY OF RELATIVITY**
  Useful to post Graduate and Advanced students
  Price : ₹ 50 or US $ 8

Order may be sent directly to Calcutta Institute of Theoretical Physics
"Bignan Kutir", 4/1, Mohan Bagan Lane, Kolkata -700 004, India

---

All rights (including Copyright) reserved by the Calcutta Institute of Theoretical Physics.
Unimage, 10, Roy Bagan Street, Kolkata-700 006 and published by Dr. S. K. Sarkar, Secretary, on behalf of Calcutta Institute of Theoretical Physics, 4/1, Mohan Bagan Lane, Kolkatta -700 004, India.

INDIAN JOURNAL OF THEORETICAL PHYSICS

VOLUME 65, 2017

C O N T E N T S

JANUARY – JUNE, 2017

JULY – DECEMBER, 2017

Detailed information about our other Journals

1. Name of the Journal : **Bengal Past & Present**
   ISSN :..... **0005-8807**
   Frequency:..... **Annually (Latest Vol. 136,2017)**
   Price: .....(a) In India: Institutions: **500-00**
   .....(b) Overseas : **$ 150-00**
   Postage:..... **Post Free**
   * Discount :.... To Subscription Agencies: **25%**
   ..... To Institutions :..... **Fixed Price**
2. Name of the Journal:..... **Journal of the Indian Anthropological Society**
   ISSN :..... **0019-4387**
   Frequency:..... **Three Issues in a year (March, July & November)**
   Price:..... (a) In India: Institutions: **1500-00 (Latest Vol. 51, 2016)**
   ..... (b) Overseas..... **$ 300-00**
   Postage:..... **Post Free**
   * Discount: To Subscription Agencies: **25%**
   ..... To Institutions :..... **Fixed Price**
3. Name of the Journal: ..... **Journal of Surface Science and Technology**
   ISSN :..... **0970-1893**
   Frequency:..... **Quarterly**
   Price:..... (a) In India: Institutions: **1800-00 (Latest Vol. 33, 2017)**
   ..... (b) Overseas..... **$ 300-00**
   Postage :.....**Post Free**
   * Discount: To Subscription Agencies: **25%**
   ..... To Institutions :..... **Fixed Price**
4. Name of the Journal: **The Journal of the Indian Academy of Philosophy**
   ISSN: .....
   Frequency:..... **Bi-Annual**
   Price:..... (a) In India: Institutions: **200-00 (Latest Vol. 52, 2013)**
   ..... (b) Overseas..... **$ 30-00**
   Postage :..... **Post Free**
   * Discount :... To Subscription Agencies: **25%**
   ..... To Institutions :..... Fixed Price
5. Name of the Journal: **The Quarterly Review of Historical Studies**
   ISSN:..... 0033-5800
   Frequency:..... **Quarterly**
   Price:..... (a) In India: Institutions: **1500-00 (Latest Vol. 57, 2017-18)**
   ..... (b) Overseas..... **$ 400-00**
   Postage:..... **Post Free**
   * Discount :... To Subscription Agencies: **25%**
   ..... To Institutions: **Fixed Price**
6. Name of the Journal: **Indo-Iranica**
   ISSN:.....03789-0856
   Frequency:..... **Quarterly**
   Price:..... (a) In India: Institutions: **1500-00 (Latest Vol. 69, 2016)**
   ..... (b) Overseas..... **$ 350-00**
   Postage:.....**Post Free**
   * Discount : To Subscription Agencies: **25%**
   ..... To Institutions :..... **Fixed Price**

For more Journals Visit our website : www.wilcoxjournals.com

*** For Foreign Subscriptions Only**

Order should be sent to :

Wilcox Books and Periodicals Co.
8/2/A, Neogi Para Road,
Kolkata - 700036 (India)
Email : wilcoxbooks@gmail.com
: wilcoxbooks@yahoo.co.in